Energetic Oxygen in the Upper Atmosphere and the Laboratory

Tom G. Slanger* and Richard A. Copeland

Molecular Physics Laboratory, SRI International, Menlo Park, California 94025

Received April 1, 2003

Contents

1. Introduction

Of the light elements that are the building blocks of nature, oxygen is unique in having three stable forms that are common in both the atmosphere and the laboratory: $O(^3P)$, O_2, and O_3. Atomic oxygen plays a role throughout the atmosphere and is the most abundant species between ~170 and 700 km. Similarly, ozone is ubiquitous and over the past 50 years has become a household word, on one hand because of its role in smog generation, and on the other because of the protection against ultraviolet radiation that it provides to the planet. We have become aware of the fragility of the very thin layer of stratospheric ozone, as we have become familiar with the effects of anthropogenic changes.

One reason that O_2 is chemically interesting is because it has two low-lying electronic states which are easily generated in the atmosphere and in the laboratory. Furthermore, the oxygen bonds in O_3 are quite weak, and as a result a variety of energetic species can be produced with modest amounts of input energy. Thus, ozone has been used as a source for many laboratory studies and often plays a similar role in the atmosphere. For instance, the glowing OH layer near 87 km is produced by the reaction of ozone with hydrogen atoms.[1] This chemical reaction is one of several that generate the terrestrial airglow.

In this review, our principal goal is to present the current state of the art in the study of the chemistry of energetic oxygen, applied to energy-transfer studies in the laboratory and to airglow observations in the atmosphere. These are synergistic disciplines, and so advances in one area find applications in the other. Most of the studies we discuss have been carried out over the past 20 years. Two comprehensive reviews of upper atmospheric studies of relatively recent vintage are those of Meriwether[1] and Solomon.[2] These contain a great many references and are important resources for those seeking more information on airglow chemistry and observations. The spectroscopy of the O_2 molecule for the states considered here was reviewed in 1988,[3] and much of that information is in the process of being updated. There is little overlap between the laboratory studies to be discussed here and the extensive and periodic NASA reviews on stratospheric chemistry.[4]

The lowest seven bound electronic states of O_2—$X^3\Sigma_g^-$, $a^1\Delta_g$, $b^1\Sigma_g^+$, $c^1\Sigma_u^-$, $A'^3\Delta_u$, $A^3\Sigma_u^+$, and $^5\Pi_g$—are all metastable with respect to radiation. The first optically allowed transition involves the $B^3\Sigma_u^-$ state, which lies 6.1 eV above the ground state. As a consequence, in many systems both in the atmosphere and in the laboratory, the lack of an efficient radiative deactivation pathway makes these seven O_2 states chemically interesting. It also makes their study at times difficult, because for laboratory in-

10.1021/cr0205311 CCC: $44.00
Published on Web 11/08/2003

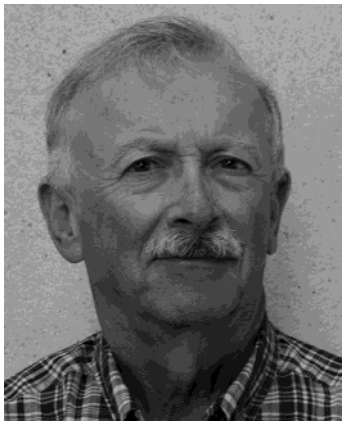

Tom G. Slanger is a native of Austria, having come to the United States in 1946. His family settled in Los Angeles, and he obtained a B.S. in 1956 in applied chemistry, and then an M.S. in 1957 in chemical engineering, both from the California Institute of Technology. Subsequently, he obtained his Ph.D. in 1965 from UCLA in physical chemistry with Professor Kyle Bayes. After a postdoctoral year spent at Saclay, France, he started work at SRI International, where he has been ever since. His research has been largely devoted to the kinetics and spectroscopy of atoms and small molecules, particularly as they relate to atmospheric processes. Most of these studies have involved electronically excited states, and he has been very active in studying and interpreting airglow processes in both the terrestrial and Venusian atmospheres. Over the past several years he has pioneered the use of astronomical sky spectra to study the terrestrial nightglow, research which has led to numerous new discoveries concerning the upper atmosphere and ionosphere.

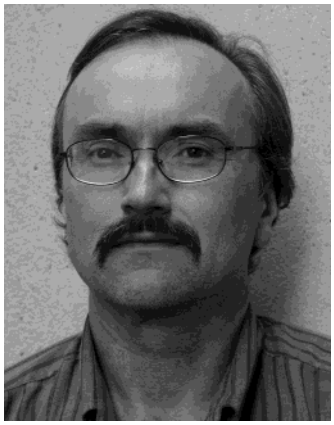

Richard A. Copeland was born in Milwaukee, Wisconsin, in 1955. He received his B.Sc. in chemistry from Valparaiso University in 1977 and his Ph.D. in physical chemistry from the University of Wisconsin–Madison in 1982 with Professor F. Fleming Crim, studying vibrational and rotational energy transfer in the hydrogen fluoride molecule. He came to the Molecular Physics Laboratory (MPL) of SRI International in 1983 as a postdoctoral fellow, studying collisional energy transfer in the hydroxyl radical and laser-based diagnostics of combustion. He became a member of the MPL staff in 1985. In 1998, he became Director of the Physics and Atmospheric Chemistry Group, and in 2000 he became Director of the Molecular Physics Laboratory. His current research interests include the collisional energy transfer and spectroscopy of molecules important in planetary atmospheres, atom recombination in the gas phase and on surfaces, and the processes occurring in low-temperature matrices containing oxygen species.

vestigations it is necessary to devise monitoring techniques beyond the inefficient radiative process.

In the upper atmosphere, solar radiation dissociates O_2, resulting in relatively large atomic oxygen densities above 80 km, with a peak near 95 km, and increasing dominance compared to other species with increasing altitude: above ~170 km, atomic oxygen [$O(^3P)$] is the primary species. Photodissociation of O_2 is balanced by three-body recombination of $O(^3P)$, and in this process the O_2 molecule is formed in the electronic states that lie below the $O(^3P) + O(^3P)$ limit. The oxygen airglow is the radiative relaxation out of the five electronically excited states. There are a number of useful reviews on aeronomy; the term is defined as the science of the upper atmospheric regions where dissociation and ionization are important, and it is now also applied to studies of the atmospheres of other planets.[1,2,5−9]

We learn about the excited states of O_2 both from the uncontrolled airglow emissions, which are found from the ultraviolet to the infrared spectral regions, and from measurements in the controlled laboratory environment. In the atmosphere, one can discern variations in emission intensity that reflect atmospheric movements and can, in principle, be related to the oxygen atom densities that are the ultimate source of the radiation. As will be demonstrated, the richness of the atmospheric O_2 emissions also provides an excellent opportunity to improve the knowledge base of O_2 spectroscopy in general. The high-resolution laboratory absorption measurements, which accurately define the upper states of the O_2 transitions, combined with the airglow emission measurements, which give unique information on the lower states, are proving to be extremely synergistic.

In the laboratory, the technique of resonance-enhanced multiphoton ionization (REMPI) has been shown to be a superb tool for studying the production and loss of highly vibrationally excited levels of the electronically excited O_2 states that lie below the 5.1 eV first dissociation limit. Earlier studies were, in general, limited to investigations of the lowest vibrational levels of the various states, but REMPI has opened a new window for such measurements. Progress has also been made in the area of theoretical calculations, particularly for vibration to vibration (V−V) and vibration to translation (V−T) energy transfer in the O_2 ground state.[10−14]

2. Electronic States and Transitions in O_2

Figure 1 shows the seven lowest bound electronic states that come from $O(^3P) + O(^3P)$ limits. There are no optically allowed transitions between any of these states, yet enough interactions occur by a variety of pathways that numerous transitions between them are known. We show the known transitions in Table 1, and when inverted transitions are excluded (i.e., $a^1\Delta_g - b^1\Sigma_g^+$ bands), as well as those involving the $^5\Pi_g$ state (because they would lie far into the infrared (IR), where observations are currently impractical), we see that there are only three unidentified systems: $A'^3\Delta_u - b^1\Sigma_g^+$, $A^3\Sigma_u^+ - a^1\Delta_g$, and $A^3\Sigma_u^+ - b^1\Sigma_g^+$. Calculations have been made of the transition strengths of these three systems,[15,16] and they are not small in comparison with known systems, with the $A'-b$ system appearing to be particularly favorable. However, these identifications have not yet been made, neither in the laboratory nor in the nightglow. Noteworthy is the fact that the $c^1\Sigma_u^- - b^1\Sigma_g^+$ bands were not included in the calculations because the

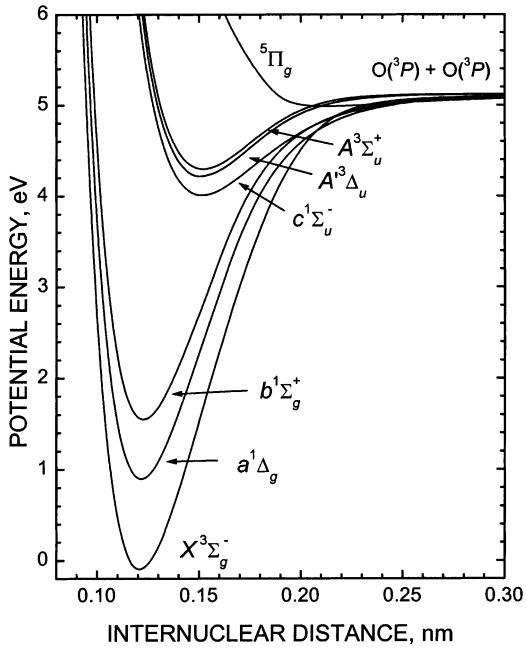

Figure 1. Bound states of O_2 arising from O(^3P) + O(^3P) limits.

Table 1. Known O_2 Transitions for States below 5.1 eV

transition	designation	0−0 band origin (cm^{-1})
$A^3\Sigma_u^+ - X^3\Sigma_g^-$	Herzberg I	35 010
$A'^3\Delta_u - X^3\Sigma_g^-$	Herzberg III	34 387[a]
$A'^3\Delta_u - a^1\Delta_g$	Chamberlain	26 346[b]
$c^1\Sigma_u^- - X^3\Sigma_g^-$	Herzberg II	32 665
$c^1\Sigma_u^- - a^1\Delta_g$		24 776
$c^1\Sigma_u^- - b^1\Sigma_g^+$		19 543
$b^1\Sigma_g^+ - X^3\Sigma_g^-$	Atmospheric	13 122
$b^1\Sigma_g^+ - a^1\Delta_g$	Noxon	5 233
$a^1\Delta_g - X^3\Sigma_g^-$	IR Atmospheric	7 889

[a] Value for the spin−orbit sub-band with $\Omega = 2$ in the $A'^3\Delta_u$ state. [b] Value for the spin−orbit sub-band with $\Omega = 3$ in the $A'^3\Delta_u$ state.

source of any transition moment was not evident. Their recent discovery in the terrestrial nightglow demonstrates that O_2 still holds surprises.[17]

3. O-Atom Electronic States

There are three O-atom electronic states of consequence in the nightglow region: the O(^3P) ground state, the O(^1D) state, and the O(^1S) state. The excited states are metastable, with the O(^1D) radiative lifetime being 114 s, and the O(^1S) lifetime, 0.84 s.[18] The so-called oxygen red lines correspond to the $^1D \rightarrow {}^3P$ transitions at 630 and 634 nm, and the oxygen green line is the $^1S \rightarrow {}^1D$ transition at 557.7 nm. O(^1S) also radiates in the $^1S \rightarrow {}^3P$ trans-auroral line at 297.2 nm, which is about a factor of 20 weaker than the green line.[19]

These states are all of great importance in the atmosphere. The O(^3P) atom is the engine that powers the nightglow by its recombination, which releases an energy of 5.1 eV. O(^1D) is important in a variety of atmospheric regions, from the stratosphere, where it is a product of ozone photodissociation, to the ionosphere, where it radiates strongly and is formed by ionic processes. The O(^1S) atom is also formed in the ionosphere, but its emission is quite intense in the atom recombination region,[20] where it is clearly associated with the O(^3P) density, but in a way that has not yet been fully defined.

Other atomic oxygen states are of consequence higher in the atmosphere, where a variety of lines are seen in the ionosphere in addition to the red and green lines. These are produced by ionic processes involving either O_2^+ or O^+.[5,6,21]

4. Molecular Transition Probabilities

To interpret the intensities of O_2 emissions in the atmosphere, it is necessary to know both the collisional lifetimes and the transition probabilities of the individual states and vibrational levels. Except for the $v = 0$ levels of the $a^1\Delta_g$ and $b^1\Sigma_g^+$ states, radiative efficiencies (the fraction of a population lost by radiation) are quite small in the atmospheric environment in which emission is observed. This inefficiency is even more pronounced under typical laboratory conditions, where densities are higher. Collisional loss rate coefficients are emerging from laboratory measurements for all the electronic states, and progress has been made on the radiative lifetimes of the excited states.

Oscillator band strengths can be derived from photoabsorption cross sections, which then lead to transition probabilities. One can calculate radiative lifetimes if the variation of the transition moment with internuclear distance is known.[22,23] A simple expression linking the absorption oscillator band strength, f, to the transition probability, A, is

$$f/A = 1.51 \times 10^{-14}(g_2/g_1)\lambda^2 \qquad (1)$$

where g_2 and g_1 are the statistical factors for the upper and lower states, respectively, and λ is the transition wavelength in nanometers.

There is a great deal of literature on this topic for the Herzberg band transitions, and the general conclusion is that, at least for the $c-X$ and $A-X$ systems, the transition moment is fairly constant with interatomic separation.[22,23] From an earlier review,[24] we can use recommended oscillator strengths and calculated Franck−Condon factors to arrive at an average of 160 ms for the $A^3\Sigma_u^+$ state lifetime and 3.7 s for the $c^1\Sigma_u^-$ state, where the latter figure does not include the fact that a $c^1\Sigma_u^-$ state molecule has other radiative pathways. Arrays of transition probabilities for the $A-X$, $A'-X$, $A'-a$, and $c-X$ band systems have been presented,[25] but the values are typically too large, as discussed elsewhere.[24,26−28]

A radiative lifetime for the upper state of the Chamberlain transition, $A'^3\Delta_u(\Omega = 3)$, is not similarly available, because there are no absorption data for the $a \rightarrow A'$ transition. The lifetime may be shorter than that for the $c^1\Sigma_u^-$ state because the Chamberlain bands are substantially more intense than the Herzberg II bands in the (terrestrial) atmosphere, but there may be other factors causing that difference.

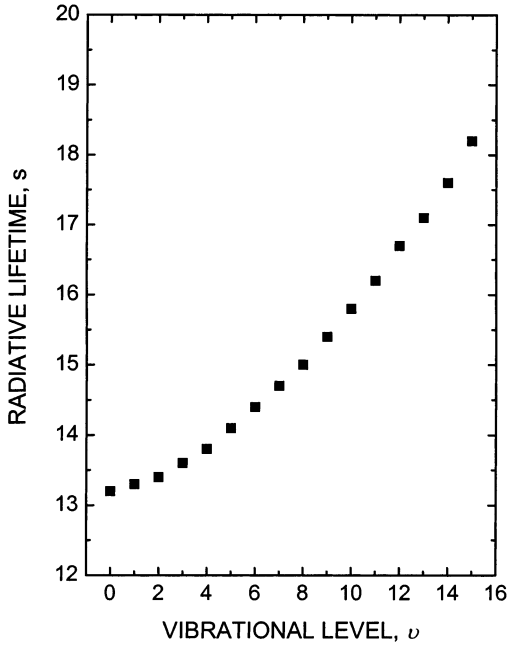

Figure 2. Calculation of the $b^1\Sigma_g^+(v)$ transition probabilities, based on the magnetic moment calculations of Minaev et al.[38] (P. C. Cosby, private communication, 2002). These are in effect the radiative lifetimes, the competing $O_2(b-a)$ radiative pathway being very weak.

Emission in the $a^1\Delta_g-X^3\Sigma_g^-$ Infrared Atmospheric system is of practical atmospheric interest, because it can be a surrogate for ozone under solar radiation.[29] Ozone dissociates in the 200−310-nm Hartley band to give a yield of $O_2(a^1\Delta_g)$ of 0.9,[4] and knowledge of radiative lifetimes, collisional removal rates, and solar flux can be used to retrieve ozone densities from satellite observations. The currently accepted radiative lifetime value is about 75 min.[30−33]

For the $b^1\Sigma_g^+$ state, there are accurate absorption cross sections for the $b-X$ 0−0, 1−0, and 2−0 bands,[33−37] from which Einstein coefficients can be deduced. Minaev et al.[38] have calculated the magnetic dipole transition moment as a function of internuclear distance, from which transition probabilities for $b^1\Sigma_g^+(v = 0-15)$ have been determined, as shown in Figure 2 (P. C. Cosby, private communication, 2002). These values are essentially equivalent to radiative lifetimes, as the $b^1\Sigma_g^+-a^1\Delta_g$ transition is much weaker than $b^1\Sigma_g^+-X^3\Sigma_g^-$.[39]

5. Photoabsorption and Photodissociation Products

O_2 absorbs radiation over a broad wavelength region. Dissociation commences at 242 nm, but absorption is still important at specific longer wavelength regions—cf. the Fraunhofer A-, B-, and γ-bands, which are, respectively, the 0−0, 1−0, and 2−0 bands of the $b^1\Sigma_g^+-X^3\Sigma_g^-$ Atmospheric band system, and the 0−0 band of the Infrared Atmospheric system, at 1.27 μ. The ultraviolet (UV) cross sections have been measured by many authors,[24,26−28,40−43] as have the $b-X$ cross sections[34−36,44−46] and the $a-X$ cross sections.[30,47]

We see that there are very distinct regions in the UV absorption. From 300 to 242 nm, there is nondissociative absorption in the Herzberg I, II, and III bands. At 242 nm the Herzberg continua start, continuing on to shorter wavelengths.[15,43,48] Although absorption cross sections associated with these continua are very small, the increasing density of O_2 with decreasing altitude makes Herzberg continua absorption an important atmospheric process, which is dominant over other O_2 photodissociation channels below 65 km.[4]

As wavelength decreases below 203 nm, absorption into the Schumann−Runge band system begins, with rapidly increasing cross section. However, the threshold for production of $O(^1D)$ is at 174 nm, and so only ground-state atoms are formed throughout the region of the Schumann−Runge bands, 174−203 nm, where predissociation yields are close to unity. There are no reports of atmospheric emission in the Schumann−Runge bands.

At 174 nm, the $O(^1D)$ limit is exceeded, and dissociation converts to the $O(^3P) + O(^1D)$ channel. Although the molecule still traverses the predissociation region, direct dissociation is now much more efficient than predissociation, and the $O(^1D)$ yield is unity for much of the Schumann−Runge continuum.[49] Nevertheless, there are repulsive states which go to the $O(^3P) + O(^3P)$, limit, and it is possible that, where they interact with the continuum of the $B^3\Sigma_u^-$ state, ground-state products will result.[50] At wavelengths shorter than 130 nm, the structure becomes more complex, and higher states become involved.[51−56]

Determinations of the products of O_2 photodissociation have been carried out down to 115 nm. Only two channels are significant—$O(^3P) + O(^3P)$ and $O(^3P) + O(^1D)$—even below the 133-nm threshold for generation of $O(^1S)$.[49,57]

6. Preparation of Excited O_2 States

There are four basic methods of preparing the excited states of O_2 under discussion.

First, there is direct photoexcitation, the limitations of which are the small absorption cross sections and the related Franck−Condon factors. As Figure 1 shows, the three lowest state potentials are nested, so in excitation from $X^3\Sigma_g^-(v = 0)$, the 0−0 bands in the $b-X$ and $a-X$ transitions are strongly favored, with Franck−Condon factors falling rapidly with increasing upper-state vibrational level.[58] In contrast, in photoexcitation to the three Herzberg states, it is the higher levels in the upper states that have the largest cross sections because of the displaced potentials, and the 0−0 bands are very weak. The dominant advantage of utilizing photoexcitation for state preparation is that there is then a known starting point and a one-component system.

Atom recombination is a second method of state generation, where the forbidden nature of the various transitions is not directly an issue. However, being a three-body process, it is very slow, and the loss processes in a flow system are far faster than production, particularly for vibrationally excited levels. Therefore, although there is a broad range of

Table 2. Threshold Wavelengths for Generating the Indicated O and O_2 States from Ozone in Spin-Allowed Photodissociation[a]

electronic state	$X^3\Sigma_g^-$	$a^1\Delta_g$	$b^1\Sigma_g^+$	$c^1\Sigma_u^-$	$A'^3\Delta_u$	$A^3\Sigma_u^+$
$O(^3P)$	1280				233.2	229.2
$O(^1D)$		310.0	266.9	175.4		
$O(^1S)$		199.3	180.5	133.5		

[a] Values in the table are in nanometers.

states and levels produced, it is not a good environment for understanding the system kinetics.

There is an extensive history of atom recombination measurements, a primary reason being the desire to simulate the atmospheric emissions in the laboratory,[40,59−64] Most of these experiments were carried out in pre-laser days, and they often raised more questions than they answered. Where attempts were made to extract rate coefficients for removal of the O_2 metastables, the derived values were typically much too small.[61,62] The complexity of the system was not fully appreciated, for we now see the interplay of the many vibrational levels of all the states. In general, the spectroscopy was not well known, and there were quite rough estimates of radiative lifetimes.

Nevertheless, it is still necessary to deal with atom recombination from the point of view of accurately defining the source term in the atmosphere.[65] The venerable value in current use for the three-body rate coefficient is now entering its fourth decade,[66] and it is hoped that there will be new measurements employing modern techniques.

A third method for O_2 state/level preparation in a prompt but nonspecific manner is by photoexcitation of the $A^3\Sigma_u^+$ state, followed by rapid collisional removal. For example, Kalogerakis et al.[67] have shown that $A^3\Sigma_u^+$ state photoexcitation followed by O_2 collisions populates high levels of the $a^1\Delta_g$ and $b^1\Sigma_g^+$ states. Thom et al.[68] have shown that the O_2 quintet state is generated in a similar manner. By following production and loss kinetics, it is possible in many cases to disentangle these processes and understand the energy flow. In a sense, such experiments are surrogates for atom recombination, where the slow three-body recombination is side-stepped.

Finally, ozone photodissociation is a fourth method by which O_2 excited states can be prepared. Because of the weakness of the $O-O_2$ bond, a range of states and levels can be generated at relatively low photon energies. In Table 2 we show the threshold for generating vibrational-level-specific O_2 states. Since the photoabsorption cross sections are large particularly below 310 nm,[4] the $O + O_2$ production rate can be large. As in O_2 photoexcitation, one has some control over the initial starting point for kinetic purposes, as the photon energy determines an upper limit to the state and level that can be produced.[69] Nevertheless, introducing another chemical component has disadvantages in that there are fast reactions, e.g., $O(^1D) + O_3$, which can present complications. There is, as yet, no evidence that ozone photodissociation produces the Herzberg states. What is known is that when the threshold for the fragmentation process to produce three oxygen atoms is reached (199 nm), that channel becomes significant, as has been noted for photodissociation at 193 and 157 nm.[70−72]

Photodissociation of ozone to produce electronically excited O_2 is both a convenient laboratory procedure and a profoundly important atmospheric process. Of greatest interest among the processes shown in Table 2 are the channels in which $O(^1D)$, $O(^3P)$, $O_2(a^1\Delta_g)$, and $O_2(b^1\Sigma_g^+)$ are formed. The strength of the $O-O_2$ bond is only 1 eV, so the molecule can be dissociated by visible light. The O_3 Chappuis band, peaking near 600 nm, is the first absorption leading to dissociation, with the production of only ground-state products. However, there is substantial excess energy, and Levene et al.[73] have shown that 560−638-nm radiation produces ground-state O_2 molecules in $v = 0-4$, the distribution monotonically decreasing with increasing vibrational level.

The next spin-allowed product channel is that to make $O(^1D) + O_2(a^1\Delta_g)$, with a threshold at 310 nm. However, the absorption cross sections of ozone starts to increase around 360 nm, in the Huggins band, and this is of great atmospheric significance because the solar flux is rising sharply with increasing wavelength in the 310−360 nm region. Thus, not only does the decreasing cross section in the Huggins band result in photoabsorption taking place deeper into the atmosphere, but there are more photons available. The Huggins band processes are multiple: there is absorption by vibrationally excited ozone, giving the $O(^1D) + O_2(a^1\Delta_g)$ products at $\lambda > 310$ nm, and there is also spin-forbidden dissociation, giving the channels $O(^3P) + O_2(a^1\Delta_g, b^1\Sigma_g^+)$ and $O(^1D) + O_2(X^3\Sigma_g^-)$.[74−80] That the Huggins band processes are potentially important has been under discussion for years, but it is only recently that a consensus on their importance has developed.[81]

The main O_3 absorption system is the Hartley band, extending from 200 to 310 nm, peaking at 255 nm and having a large cross section. Here the products are $O(^1D) + O_2(a^1\Delta_g)$, and photodissociation within the band is often used to generate each of these species. The Hartley band photoabsorption process is responsible for the fact that ozone offers protection to life on Earth from the effects of solar UV radiation in the wavelength region longward of 200 nm.

Although photodissociation of ozone in the Hartley band is dominated by the 90% yield of the $O(^1D) + O_2(a^1\Delta_g)$ channel, the 10% channel generates ground-state products with enormous internal energy in the O_2.[82−85] At the peak of the Hartley band, the dissociation must dispose of 90 kcal mol^{-1}. It has been shown[82] that 248-nm ozone photodissociation generates $X^3\Sigma_g^-(v)$ almost up to the thermodynamic limit of $v = 25$, confirming numerous earlier measurements dealing with this very energetic pathway.[86,87] There have been a variety of subsequent measurements[83,84,88−94] that define the O_2 vibrational distribution as a function of input photon energy. In contrast to the $X^3\Sigma_g^-(v)$ produced in the Chappuis band and the $a^1\Delta_g(v)$ produced in the Hartley band, the $X^3\Sigma_g^-(v)$ distribution in the Hartley band does not

peak at $v = 0$. For example, at 226 nm excitation, there is a peak at $v = 13-16$ and a second peak at $v = 26$.[88]

There have been few measurements of the products of ozone photodissociation below 200 nm, but this region is interesting because of the opening of new channels. Taherian and Slanger[70] established that a major pathway at 157 nm is the fragmentation of the ozone molecule into three ground-state oxygen atoms, the threshold for such a process being at 199 nm. In addition, the other major channel is the $O(^1D) + O_2(b^1\Sigma_g^+)$ pathway, where the $O_2(b^1\Sigma_g^+)$ product is generated with a broad vibrational distribution. Similar results were obtained by Turnipseed et al.[71] at 193 nm, with lower yields for the photofragmentation process.

7. Detection of Excited States

There are three techniques that have proven practical in detection of populations of excited states of O_2. Historically, fluorescence is the oldest of these, being used extensively to make measurements in flowing afterglows. In such a system, the excited levels are produced as they are in the atmosphere, by three-body atom recombination following O_2 dissociation, typically by a microwave discharge. In this manner, all the excited O_2 states below the first dissociation limit can be generated, although the $^5\Pi_g$ state has not been detected by fluorescence; its emission would be in the far IR. There is considerable literature on the production of the Herzberg states, although predominantly of the $A^3\Sigma_g^+$ state, the Herzberg I source.[60-64,95-97]

Excellent O_2 afterglow spectra of the near UV[60] were published at a time when the identifications of the bands were still evolving. Unidentified bands were noted, and connections were made to bands at the same wavelengths in nightglow spectra published by Chamberlain.[98] These bands were the strongest of those in the Chamberlain system and correspond to lower state ($a^1\Delta_g$) levels of $v = 2, 3$. Subsequently, an afterglow spectrum published by Degen again considered these as unknown bands.[95] Later, the bands were definitively identified, and a full analysis of the high-resolution spectrum of the 4−3 band published by Degen was carried out.[99] Always confusing the issue was that in the work of Herzberg,[100] in which the $A'^3\Delta_u - X^3\Sigma_g^-$ system was identified in absorption, only sub-bands corresponding to the $A'^3\Delta_u(\Omega = 1,2)$ spin sublevels were detected, whereas emission in the $A'^3\Delta_u - a^1\Delta_g$ system strongly favors the $\Omega = 3$ level. It should be noted that the $A'^3\Delta_u$ state was earlier known as the $C^3\Delta_u$ state.

The Herzberg II emitter, the $c^1\Sigma_u^-$ state, was not identified in emission until 1968,[95] at which time it was pointed out that the original vibrational numbering of the $c^1\Sigma_u^-$ state was in error by five units.[100] The same spectral data set was further analyzed and found to contain a variety of upper-state vibrationally excited levels for all three transitions: Herzberg I, Herzberg II, and Chamberlain.[101]

Much of the early work on the Herzberg states was spectroscopic in nature, but attempts were made by Young and Sharpless[61] and Young and Black[62] to deduce removal rate coefficients in an atmospheric environment (i.e., in O_2, N_2, and $O(^3P)$), to elucidate the processes taking place in the upper atmosphere; this work was not limited to the Herzberg states (only the $A^3\Sigma_u^+$ state was considered) but also included the $b^1\Sigma_g^+$ state and the atomic oxygen green line. The interest was in understanding the relationship between the atomic oxygen density and the green line intensity, so that the latter could be used to remotely measure the mesospheric atom density. This quest has not yet been completed.

The measurements made by Young and co-workers were handicapped by the lack of knowledge of the radiative properties of the emitters, that is, the radiative lifetimes, and also by the complexity of the system. It is now reasonably well established that none of the observed O_2 emissions are part of a nascent distribution, and that the low-lying vibrational levels of the excited states all have higher precursors. Thus, a steady-state system such as an afterglow provides misleading kinetic results: a change in a component affects both the emitter under consideration and its precursor(s) as well.

Afterglow kinetics measurements were further pursued in the work of Ogryzlo and co-workers,[97,102-105] with detailed measurements being reported for both the $A^3\Sigma_u^+$ and $c^1\Sigma_u^-$ states. These measurements, limited to low vibrational levels, have not yet been repeated by other methods (REMPI measurements described below are for higher vibrational levels and have not yet been extended to lower levels), yet it appears likely that the measured rate coefficients of O_2, N_2, and $O(^3P)$ as quenchers will be found to be underestimated for the $A^3\Sigma_u^+$ state, based on what is now known of the higher levels and the influence of cascade processes.

The technique of laser-induced fluorescence (LIF) is quite effective in the study of vibrationally excited levels of the O_2 ground state,[84,89,91,106,107] as advantage can be taken of the first optically allowed transition, the Schumann−Runge $B^3\Sigma_u^- - X^3\Sigma_g^-$ system. As used here, we reserve the use of "LIF" to those processes where O_2 is excited by the laser; photodissociation of ozone can also result in O_2 emission but does not involve resonance with an O_2 transition.

As the $B-X$ transition is optically allowed, its use for monitoring $X^3\Sigma_g^-(v)$ predates that of laser availability. There are numerous examples where this band system has been used in both emission and absorption, and both types of measurements are strongly influenced by predissociation in the upper state, which affects all vibrational levels.[106,108-112] Those levels near the dissociation limit are the least affected, while the $B^3\Sigma_u^-(v = 4)$ level shows line widths in excess of 4 cm^{-1}. As a result, although the transition is strong, radiative efficiencies are low, never exceeding 1%.[82,106,113] There is now considerable information on collisional removal of ground-state vibrational levels by O_2 and N_2, spanning the $v = 1-30$ range.[82,84,89,114,115] Furthermore, calculations[12,13] have been carried out for an extensive range of vibrational levels with O_2 collider, and agreement with experiment is found to be good.

The most recently developed technique for monitoring excited states and levels in O_2 is that of REMPI. Initial measurements were carried out in afterglow systems,[116,117] but in such an environment there is rapid relaxation of vibrational levels, so most observed transitions involved the $v = 0$ level of the state being sampled. Numerous series of bands were found, corresponding to a variety of Rydberg states and levels in the upper O_2 states excited by two-photon resonances. All of the O_2 states lying below the first dissociation limit, including the $^5\Pi_g$ state, have optically allowed pathways via one- or two-photon absorption to Rydberg, valence, or ion-pair states,[67,68,118,119] and thus the dominant restriction is the FCF between the initial excited state and the intermediate state to ionization.

8. The Oxygen Nightglow

There are three basic classes of atmospheric emission: dayglow, nightglow, and aurora. Of these, there are considerable similarities between dayglow and aurora, but nightglow emissions are quite different. Although the nightglow constituents are of course present at all times, they are weaker than the dayglow and auroral emissions. The latter processes typically originate with direct photoexcitation, excitation by fast electrons, or ion recombination, and are generally seen at higher altitudes than the ~95 km oxygen nightglow.

The realization that the night atmosphere is luminous originated about a century ago.[120] Aurora were well known, if not understood, and dayglow emissions were not possible to observe until rockets became available. The basic observation from which the existence of the nightglow was deduced was that, on nights when the nightglow is particularly strong, the intensity increases still further when scanning from the zenith to the horizon, as the path length through the atmosphere increases.

The first spectral feature to be identified was the 557.7-nm atomic oxygen green line, but for many years it was not realized that this was a permanent feature in the nightglow, and not of auroral origin. The correct identification of the transition came somewhat later from laboratory studies, and Chapman[121] then proposed that the source in the atmosphere was recombination of oxygen atoms, with oxygen atoms also acting as the third body and carrying away the recombination energy in electronic excitation.

An alternative to this idea was put forward by Barth and Hildebrandt,[122] where the process was split into two reactions, the first utilizing O_2 as the third body, and the resulting activated O_2^* transferring its energy (at least 4.17 eV) to an oxygen atom. The electronic state of the O_2^* molecule has been a matter of dispute for years, with the $c^1\Sigma_u^-$ state being the most favored precursor.[7] However, the question has not yet been settled. It is an intriguing fact that the source of the green line emission associated with the O-atom recombination region, observed for more than 100 years, is still debated.

Identification of the molecular O_2 emissions proceeded more slowly. It was not until the 1950s that it was proposed that the UV emissions were due to the Herzberg I $A^3\Sigma_u^+ - X^3\Sigma_g^-$ bands, identified 20 years earlier in absorption.[123] The $A'^3\Delta_u$ and $c^1\Sigma_u^-$ states were also first seen in absorption by Herzberg,[100] and soon thereafter Chamberlain[98] concluded that certain near-UV nightglow emission bands did not belong to the Herzberg I system and appeared to be due to the $A'^3\Delta_u - a^1\Delta_g$ system, which now bears his name.

Two bands of the Herzberg II emission ($c^1\Sigma_u^- - X^3\Sigma_g^-$) were identified in the laboratory spectrum published by Degen,[95] but in the nightglow the first identification was not in the terrestrial atmosphere but at Venus.[124] In the nightglow of that planet, $c-X$ emission is far stronger than the combined UV and visible O_2 emission in the terrestrial nightglow and originates from only the $v = 0$ level of the $c^1\Sigma_u^-$ state. On Earth, weak Herzberg II emission was subsequently identified,[125] but with an intensity too low for meaningful measurements to be made. As discussed below, it seems that the alternative $c^1\Sigma_u^- - b^1\Sigma_g^+$ system will be more useful for $c^1\Sigma_u^-$ state studies.

The origin of the O_2 nightglow is oxygen atom recombination under almost all circumstances, where the atoms are created in the daytime by solar photodissociation of O_2. Photoabsorption occurs from the far UV down to the first photodissociation limit, at 242 nm, with a generally decreasing cross section with increasing wavelength. Thus, the shorter wavelength radiation is deposited higher in the atmosphere, while beyond 200 nm absorption is mainly in the stratosphere. An exception to this statement is the intense solar Lyman-alpha feature at 121.6 nm, which occurs at a deep minimum in the O_2 photoabsorption spectrum and thus penetrates well into the mesosphere.[51] The various O_2 spectral features are segregated as they penetrate the atmosphere. Above 90 km, the Schumann−Runge continuum accounts for most of the absorption. The Schumann−Runge bands are then the dominant absorption feature down to 65 km, and below this altitude it is the Herzberg continuum.[126]

The oxygen nightglow is generated by the process

$$O(^3P) + O(^3P) + M \rightarrow O_2^* + M \qquad (2)$$

where M is O_2/N_2, although it is, in principle, possible for M to be a third oxygen atom, as originally proposed by Chapman to explain $O(^1S-{}^1D)$ 557.7 nm emission. O_2^* represents any of the seven states lying below the first dissociation limit, and it has been argued by Bates and others that the population distribution between these states can best be estimated statistically, in which case the $^5\Pi_g$ state should be generated in about 40% of all collisions.[65,127,128]

However, being able to see a true nascent distribution following stabilization of the O_2^* entity is improbable, because in a real system the molecules suffer many collisions before being detected. Current laboratory experiments demonstrate that molecules in a given state do not necessarily remain in that state but experience population redistribution. The

question of the nascent distribution is therefore not closely linked to actual observations. In any case, the $^5\Pi_g$ state has not yet been seen in the nightglow because it could only be observed in the far infrared well beyond 10 μm, a consequence of its large interatomic spacing, leading to small Franck−Condon factors for shorter wavelength transitions. Observational knowledge on this state comes entirely from laboratory REMPI measurements, as described below.

The O_2 nightglow is mainly represented by four band systems, with a fifth having recently come into prominence. These are, in order of increasing wavelength, the Herzberg I system ($A^3\Sigma_u^+ - X^3\Sigma_g^-$), the Chamberlain system ($A'^3\Delta_u - a^1\Delta_g$), the new $c^1\Sigma_u^- - b^1\Sigma_g^+$ system, the Atmospheric system ($b^1\Sigma_g^+ - X^3\Sigma_g^-$), and the Infrared Atmospheric system ($a^1\Delta_g - X^3\Sigma_g^-$). Band systems which are more difficult to observe include Herzberg II ($c^1\Sigma_u^- - X^3\Sigma_g^-$), Herzberg III ($A'^3\Delta_u - X^3\Sigma_g^-$), and $c^1\Sigma_u^- - a^1\Delta_g$. There is also evidence for the $B^3\Sigma_u^- - b^1\Sigma_g^+$ system, where the data relate to the continuum of the upper state.[129,130]

9. Excited Oxygen in Other Atmospheres

Somewhat surprisingly, there is only limited information on O_2 emissions in other atmospheres in our solar system. In fact, observations are limited mainly to Venus, with only $O_2(a-X)$ 0−0 band dayglow emission reported from Mars.[131,132]

As noted above, the $c^1\Sigma_u^- - X^3\Sigma_g^-$ Herzberg II bands are minor emitters in the terrestrial atmosphere. It was thus a great surprise, and an initial cause for confusion, to find that these bands are the dominant emission in the visible spectral region on Venus, and that their intensity is an order of magnitude greater than the terrestrial Herzberg emissions. They were first seen from the Venera 9/10 probes[124] and initially attributed to CO fourth positive emission.[133] Subsequently, a new CO_2 band system was proposed, but eventually Lawrence et al.[134] showed that it was the $v' = 0$ progression of the Herzberg II system. The critical experiment was to show that a conventional O_2 afterglow spectrum, dominated by Herzberg I emission, was converted to the Herzberg II progression upon addition of CO_2, thus mimicking the Venus atmosphere. These results were duplicated,[135] and the appearance of the Chamberlain bands in the laboratory spectrum then led directly to identifying the Chamberlain $v' = 0$ progression as an additional feature in the Venera spectra.[136]

The next observation of the Venus visible emission was from the Pioneer Venus Orbiter[137] when unresolved visible emission was measured with the star tracker. One of the conclusions from this unplanned experiment was that the visible emission is relatively stable in intensity, the average value being within a factor of 2 of that measured by the Venera spacecraft. This is no small point, because other emissions vary drastically. Crisp et al.[138] have seen from ground-based measurements that the 1.27 μm $a-X$ emission is quite variable across the disk of the planet, and that there are times when it is not discernible. These differences amount to a 2 orders of magnitude variation in intensity, and it is difficult to understand why the other O_2 band system seems not to behave in a similar manner. The situation is exacerbated by the recent measurement of the atomic oxygen green line on Venus, with an intensity similar to the ∼150 Rayleigh terrestrial intensity,[139] whereas it was not detected on the Venera 9/10 missions.[140] The questions raised by these studies must be at the forefront of subsequent atmospheric investigations, as emission is a window on atmospheric dynamics.

10. Nightglow Observations

Ground-based and space-based measurements each have their strengths and weaknesses. Larger and more precise instruments can be used from the ground, but they sample only a limited region of space and do not directly measure the altitude of the emission. Furthermore, they are limited in wavelength capability. At the blue end of the spectrum is the ozone cutoff at 310 nm, and at the red end, beyond 1 μm, is atmospheric absorption due to water, CO_2, and various trace species. From space, wavelength accessibility is limited only by the detector response.

There are basically three molecular oxygen features that have been studied in the nightglow prior to the recognition of the wealth of spectral information available in astronomical sky spectra: the Herzberg I bands, the 0−0 and 0−1 Atmospheric bands, and to a much more limited extent, the 0−0 IR Atmospheric band. There is relatively little work that has been done on O_2 emissions in aurora, primarily because N_2, N_2^+, and O-atom emissions are the dominant features. However, it is evident that increased concentrations of $O(^1D)$ in aurora result in greatly enhanced $b^1\Sigma_g^+(v = 0)$ emission rates.[141]

10.1. Ground-Based and Flight-Based Nightglow Measurements

The first high-quality spectrum of the UV nightglow was produced by Chamberlain,[98,142] showing partially resolved lines of the Herzberg I bands down to the ozone cutoff, and the additional spectral features now known as the Chamberlain bands. In medium-resolution spectra, the structures of the two band systems make it easier to recognize the rotational development of the Herzberg I bands than the denser Chamberlain bands.

Broadfoot and Kendall[143] produced a nightglow spectrum at 0.5 nm resolution over a very broad spectral region, from the ozone cutoff to 1000 nm. This has been an aeronomical standard for many years and is particularly useful at the short wavelength end to identify the Herzberg I and Chamberlain bands and in the longer wavelength regions to identify the OH Meinel band lines.

A key issue in nightglow observations since their detailed study began has been to deduce the oxygen atom density in the mesosphere/lower thermosphere without measuring it directly. It seemed that if one knew the atom recombination rate, the yield for making the emitting state in that process, the emitter intensity, its radiative lifetime, and its collisional

removal rate, that would be sufficient to retrieve the O-atom density. In particular, if it were possible to calibrate the most intense emission, the 557.7-nm atomic oxygen green line, in terms of a corresponding O-atom density, then the problem would be solved.

This has proven to be somewhat of a will-o'-the-wisp. If the original Chapman mechanism to produce the green line had been valid, then it would have been possible to extract the O-atom density, but the introduction of the transfer of energy from an activated O_2^* molecule as an intermediate step requires the identification and characterization of that entity, or of the multiple O_2^* species that might be responsible, which have energies between the 4.2 eV energy of $O(^1S)$ and the 5.1 eV O_2 dissociation limit.

Although much progress has been made in recent years on the O_2^* states in that energy range,[144−147] there is substantial difficulty in studying their interactions with $O(^3P)$ as the collider. This is because most of these levels/states are rapidly removed by the parent gases, cf. O_2 or O_3, so it is hard to isolate the effects of the atoms.

At present, the assumption is that the $c^1\Sigma_u^-$ state, with $v \geq 2$, is the transfer agent. This argument is not persuasive, since it is based on analysis of the Herzberg I bands and the demonstration that $O_2(A^3\Sigma_u^+)$ is apparently not the appropriate O_2^*.[148] It is then assumed that the Chamberlain bands are kinetically similar to the Herzberg I bands, which by elimination leaves the $c^1\Sigma_u^-$ state. The $c^1\Sigma_u^-$ state, in the Herzberg II system, cannot be studied from rockets or satellites because its emission is weak and it is not normally resolvable from the Herzberg I bands. With the recent identification of the $O_2(c-b)$ bands in the near-UV nightglow,[17] it is possible to test the relationship between these emissions and the green line,[149] although we cannot be sanguine that the goal of extracting the O-atom density from the nightglow will then be attainable.

There is, in fact, a new complication created by the advances made in both nightglow observations and laboratory measurements. We now realize that the atmosphere contains broad distributions of the vibrational levels of the lower O_2 states. Astronomical sky spectra have established that the $b^1\Sigma_g^+$ state is seen up to $v = 15$,[150] while laboratory studies of the Herzberg states have shown that, following O_2 collisions, these states evolve to very high vibrational levels of both the $b^1\Sigma_g^+$ and $a^1\Delta_g$ states, with the highest levels equaling $v = 15$ and 19, respectively.[67] It is likely that the ground state may be similarly populated. Thus, the energy necessary to excite $O(^3P)$ to $O(^1S)$ upon O_2^* collisions is available in a variety of guises. A point that should be borne in mind is that the green line represents a small fraction of the total recombination rate, less than 1% (collisional quenching is not important). Being a minor process, the disentangling of the particular channel(s) producing $O(^1S)$ is a considerable challenge. A further difficulty arises from the fact that it is now clear that the $O_2(^5\Pi_g)$ state is stable, with a $v = 0$ energy near 5.0 eV.[151] Although emission from this state is not seen, it is a product of O-atom recombination and is therefore another candidate for the O_2^* that makes $O(^1S)$.[151,152]

It has recently been found that the oxygen green line is also an emitter in the atmosphere of Venus.[139] This is an intriguing discovery, because the principal O_2 emitter there is the $c^1\Sigma_u^-(v = 0)$ level, which has insufficient energy to generate $O(^1S)$ upon O-atom collisions. However, the necessary efficiency of $O(^1S)$ production from O-atom recombination is also very low at Venus, so various pathways are possible.

Much of the work in recent years on the nightglow emissions viewed from the ground has to do with atmospheric motion and winds. Since the various emissions—OH, Na, $O_2(b^1\Sigma_g^+)$, and $O(^1S)$—lie at somewhat different altitudes, studies of the intensity phase lag between such emissions provide information on the passage of gravity waves propagating downward or upward in the atmosphere. Each of these emissions also contains information on temperature—the molecules by their rotational distributions, and the atoms by their emission line widths.

There are many ground-based observations of atmospheric oxygen features, carried out with instruments that sample a more limited spectral region than in the survey of Broadfoot and Kendall.[143] In the UV region, studies have been carried out by Stegman and Murtagh[153,154] and by Stegman[155] on the vibrational distributions of the Herzberg states and on the correlations between different oxygen features, cf. the Herzberg I and II bands, the Chamberlain bands, and the atomic green line. Emphasis was placed on two spectral regions, 320−330 and 341−353 nm, which were measured and modeled over a range of intensity conditions. The Herzberg III bands were also included in the model, but their presence is difficult to confirm. The same is true for the much higher resolution sky spectra described below.

Examples of coordinated measurements are the ALOHA-90 and ALOHA-93 campaigns, in which both ground-based and flight-based measurements were made. A variety of observations of oxygen emission features were carried out, primarily of the 864.5-nm 0−1 O_2 Atmospheric band and the atomic green line. Gravity waves involving these emissions were observed[156−158] and correlated with emissions of other features, cf. sodium and OH.

Ground-based studies of O and O_2 emissions have been made over a great number of years. Many of these are reviewed by Meriwether[1] and by Solomon,[2] and much valuable information continues to come out of such investigations.[159−163] The demonstration of the utility of astronomical sky spectra enhances studies of this nature.[164]

10.2. Rocket Measurements

To clarify many questions about nightglow observations, it is essential to have altitude information, which is not typically available from ground-based studies. Measurements from rockets as they penetrate the airglow layer provide the additional dimension. The "Energy Transfer in the Oxygen Nightglow" (ETON) campaign of 1986 was particularly useful in this respect, in that a variety of emissions

were measured over a relatively short period of time.[20,148,165,166] As the atmosphere is dynamic, an emitting layer can vary substantially in altitude in a short period. A unique feature of this study was the direct measurement of the O-atom density by a resonance fluorescence technique.

The first paper in the series[20] presents an extensive set of altitude profiles, measured with multiple rockets. These include the O_2 Herzberg I and Chamberlain systems in the UV, the O_2 0−0 Atmospheric band and the O_2 0−0 IR Atmospheric band in the IR, the atomic oxygen green line, and atomic oxygen as well as OH and the nightglow continuum (believed to be due to the reaction between $O(^3P)$ and NO).

The second paper[148] attempts to deduce the mechanism for formation of $O_2(b^1\Sigma_g^+)$ and $O(^1S)$ in the atmosphere, from the perspective that they are not directly formed in the three-body O-atom recombination step. Efficiencies of energy transfer and quenching ratios involving the presumed precursors are deduced.

In the third paper of the series,[165] the nightglow continuum is investigated, and comparisons are made to the measured atomic oxygen profiles, since in principle the continuum, if it is due to O + NO, can provide information on atmospheric NO. An interesting result is that one of the wavelengths chosen for the continuum measurements, 714 nm, is coincident with what we now know to be the relatively strong O_2 4−3 Atmospheric band.[150] It was deduced from the excess emission that there must be an additional emitter, and the idea was correctly put forth that it might be the 4−3 band.

The fourth paper in the series[166] deals with atmospheric Herzberg I emission, where optical filters are chosen to sample both high and low $O_2(A^3\Sigma_u^+)$ vibrational levels. Little difference is seen in their altitude profiles, suggesting that their O_2/N_2 removal rate coefficients are not very different for high and low v. It is also concluded that, where there is overlap with the laboratory measurements in terms of the vibrational levels sampled,[97,102,104] the laboratory collisional removal values are much too small. The laboratory values obtained since that time are much larger, for O_2 and particularly for N_2,[145−147,167] and are also substantially larger than the values deduced from the ETON measurements. The question of possible removal of the $A^3\Sigma_u^+$ levels by O-atoms is discussed, but the magnitude of the new O_2 and N_2 rate coefficients makes this unlikely for high vibrational levels.

There is a substantial body of information obtained from rocket flights covering a variety of different aspects of atomic and molecular oxygen emission, including observations of these emissions in aurora.[168−179]

In addition to observing emissions from oxygen species, rocket and satellite missions provide the opportunity to sample the neutral atmosphere by viewing UV emissions through different thicknesses of absorbing gas. This type of experiment can also be done by solar and stellar occultation. An example is the work of Dymond et al.,[180] where O^+, $O(^3P)$, and O_2 densities were measured from a sounding rocket.

10.3. Satellite Measurements

Measurements from satellites are associated with missions, cf. ATLAS,[181] UARS,[182] MSX,[183] and GLO studies from the space shuttle.[141] With the launch of the TIMED mission in 2001, these studies are continuing, and measurements are being made for a variety of reasons on the usual target emissions: the atomic oxygen red and green lines, the O_2 0−0 Atmospheric band, and the O_2 0−0 IR Atmospheric band, as well as the many other emissions of species in the UV and the IR. There are studies of atmospheric tides, gravity waves, winds, temperatures, and the coupling of energy through different parts of the atmosphere.

The highest resolution with which the UV Herzberg bands have been studied from space is 0.2 nm on the ATLAS/ISO mission.[181] Although these data have some problem with the assigned altitudes, the spectra themselves can be evaluated in terms of the relative intensity of the Herzberg I and II emissions. The authors have done this for the 275−300 nm region, where the Herzberg II emission is the most intense, and concluded that the HzI/HzII ratio in that region is greater than 6.

The S3-4 military satellite observed the Herzberg band emission with 0.6 nm resolution, and simulations of the emission were carried out for the Herzberg I, II, and III bands over the 250−290 nm range.[184] In this region, where all three of the band systems are strongest, the conclusion was reached that the intensity ratio between them was 4.5:1.0:0.7, respectively. We have confirmed (R. W. Eastes, private communication, 2003) that the above ratio is correct, rather than the ratio quoted in the original paper. A further analysis of the ATLAS/ISO data was attempted,[185] and the best fit indicated a ratio of 10−15 for the Herzberg I/II and I/III ratios. An estimate was also made of the HzI/HzII ratio from rocket data,[176] a ratio of 7 being found. It is evident that this uncertainty is due to the weakness of the Herzberg II band system, and it is hoped that the recognition of the presence of the $O_2(c-b)$ band system in the nightglow[17] will simplify $c^1\Sigma_u^-$ state studies.

11. $O_2(a^1\Delta_g–X^3\Sigma_g^-, b^1\Sigma_g^+–X^3\Sigma_g^-)$ Dayglow Measurements

As a consequence of the accuracy with which the yield of the $O(^1D) + O_2(a^1\Delta_g)$ channel in the Hartley band is known, the intensity of the 1.27 μm emission in the dayglow may, in principle, be used to infer the ozone density.[29,186−188] To do so requires knowledge of the radiative lifetime of the state, the quenching parameters, the solar flux in the Hartley band and its modification with solar zenith angle, and information concerning other possible sources of the $O_2(a^1\Delta_g)$ state. Being of necessity a space-based observation, it is also required that the appropriate observational inversion techniques be correctly applied. The radiative lifetime of $a^1\Delta_g(v = 0)$ has been a matter of some controversy[189,190] but now appears to have settled at a value near 75 min,[30−33,47] which is 17% longer than the much earlier value reported by Badger et al.[189]

This new radiative lifetime is consistent with that obtained from microwave observations by Sandor et al.[191]

The $O_2(a^1\Delta_g)$ state is quenched very inefficiently by all species in the upper atmosphere,[4] but that fact is offset by its long radiative lifetime. O_2 itself is the only significant quencher, with a 300 K removal rate coefficient of 1.7×10^{-18} cm^3 s^{-1}.[4] The density at which quenching and the radiative rate are equal is then $[O_2] = 2 \times 10^{14}$ cm^{-3}, which corresponds to an altitude of 75 km. Below about 85 km, it is necessary that the observed $O_2(a^1\Delta_g)$ emission intensity be corrected for the effect of O_2 quenching.[29]

The $O_2(b^1\Sigma_g^+)$ state is also generated in the dayglow, but by different mechanisms. The $b-X$ transition is much stronger than the $a-X$ transition, by a factor of 300 in terms of radiative lifetimes. As a result, the $b-X$ transition is induced by solar radiation, and of the several atmospheric $b^1\Sigma_g^+$ dayglow sources, this is the dominant one between 65 and 100 km.[29,188,192] A zenith intensity of 300 kilorayleighs has been measured, with a maximum in the 50−65 km range.[193,194] Another manifestation of $b-X$ absorption is the Fraunhofer A-band, where solar radiation at the wavelengths of the $b-X$ 0−0 band rotational lines is absorbed lower in the atmosphere.[195]

Although there is no known channel within the Hartley band giving $O(^1D) + O_2(b^1\Sigma_g^+)$ products, the $O(^1D)$ that accompanies $O_2(a^1\Delta_g)$ production is efficiently converted to $O_2(b^1\Sigma_g^+)$ in the energy-transfer reaction

$$O(^1D) + O_2 \rightarrow O(^3P) + O_2(b^1\Sigma_g^+, v = 0, 1) \quad (3)$$

It is believed that the yield for this reaction is close to unity,[196] although the overall atmospheric yield is about 35%, because N_2 is an efficient quencher of $O(^1D)$.[4] Again, the altitude of emission is limited by quenching, but for $O_2(b^1\Sigma_g^+)$ in the $v = 0$ level, the relevant quencher is N_2, not O_2. It is important to note that the product of quenching $O_2(b^1\Sigma_g^+, v = 0)$ by most colliders is $O_2(a^1\Delta_g)$,[197] so that when making an inventory of $O_2(a^1\Delta_g)$ dayglow sources, this additional source from Hartley band ozone photodissociation must be included. As we discuss below, $O_2(b^1\Sigma_g^+)$ is also produced higher in the atmosphere by reaction 3, where the $O(^1D)$ source is not ozone photodissociation but O_2^+ dissociative recombination.

12. Large Telescopes and Sky Spectra

A recent addition to the arsenal of instruments in use to investigate the terrestrial nightglow is the array of major telescopes throughout the world. So-called "sky spectra" are providing a new dimension in the study of nightglow phenomena, particularly in the area of O_2 spectroscopy, but also in other areas.

A sky spectrum is the correction that astronomers need when carrying out spectral analysis of a stellar object. It is the sum of all extraneous emissions, a large component of which is the terrestrial nightglow. The sky spectrum is obtained from a long-slit observation, where the object is centered in the slit, while above and below is blank sky. The sky spectrum is then digitally subtracted from the stellar spectrum and either archived or discarded.

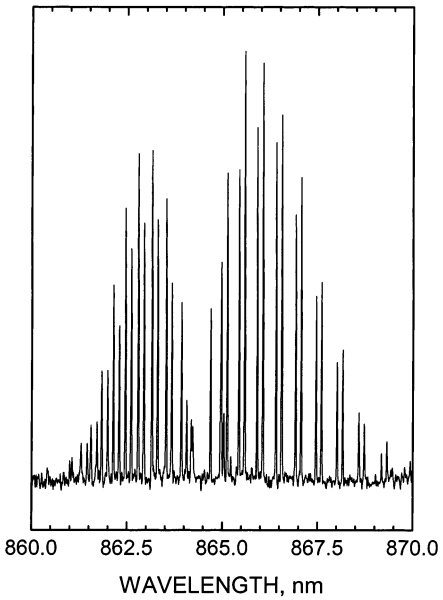

Figure 3. Nightglow sky spectrum of the $O_2(b-X)$ 0−1 band recorded by Keck I/HIRES; 50-min data collection.

Telescopes with large echelle spectrometers and CCD detection generate high-resolution data, with broad spectral coverage and high sensitivity. As an example, the HIRES echelle spectrometer on the Keck I telescope in Hawaii is typically operated at a resolution of 40 000, with a spectral range of 200 nm. The quality of the spectra obtained by HIRES is shown in Figure 3, the $O_2(b-X)$ 0−1 band, a frequent target of aeronomical investigations.

As such spectra are obtained during the course of an astronomer's observations, they are not subject to the whims of aeronomers. Data collection is typically carried out for a period of 50 min, so temporal fluctuations in the nightglow on a much shorter scale cannot be followed. The telescope moves across the sky at the appropriate rate to track a given object, and astronomers view 4−6 objects in the course of a night, often in different portions of the sky. Still, it is not necessarily true that such a protocol is undesirable for aeronomical studies, since even with a fixed viewing direction the atmosphere is dynamic.

13. O_2 Systems in Sky Spectra

The four emission systems that are readily discernible in sky spectra—Herzberg I ($A-X$), Chamberlain ($A'-a$), Atmospheric ($b-X$), and the new $c-b$ system—will be discussed in turn. Of particular importance is that large ranges of vibrational levels in the upper and lower states are available in each case, and so we are able to carry out highly redundant determinations of spectroscopic constants for the $X^3\Sigma_g^-$, $a^1\Delta_g$, and $b^1\Sigma_g^+$ states. As a result, great improvements can be made in determining their potentials. We are satisfied with the quality of the existing data for the upper states—$A^3\Sigma_u^+$, $A'^3\Delta_u$, and $c^1\Sigma_u^-$—and therefore in the analyses these are taken as invariant and are based on the absorption data

reported by Jenouvrier,[43] Ramsay and co-workers,[198−200] and Yoshino and co-workers.[26−28]

13.1. Herzberg I Bands

Herzberg band emission extends to the dissociation limit of 242 nm, but as viewed from the ground, the limit of detectability is determined by the ozone cutoff, approximately 315 nm. Although the bands become stronger to shorter wavelength, with the Keck/HIRES instrument, sensitivity measurements can be made in the 400−600 nm region, where there have been no previous observations, but where emission is observed from bands that terminate on high ground-state vibrational levels.

Figure 4 shows an example of a Herzberg I band region. Figure 4a contains the $A-X$ 3−10 and 5−11 bands, which are simulated in Figure 4b at 200 K, using the DIATOM spectral simulation program.[201] In the simulation, the [5−11]/[3−10] ratio is 60:40. We are unaware of any published nightglow spectrum of the Herzberg I system exhibiting the equivalent spectral resolution. Since it is spectral quality that is desirable, the spectrum is a co-addition of 20 h of observation. Unless spectral calibration is very accurate, co-addition may broaden the spectral lines, but we have never detected any such problem. The calibration source for all the HIRES spectra is a thorium/argon lamp. The sky spectra have been tested for the quality of calibration against NIST-based atomic line positions for lines appearing in the nightglow, cf. O I, K I, Na I, Hg I, and H I, and typical deviations are 0.0003 nm.[202]

In Table 3 is shown a matrix of bands that have been rotationally analyzed from Keck spectra in the Herzberg I system. It is extensive and contains many duplication of upper and lower vibrational levels. It is therefore possible to fit the data set simultaneously in order to make improvements in the spectroscopy of the O_2 ground state. Moreover, the data can be supplemented by the Keck measurements on another ground-state transition, the $b^1\Sigma_g^+-X^3\Sigma_g^-$ Atmospheric band system. Between the two transitions, there are 70 accurately measured bands involving the ground state. In combination with the extensive high-resolution absorption measurements of the $A-X(v = 0)$ transitions by Jenouvrier et al.[43] and the precise constants for $X^3\Sigma_g^-(v = 0-3)$ derived by Rouillé et al.,[203] the present measurements provide, for the first time, an accurate determination of the O_2 ground-state level energies over the full range of $v = 0-14$ with a precision better than 0.02 cm^{-1}.

Table 3. Herzberg I Bands Rotationally Analyzed in the Keck Spectra[a]

$X^3\Sigma_g^-$ state (v'')	$A^3\Sigma_u^+$ state (v')								
	0	**1**	**2**	**3**	**4**	**5**	**6**	**7**	**8**
4	−	−	×	×	×	−	−	−	−
5	−	×	×	×	×	−	−	−	−
6	−	×	×	×	−	−	×	×	−
7	×	×	×	−	−	×	×	×	−
8	×	×	−	−	×	×	−	−	−
9	×	−	−	×	×	−	−	×	−
10	×	−	×	−	−	−	×	×	−
11	×	−	×	−	−	×	×	−	−
12	−	−	−	−	×	×	×	−	×
13	−	−	−	×	−	−	×	×	−
14	−	−	−	−	−	×	−	−	−

[a] Transitions marked with symbol × are observed.

13.2. Chamberlain System

The Chamberlain band system is seen in the atmosphere in high resolution for the first time in the Keck sky spectra. Previously, the clearest Chamberlain band nightglow spectrum was the discovery spectrum.[98] In Figure 5 we present a co-added spectrum for the 6−2 band, and DIATOM simula-

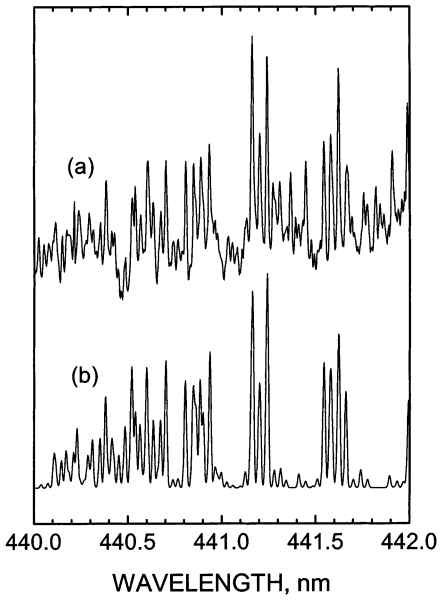

Figure 4. Keck I/HIRES sky spectrum of Herzberg I bands (a) and DIATOM simulation (b). The simulation consists of 60% $A-X$ 5−11 and 40% $A-X$ 3−10. The Chamberlain 7−6 band commences at 441.3 nm. The spectra were accumulated for 10 h.

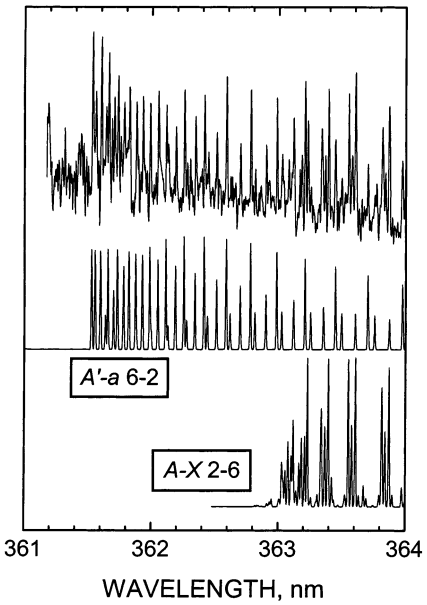

Figure 5. Keck I/HIRES sky spectrum of the Chamberlain 6−2 band and the Herzberg I 2−6 band (top). The lower two panels are DIATOM simulations. The spectra were accumulated for 10 h.

Table 4. Chamberlain Bands Rotationally Analyzed in the Keck Spectra[a]

$a^1\Delta_g$ state (v'')	$A'^3\Delta_u$ state (v')							
	2	**3**	**4**	**5**	**6**	**7**	**8**	**9**
0	–	–	–	–	–	–	–	–
1	–	–	–	×	×	×	–	–
2	–	–	×	×	×	×	×	×
3	–	×	×	×	×	×	×	–
4	×	×	×	×	–	–	–	–
5	×	×	–	–	–	×	×	×
6	–	–	–	×	×	×	–	–
7	–	–	×	×	–	–	–	–
8	–	–	–	–	–	×	×	–
9	–	–	–	–	×	×	–	–
10	–	–	–	×	–	–	–	×

[a] Transitions marked with symbol × are observed.

tions of that band and the $A-X$ 2−6 band. The agreement is seen to be very good. Because the lower state is not the ground state, the bands are displaced toward longer wavelengths from the strong Herzberg I bands, and with the sensitivity inherent in the sky spectra, it is possible to measure many bands in the 350−500 nm region.

Table 4 is a matrix of the bands that have been analyzed, and it is seen that the $a^1\Delta_g$ state vibrational range is $v = 1-10$. This is substantially greater than any previous measurements. Nieh and Valentini[69] reported CARS measurements for the $v = 0-6$ range, but with limited rotational distributions. For instance, for $a^1\Delta_g(v = 1)$ the rotational range was $J = 25-44$, but for $v = 5$ and 6, only three levels were reported, $J = 16$, 18, and 20 for $v = 5$, and $J = 2$, 4, and 6 for $v = 6$. More than 1270 Chamberlain band lines have been rotationally identified in the Keck spectra. In combination with the extensive high-resolution measurements of the $A'-X(v = 0)$ transitions by Jenouvrier et al.,[43] the present measurements give an accurate determination of the $a^1\Delta_g$ state levels $v = 0-10$.

13.3. Herzberg II and $c^1\Sigma_u^-$–$b^1\Sigma_g^+$ Bands

Until the analysis of the Keck spectra in the 400−500 nm range, the only well-characterized $c^1\Sigma_u^-$ state transition was the Herzberg II $c^1\Sigma_u^- - X^3\Sigma_g^-$ system. The $c^1\Sigma_u^- - a^1\Delta_g$ state system has been reported in a flowing afterglow[135] and in rare gas matrices,[204] but with little spectroscopic information.

The $c-X$ emission bands were initially identified and analyzed in a laboratory spectrum by Degen[95] and subsequently observed in the Venus nightglow.[124,134] The claim was later made[205] that $c-X$ emission could also be discerned in the terrestrial nightglow, from the 0.5-nm resolution spectrum of Broadfoot and Kendall.[143] The bands thus identified cannot be confirmed in the 0.01-nm resolution Keck spectra, and we now believe that the $c-X$ system is relatively quite weak in the terrestrial atmosphere.

However, analysis of the near-UV Keck spectra revealed a series of sparse yet prominent lines, shown to belong to the $O_2(c-b)$ system, with $c^1\Sigma_u^-(v = 4-11)$ and $b^1\Sigma_g^+(v = 0-3)$.[17] Confirmation is straightforward, since the upper and lower term

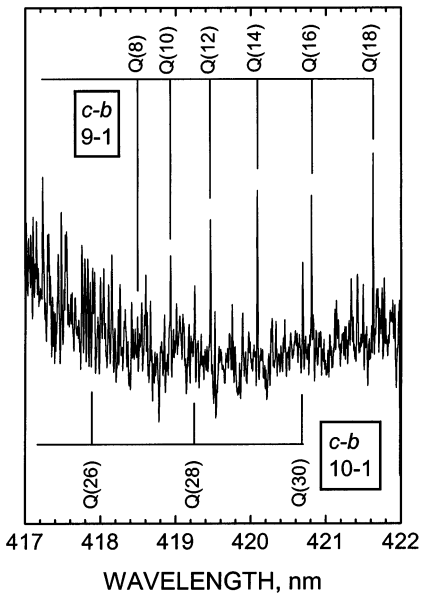

Figure 6. Keck I/HIRES sky spectrum of the $O_2(c^1\Sigma_u^- - b^1\Sigma_g^+)$ system, containing portions of the 9−1 and 10−1 bands. The spectra were accumulated for 10 h.[17]

Table 5. Q(16) Line Positions for $O_2(c^1\Sigma_u^- - b^1\Sigma_g^+)$ Bands[a]

$c^1\Sigma_u^-$ state (v')	$b^1\Sigma_g^+$ state (v'')			
	0	**1**	**2**	**3**
4	–	478.49	512.11	549.96
5	–	464.20	495.78	531.19
6	–	451.43	481.25	514.54
7	–	440.02	468.31	–
8	405.45	429.85	456.80	–
9	397.39	420.80	446.60	–
10	390.25	412.80	437.59	–
11	383.95	405.77	–	–

[a] Positions are the wavelengths in nanometers in air.

energies are precisely known. The $c-b$ 9−1 and 10−1 bands are shown in Figure 6.

Spectroscopically, the transition is quite unusual and is only the second known example of a $^1\Sigma_u^- - ^1\Sigma_g^+$ spectrum in a diatomic molecule,[206] and the first emission spectrum. The spectrum is sparse because there is only a Q-branch, and only alternate rotational levels are populated. Furthermore, only rotational coupling with a $^1\Pi_u$ perturbing state can provide a transition moment, and in such a case, the intensity expression for the rotational distribution contains a J^3 term in front of the exponential. As a consequence, emission favors high rotational levels, and the band structure extends over a wide spectral region. At 200 K, the Q(16) line is the most intense, and Table 5 shows the line positions of the Q(16) lines in the stronger bands.

It is believed that the barely bound $O_2(1^1\Pi_u)$ state is the perturber that interacts with the $c^1\Sigma_u^-$ state. As it lies near the latter at large interatomic distances,[50] it affects high $c^1\Sigma_u^-$ state levels preferentially, and its effect rapidly decreases with decreasing vibrational level; the last level from which $c-b$ emission is seen is $c^1\Sigma_u^-(v = 4)$. This conclusion is in accord with observations of the Venus nightglow[124] and laboratory studies,[134,135] where extremely strong

emission is seen from the $c^1\Sigma_u^-(v = 0)$ level in the Herzberg II bands, yet there is no indication of $c-b$ emission in the 650−750 nm wavelength range from bands in the $v' = 0$ progression, which might otherwise be expected. We thus conclude that, due to the different vibrational distributions, that the $c-b$ system is the predominant $O_2(c^1\Sigma_u^-)$ emission in the terrestrial atmosphere, while the $c-X$ emission dominates at Venus.

13.4. The $b^1\Sigma_g^+-X^3\Sigma_g^-$ Atmospheric Band System

The number of bands previously seen in the nightglow in the O_2 Atmospheric band system is very limited. From the ground, one sees the 0−1 band (Figure 3), a prime target for aeronomic observations. From space the 0−0 band is very intense, but it is absorbed in the atmosphere and is historically noteworthy as the Fraunhofer A-band seen in solar spectra viewed through the Earth's atmosphere.[195] There have been auroral observations of emission from higher $b^1\Sigma_g^+$ vibrational levels, but always at low resolution.[207]

Solar absorption measurements provide high-resolution data on the $b-X$ system for lower vibrational levels. The bands observed[195] include 0−0, 1−0, 2−0, 3−0, 1−1, 2−1, and 3−1, as well as the 0−0 and 1−0 bands of the $^{16}O^{18}O$ and $^{16}O^{17}O$ isotopes. The 0−0 band (the Fraunhofer A-band) is greatly broadened by passage through the atmosphere, but the others are narrow. The $^{16}O^{18}O$ and $^{16}O^{17}O$ 0−0 band lines can been seen in *emission* in the Keck spectra,[208] because the number density of the isotopic molecules in the atmosphere is not high enough to block transmission of the isotopic radiation. A portion of the R-branch of the A-band is shown in Figure 7b, along with a solar spectrum (Figure 7a). One sees that the unsaturated isotopic lines appearing in the solar spectrum, in absorption, are at the positions of emission features in the nightglow spectrum. As expected, there is complete agreement between the nightglow spectrum and the solar spectrum for those lines. The broad absorption lines in the nightglow spectrum mirror the same lines in the solar spectrum, and the fact that the $^{16}O^{16}O$ absorption lines appear at all in a nightglow emission spectrum shows that there is a continuum background; the current belief is that it is caused by O + NO recombination and is therefore the NO_2 continuum.[165,209] The strong feature at 759.8 nm in the nightglow spectrum is the OH Meinel 4−0 $P_1(3.5)$ line.

Emission out of the $b^1\Sigma_g^+(v = 0)$ level is a prime observable from the ground and from space. However, the sky spectra reveal a great deal more about the Atmospheric band system. Using co-added spectra, 30 bands have been identified, with $b^1\Sigma_g^+$ levels from $v = 0$ to $v = 15$, and ground-state levels from $v = 0$ to $v = 12$.[150] As there has been no previous spectroscopy reported that involves $b^1\Sigma_g^+$ state levels above $v = 3$, this represents a great step forward. In Figure 8 is presented a sky spectrum in which both the $b-X$ 6−5 and 12−10 bands appear, additional lines belonging to the 8−3 OH Meinel band.

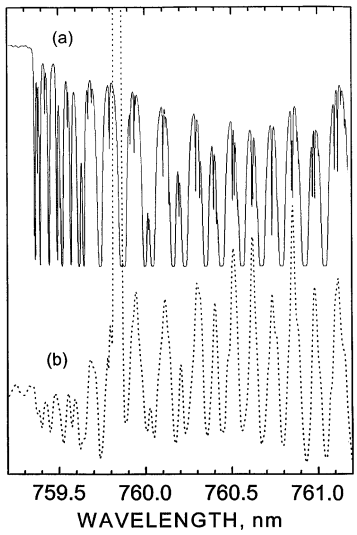

Figure 7. Comparison of the solar absorption spectrum (a) with Keck I/HIRES sky spectrum (b) of the Fraunhofer A-band region. The solar spectrum shows intense broadened absorption lines due to the $O_2(b-X)$ 0−0 transition. Between the broad $^{16}O^{16}O$ lines are narrow $^{18}O^{16}O$ absorption lines which are not saturated. The sky spectrum shows isotopic emission lines at the positions of the solar isotopic absorption lines. The $^{16}O^{16}O$ absorption lines are also reproduced in the sky spectrum, an indication that there is a continuum background in the nightglow, from which O_2 absorbs radiation just as in the solar spectrum. The strong feature at 759.8 nm is the $P_1(3.5)$ line of the OH 4−0 Meinel band, which is only slightly affected by passage through the A-band region.

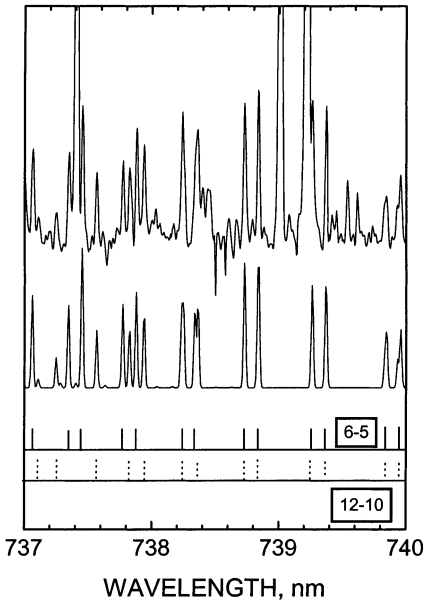

Figure 8. Keck I/HIRES sky spectrum of the 6−5 and 12−10 bands of the $O_2(b-X)$ system (top) and DIATOM simulation (below). The strong lines belong to the 8−3 Meinel OH band.

Analysis of the data over the 600−900 nm range leads to a vibrational intensity distribution, presented in Figure 9, where the intensity scale is set by comparison against an average OH nightglow spectrum. The distribution is remarkable with respect to its trimodal character. The intense $v = 0$ emission is understandable in comparison to $v = 1$, because of the very large difference in quenching

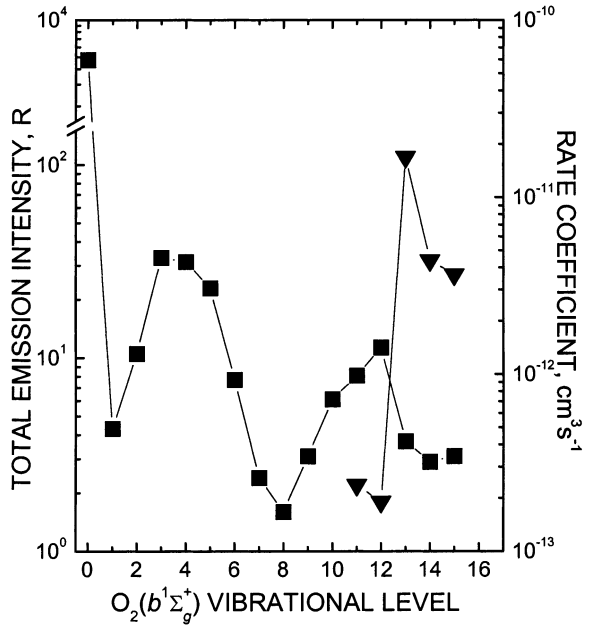

Figure 9. Vibrational distribution of the $O_2(b^1\Sigma_g^+)$ state in the nightglow (squares).[150] The left axis gives values for the total emission intensity out of each level, while the right axis refers to the rate coefficients for $v = 11-15$ removal by O_2 (triangles).[247] Note that the very large difference between the rate coefficients for $v = 12$ and $v = 13$ is only modestly mirrored in the populations.

efficiencies. The strong dip at $v = 8$ is also likely to be due to rapid quenching, and Kirillov[210] has carried out calculations of rate coefficients using Landau−Zener and Rosen−Zener approximations for the $b^1\Sigma_g^+(v) + O_2$ system in which rapid $v = 8$ quenching is attributed to the nearly resonant process

$$O_2(b^1\Sigma_g^+, v = 8) + O_2(X^3\Sigma_g^-, v = 0) \rightarrow O_2(X^3\Sigma_g^-, v = 7) + O_2(b^1\Sigma_g^+, v = 0) + 41\ cm^{-1} \quad (4)$$

A full understanding of the development of this vibrational distribution will require measurements of removal of the $b^1\Sigma_g^+(v)$ levels by all the colliders. Progress is being made with O_2 and N_2, but it is important that the results of collisions with $O(^3P)$ also be evaluated.

Also shown in Figure 9 are O_2 removal rate coefficients measured for $b^1\Sigma_g^+(v = 11-15)$ with O_2 as a collider,[67] and noteworthy is the very large difference between the $v = 12$ and 13 levels. It does not mirror the modest decrease in the nightglow population between $v = 12$ and 13, and is further discussed below.

13.5. The $a^1\Delta_g$–$X^3\Sigma_g^-$ IR Atmospheric Band System

The IR Atmospheric system is less often viewed than the UV and visible O/O_2 emissions, but it is of particular interest because it is the lowest emitting state, and therefore can be thought of as a collector for the complicated processes involved in O-atom recombination. Emission is seen only from the $a^1\Delta_g$-($v = 0$) level, because the higher vibrational levels (at least $v = 1$ and 2 and levels above $v = 17$) are very rapidly quenched by O_2.[211−213]

It is useful to compare the volume emission rate in the 95 km region where O-atoms are recombining with the three-body atom recombination rate. The recombination rate of O-atoms in N_2 is 4.7×10^{-33}-$(300/T)^2$ cm^6 s^{-1}, or 1×10^{-32} cm^6 s^{-1} at 200 K.[66] For an average peak O-atom density of 5×10^{11} cm^{-3} and a total density of 3×10^{13} cm^{-3}, the atom recombination rate is 7.5×10^4 cm^{-3} s^{-1}. This is quite close to the $a-X$ 0−0 volume emission rate from SME measurements given by Howell et al.[214] and from ETON measurements.[215]

It therefore appears that each O-atom recombination event produces one $a^1\Delta_g(v = 0)$ molecule. However, in a sense this is not a large yield, because the recombining O-atoms must dispose of 5 eV per event, whereas an $O_2(a^1\Delta_g, v = 0)$ molecule only accounts for 20% of the total—80% of the energy goes elsewhere. It is important to determine the disposition of this fraction, which may well involve the ground state, possibly with a broad vibrational distribution.[82,84,89]

14. Hot $O_2(b^1\Sigma_g^+, v = 0, 1)$ in the Ionosphere

The many new O_2 Atmospheric bands are mainly formed in the nightglow by oxygen atom recombination. However, the $b^1\Sigma_g^+(v = 0,1)$ vibrational levels can be produced whenever $O(^1D)$ and O_2 are present, via reaction 3. Apart from ozone photodissociation, there are no known $O(^1D)$ sources in the normal 85−105 km nightglow region.

It is worth mentioning that there are a variety of potential $O(^1D)$ sources, the class of reactions where O-atoms are the colliders. Thus, any of the O_2 vibronic states with energies above 2 eV could, if quenched by $O(^3P)$, be sources of $O(^1D)$. Of particular interest, historically and perhaps practically, is the three-body O-atom interaction,

$$O(^3P) + O(^3P) + O(^3P) \rightarrow O_2^* + O^* \quad (5)$$

First proposed by Chapman[121] to account for green line production, where O^* is $O(^1S)$, another possible product is $O(^1D)$. Whereas $O(^1S)$ radiates efficiently in the 95 km nightglow region where it is observed, the same will not be true for $O(^1D)$, as its radiative lifetime is larger by a factor of ∼200, and it is quenched much more rapidly by O_2 and N_2. $O(^1D)$ is typically not observed below 200 km. Nevertheless, if it is formed via reaction 5 in the mesopause region, then it will manifest itself by $b^1\Sigma_g^+(v = 0,1)$ generation, which would be an additional source beyond that from O-atom recombination.[216,217]

An obvious example of $b^1\Sigma_g^+(v = 0,1)$ generation is found in the ionosphere, where there is no possibility of confusion with the three-body recombination source because of the very low density. In this case, $O(^1D)$ is produced by dissociative recombination,

$$O_2^+ + e \rightarrow O(^1D) + O(^3P) \quad (6)$$

where the principal source of the ion is charge

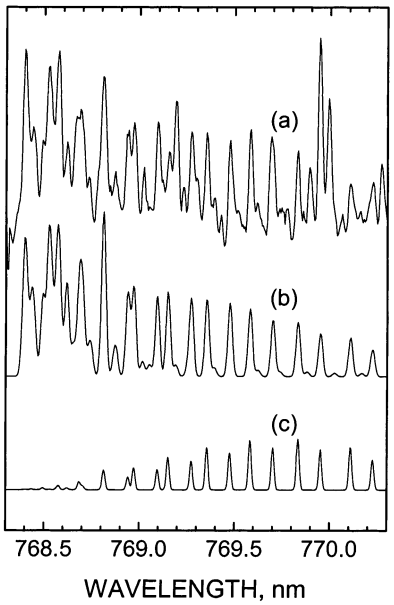

Figure 10. Demonstration of ionospheric emission in a sky spectrum from Keck I/HIRES from the $O_2(b-X)$ 1−1 band (a). A DIATOM simulation at a temperature of 1000 K is shown (b), along with a 200 K simulation (c) that represents the normal mesospheric rotational distribution in this band. The spectrum was recorded at 1822−1852 local time on Jan 11, 2000.[218]

exchange with O^+ that has been formed during the day by photoionization:

$$O^+ + O_2 \rightarrow O + O_2^+ \qquad (7)$$

O_2^+ and O^+ disappear slowly throughout the night, as do the electrons, and thus $O(^1D)$ is continually generated.

Although the O_2 density rapidly decreases above 110 km, reaction 3 proceeds at some low level, the evidence being that, on occasion, strong emission is seen in the $b-X$ 1−1 band. Its origin in the ionosphere is confirmed by the fact that the temperature calculated from its rotational distribution does not correspond to the ~200 K temperature of the mesopause, which can be extracted from the distribution seen in Figure 3. Instead, in the example shown in Figure 10a, the temperature is about 1000 K, which is appropriate to an altitude near 200 km at solar maximum.[218] Figure 10b,c shows DIATOM simulations for 1000 and 200 K; clearly, the 1000 K simulation represents the data well. Although the 95 km emission is still present, it is totally dominated by the higher altitude emission, which can be recognized by the fact that the strong OH lines typically seen in this region[219] are now dominated by the 1−1 band emission. A rough estimate of the total ionospheric emission from $b^1\Sigma_g^+(v = 0,1)$ under the conditions of Figure 10 is 500 rayleighs (when viewed from above the atmosphere).

Wallace and Chamberlain[220] demonstrated that the $O_2(b-X)$ 1−1 band emission is a prominent auroral feature, and it has been shown[207,221] that higher $b^1\Sigma_g^+$ state bands are also discernible, up to $v' = 5$. Gattinger and Jones[207] correctly deduced that the $b^1\Sigma_g^+(v = 1)$ level must be much more rapidly quenched than the higher levels, as the 1−1 band emission becomes much brighter relative to emission from higher levels as the auroral altitude increases. It has been suggested that $O_2(b^1\Sigma_g^+)$ vibrational excitation in aurora is due to charge exchange between O_2^+ and NO.[222]

15. Recent Laboratory Measurements

Considerable progress has been made in recent years in determining loss rate coefficients and kinetic pathways for all of the O_2 states that are involved in atom recombination. Attempts to determine where energy goes after an initial excitation step is of relatively recent vintage, since unless there is a well-defined starting point, it is a difficult if not impossible task to deal with the myriad of relaxation pathways available to a molecule with 5 eV excess energy. Thus, the best experiment in an O_2 system involves direct laser excitation of an electronic state in a single vibrational level. In most cases rotational equilibration is rapid, but the vibrational loss processes are often fast and near dissociation of comparable magnitude to rotational redistribution.

McDade[223] has discussed the importance of further laboratory measurements on the $O/O_2/N_2$ systems, pointing out that only a fuller understanding of the kinetics and reactive pathways will facilitate the use of the emission data collected from the ground, from rockets, and from satellites to extract the basic source parameter, the O-atom density. He stresses the need to consider O-atom removal for many of the levels present in the atmosphere.

An early attempt to detect fluorescence from laser-excited $O_2(A^3\Sigma_u^+)$ was only able to achieve a lower limit on the rate coefficient for $v = 8$,[224] which was orders of magnitude higher than values reported for lower vibrational levels.[97,102] Such studies advanced significantly when Wildt et al.[225] obtained $O_2(b^1\Sigma_g^+)$ fluorescence signals following excitation of O_2 to vibrational levels of all three Herzberg states: $A^3\Sigma_u^+$, $A'^3\Delta_u$, and $c^1\Sigma_u^-$. They excited these with an excimer-pumped dye laser in the 248 nm region and looked at the resulting emission in the $O_2(b-X)$ 0−0 band. No attempt was made to trace the pathway by which this energy degradation takes place. One of the important observations was that the excitation spectrum of the $b-X$ emission looked like the O_2 absorption spectrum, leading to the conclusion that, no matter which of the three O_2 states is initially prepared, the efficiency of conversion to $b^1\Sigma_g^+(v = 0)$ is similar. The implication is that the three upper states are collisionally coupled, and the system quickly loses its memory as to how the energy deposition was initiated. A further conclusion that can be drawn is that, in order to study the details of the dissipation of energy in the atom recombination process, it is not necessary to start with separated atoms; it is sufficient to put in the energy close to the O_2 dissociation limit.

A second important result was that the production of $b^1\Sigma_g^+(v = 0)$ is rapid, in fact faster than the experimental time resolution of ~1 μs. At the O_2 pressure used, it was concluded that the effective rate

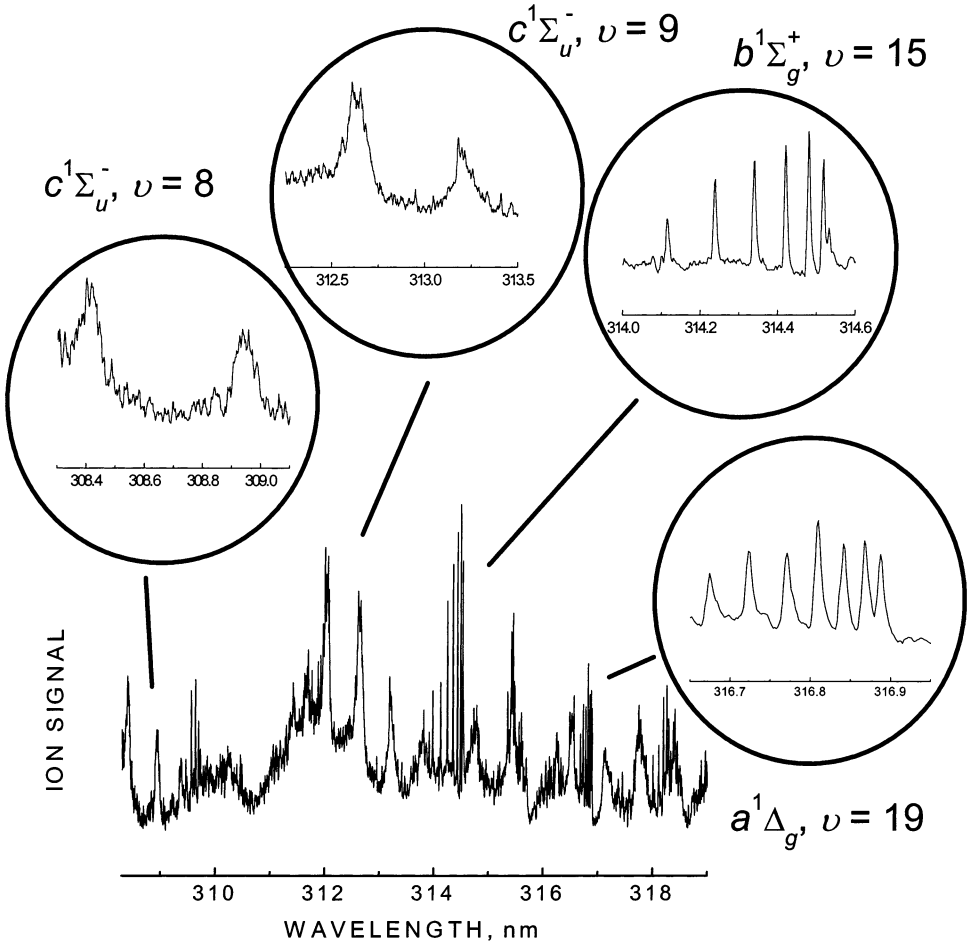

Figure 11. Ion signal as a function of ionization laser wavelength following excitation of O_2 to the $\upsilon = 7$ level of the $A^3\Sigma_u^+$ electronic state. The experimental spectrum was measured at 9.6 Torr of O_2 and 155 K with a delay between the excitation and ionization laser pulses of ~50 ns.[67]

constant limit for the overall relaxation process is $>1 \times 10^{-11}$ cm^3 s^{-1} for removal of $A^3\Sigma_u^+(\upsilon = 8)$ and production of $b^1\Sigma_g^+(\upsilon = 0)$. This is much larger than loss rate coefficients reported earlier[97,102,103] for lower $A^3\Sigma_u^+$ levels. Subsequently, the quantum efficiency for $b^1\Sigma_g^+(\upsilon = 0)$ production following $A^3\Sigma_u^+(\upsilon = 8)$ excitation was evaluated, but a number of revisions were subsequently made.[226,227] As a result, the current recommended value for the yield with O_2 collider is 0.14 ± 0.06, and for N_2 collider, 0.42 ± 0.18.[227] That the N_2 yield is larger is surprising and is uncorroborated by the SRI REMPI measurements described below.

There is, in fact, evidence to the contrary on this point. In a fast-flow system of a mixture of O(^3P) and N_2, it has been shown that addition of small amounts of O_2 downstream of the discharge—much less than the N_2 concentration—causes the efficient creation of both $O_2(a^1\Delta_g)$ and $O_2(b^1\Sigma_g^+)$.[105,228] The implication is that O_2 is substantially more effective than N_2 in causing the $O_2(a^1\Delta_g, b^1\Sigma_g^+)$ precursor, presumably the O_2 Herzberg states, to generate these two lower states. A mechanism has been identified for this process with O_2 collider,[67] but it is not evident how N_2 could be as effective.

The next significant advance in the study of O_2 energy transfer was the development of active probes, laser-based methods to detect product states with high time resolution. These are typically two-laser experiments, one laser for excitation, and the other for probing the evolving population. The two techniques of this sort are LIF and REMPI. As described above, LIF measurements are best applied on allowed optical pathways, and the only useful one in O_2 is the Schumann−Runge transition, therefore limiting O_2 LIF to studies of the vibrational levels of the ground state.[229]

REMPI is a more generally applicable technique than fluorescence to study the O_2 electronic states, because the vibrationally excited levels of all the states being considered are collisionally removed so rapidly that their fluorescence yields preclude observation. In the present REMPI experiments, the first laser is tuned to an absorption feature in O_2, e.g., a rotational line of the $A-X$ 7−0 or the $b-X$ 1−0 bands, and the second (ionization) laser is scanned. What is thereby traced out is a snapshot of the entities present in the system at the instant in time set by the separation between the pulses of the two lasers.

When the second laser is set to a known ionization feature and the photoexcitation laser is scanned, the trace represents the photoabsorption spectrum, e.g., $A-X$ 7−0 or $b-X$ 1−0, which becomes progressively weaker as the delay between the two lasers is increased. If the ionization laser is set to a feature

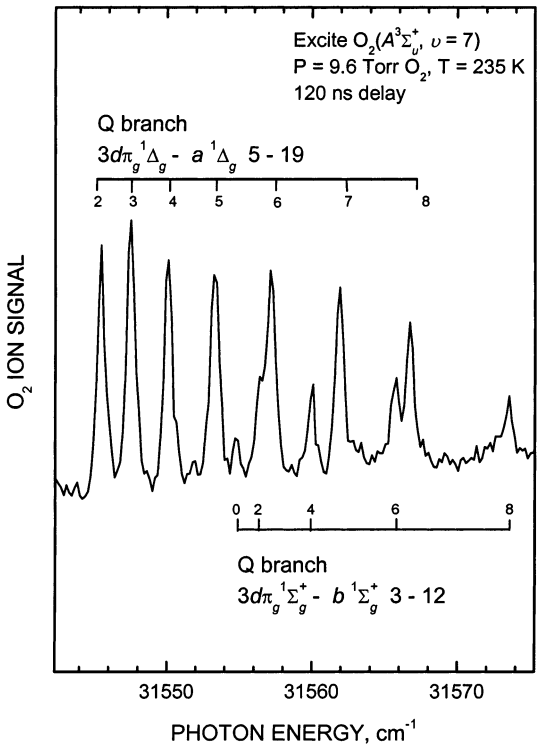

Figure 12. Ion signal as a function of photon energy following excitation of O_2 to the $v = 7$ level of the $A^3\Sigma_u^+$ electronic state. The REMPI spectrum was obtained at 9.6 Torr of oxygen at a temperature of 235 K and a time delay of 120 ns between the excitation and ionization laser pulses.[67] The strong features are assigned to the Q branch of the 5−19 band of the 2 + 1 REMPI transition, $3d\pi_g{}^1\Delta_g - a^1\Delta_g$.[230,231] The weaker rotational features are assigned to the Q branch of the 3−12 band of the 2 + 1 REMPI transition, $3d\pi_g{}^1\Sigma_g^+ - b^1\Sigma_g^+$.[230,231]

not initially excited by the first laser, then the ionization signal can initially increase with delay time before decreasing. Still, the observed spectrum reflects the initial photoabsorption process.

The intermediate states used for the REMPI measurements are singlet and triplet *gerade* Rydberg states, of which there are a great number.[118,119,230,231] For the lower O_2 *gerade* states these are reached by two photons, while the *ungerade* Herzberg states are excited by one photon. The $^5\Pi_g$ quintet state is excited by two photons to a $^5\Pi_g$ ion-pair state.[147,232]

Figure 11 shows the richness of a REMPI spectrum, where the first laser excites the O_2 to the $A^3\Sigma_u^+(v = 7)$ level, and the system is sampled with the ionization laser after 50 ns at 9.6 Torr of O_2. There are a number of unidentified features, but there are unambiguous spectra from $c^1\Sigma_u^-(v = 8,9)$, $b^1\Sigma_g^+(v = 14,15)$, and $a^1\Delta_g(v = 18,19)$. The $O_2(a^1\Delta_g, v = 19)$ region is expanded in Figure 12, to demonstrate that there is an overlapping transition for some rotational lines assigned to ionization of O_2 in the $v = 12$ level of the $A^3\Sigma_u^+$ state. Ionization laser scans in other spectral regions reveal other states and levels. We discuss the individual states in order of decreasing energy, but we start with the $A^3\Sigma_u^+$ state, since in the experiments carried out at SRI it is the precursor to the higher-lying $^5\Pi_g$ state.

Nevertheless, even with a specific starting point in the scheme of energy degradation and a pure O_2 system, tracing the pathways through which the energy flows is a daunting task. In what follows, we provide examples for each of the seven states associated with ground-state atoms. However, it is not yet possible to present a full picture. For this there are two reasons: the whole range of vibrational levels cannot be sampled for a given state, and there has not been any attempt to investigate the possible transfer of energy into the ground-state manifold.

Significant repositories of energy deposited high in the Herzberg states are the $v = 0$ levels of the $a^1\Delta_g$ and $b^1\Sigma_g^+$ states.[225,227,233] However, the yields into these levels are in the 10−60% range,[226,227] while if all the energy from an initially excited 5-eV level were converted to $a^1\Delta_g(v = 0)$ (having 1-eV excitation), then the yield could be as high as 500%, or analogously, 300% for $b^1\Sigma_g^+(v = 0)$. It is thus apparent that we account for a small fraction of the input energy and do not yet possess a complete picture. The relaxation of highly vibrationally excited ground-state O_2 is known to be quite slow in O_2 collider,[13,82,84,89,114,115] and so the many examples of the rapid disappearance of the population from one level and its prompt appearance elsewhere may not adequately reflect the energy degradation of the system as a whole. Typical collisional cascading removal rate coefficients of $O_2(X^3\Sigma_g^-,v)$ in high vibrational levels are in the 10^{-14} cm^3 s^{-1} regime, and much less at low temperature.[13] If O_2 rather than $O(^3P)$ is the dominant quencher of $X^3\Sigma_g^-(v)$ in the nightglow region of the atmosphere, then the relaxation time of such energetic molecules is in the range of tens of seconds.

15.1. The $A^3\Sigma_u^+$ State

Production of the three Herzberg states is carried out by direct photoexcitation.[145,146,167,225] Nevertheless, the Franck−Condon factors (FCFs) present a limitation. Because photoexcitation from the ground state is in all cases an optically forbidden process, the FCFs need to be of adequate magnitude. Their rapid decrease with decreasing $A^3\Sigma_u^+$ state vibrational level precludes preparation of the lower vibrational levels by this method,[23] and the current measurements have not been carried out for $A^3\Sigma_u^+(v < 6)$. Moreover, even if such levels are collisionally generated, which they surely are as energy degrades, and as the terrestrial nightglow demonstrates, a method of sampling them has not yet been found. This is because the FCFs between such levels and the Rydberg and valence intermediate levels also rapidly decrease with decreasing $A^3\Sigma_u^+(v)$.

The fluorescence studies described in the preceding section only obtained limits on the rate coefficients for removal of O_2 in high vibrational levels of the $A^3\Sigma_u^+$ state.[224,225] An approach other than detecting the fluorescence was required to make quantitative measurements of the rate constants. In the mid-1990s, Copeland[234] developed a REMPI method to probe high vibrational levels in the $A^3\Sigma_u^+$ state with

a pulsed laser via excitation through the $v = 5$ level of the $C^3\Pi_g$ Rydberg state and combined the REMPI detection with state-specific excitation. Initial experiments on $O_2(A^3\Sigma_u^+, v = 7)$ were performed with O_2 collider, yielding the first quantitative determination for a high vibrational level. The measurements were then extended to other colliders, including N_2 and CO_2, and expanded to vibrational levels $v = 6$ and 9.[146] Other intermediate states, including some long-lived, weakly bound valence levels, were identified as efficient intermediate states to ionization.[146] It was surprising to find that the rate coefficient for N_2 was only about a factor of 2 smaller than that for O_2, and thus N_2 is the dominant collisional partner for removing O_2 molecules from these vibrational levels in the Earth's atmosphere. These results significantly changed the models of the atmospheric emission, since previously aeronomers thought only O_2 and $O(^3P)$ would affect the excited O_2.[7]

For direct atmospheric model input, the rate coefficients must be measured between 150 and 250 K, the temperature of the emitting region. The first temperature dependence of the energy-transfer rates was published in 1997,[145] finding that rate coefficients were similar from room temperature down to about 200 K, with a significant increase (a factor of ~2) going to 150 K. Similar temperature behavior was observed for the vibrational levels $v = 6$ and 7 in subsequent investigations.[167,235] Specific data from these investigations are presented below in the discussion of the pathways for the removal of energy.

The direct approach of exciting and monitoring the excited electronic state has thus far been limited to $v = 6$, 7, and 9 because of interferences in the detection by 2 + 1 REMPI of ground-state O_2 and the FCFs for excitation of a specific vibration level. Concurrent with the above investigation, studies of possible reactions of O_2 in the $A^3\Sigma_u^+$ state were undertaken. O-atoms are produced efficiently following excitation of O_2 to vibrational levels $v \geq 9$, with the yield decreasing to less than 10% for $v = 8$ and below.[236] Clearly, more than electronic energy transfer can be occurring at these energies. Since it was hypothesized that O_3 was generated via an $O_2^* + O_2$ reaction, the possibility of N_2O production was also considered. Careful studies employing long duration excitation of the $A^3\Sigma_u^+$ state in background N_2 found no detectable yield.[237] The upper limit for production excluded this reaction as a significant source of N_2O in the Earth's atmosphere.

Other than reaction, the pathways of energy relaxation are clearly important. Mapping out the relaxation is a significant task, and several advances and examples in achieving this goal are given below. Figure 13 shows the photoexcitation spectrum of $A^3\Sigma_u^+(v = 7)$ at zero delay, with ionization via the $C^3\Pi_g(v = 5) - A^3\Sigma_u^+(v = 7)$ band, and traces out the $A-X$ 7−0 absorption spectrum. The intense line that appears at 252.4 nm is a 2 + 1 REMPI transition in xenon, caused by the excitation laser alone. Another such line appears in the excitation spectrum of the $A-X$ 6−0 band, at 255.95 nm. These lines are also easily observable from air, where xenon is present at a concentration of 87 ppb.

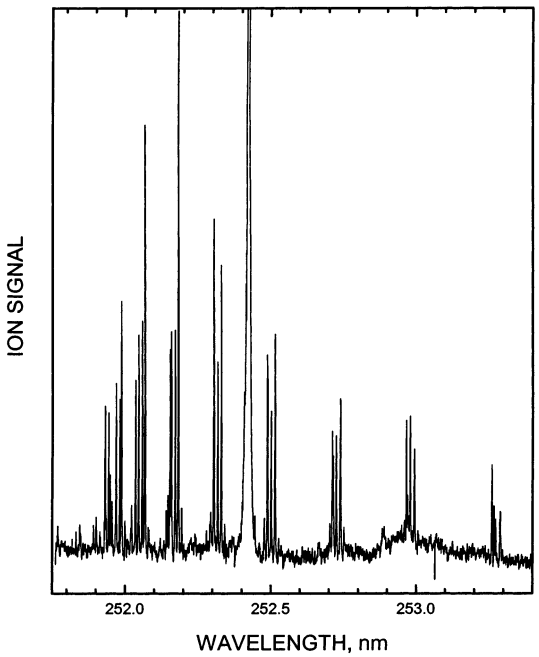

Figure 13. Excitation spectrum of the $A^3\Sigma_u^+(v = 7)$ level, with no delay between the excitation and ionization lasers. The $A-X$ band is scanned, and the ionization laser is set at 282.5 nm, resonant at the one photon level with features in the $O_2(C-A)$ 5−7 band. The intense line at 252.4 nm is caused by a 2 + 1 ionizing transition in xenon, traces of which are typically found in an O_2 gas cylinder.

Measurements on the $O_2(A^3\Sigma_u^+)$ state were carried out over a broad range of vibrational levels and with the three atmospherically important colliders, O_2, N_2, and CO_2, where the latter is of greatest importance at Venus and Mars. The REMPI signal from the $A^3\Sigma_u^+(v = 7)$ level is shown in Figure 14, where the lower trace shows a one-laser background signal from cold O_2, while the upper trace shows the appearance of the $A^3\Sigma_u^+(v = 7)$ population following a pulse of the excitation laser.

In the upper trace of Figure 15 a decay plot for $A^3\Sigma_u^+(v = 6)$ is shown, demonstrating that when observing the initially excited level, there is very little build-up phase in the signal. In contrast, the lower trace shows the temporal behavior when $v = 7$ is excited and $v = 6$ is sampled, and here the population build-up is evident. The behavior is modeled for different fractions of $A^3\Sigma_u^+(v = 7)$ cascading to $A^3\Sigma_u^+(v = 6)$, and the $A^3\Sigma_u^+(v = 6)$ yield with O_2 collider is found to be approximately 35%, with some of the population being detected in the $c^1\Sigma_u^-$ manifold. Similar determinations with N_2 and CO_2 colliders reveal their yields for the $A^3\Sigma_u^+(v = 7 \rightarrow 6)$ cascade to be 10% and 75%, respectively. This is an important result, because the fraction of the $A^3\Sigma_u^+(v = 7)$ population removed by N_2 rather than O_2 in the atmosphere is about two-thirds, so between these two levels cascading is not the predominant process. The branching ratios show little or no temperature dependence.[167,238]

Figure 16 plots the measured $O_2(A^3\Sigma_u^+)$ removal rate coefficients by O_2 for the five vibrational levels for which measurements were made. The error bars

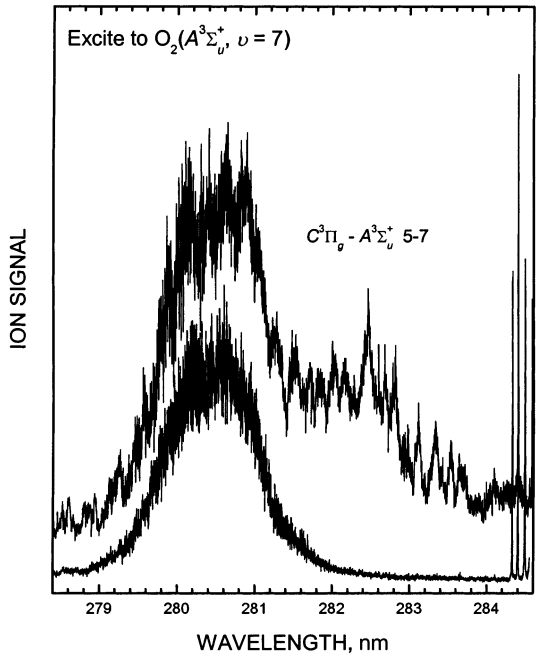

Figure 14. Ion signal as a function of ionization laser wavelength. The upper spectrum is obtained following excitation of O_2 to the $v = 7$ level of the $A^3\Sigma_u^+$ electronic state. The lower spectrum is taken with the excitation laser off-resonance with any O_2 Herzberg feature and shows background ionization of the ground-state O_2. For both spectra the O_2 pressure was 5.1 Torr and the delay between the excitation and the ionization laser pulses was 100 ns. The spectra were measured at 230 K. The $A^3\Sigma_u^+(v = 7)$ population is allowed to rotationally equilibrate before ionization. The upper spectrum displays strong features due to the $C\ ^3\Pi_g - A^3\Sigma_u^+$ 5−7 band between 280 and 284 nm.[167] The wavelength scale is only accurate to 0.01 nm.

are of the magnitude of the data circles for $v = 6$, 7, and 9, while for $v = 10$ and 11 lower limits are given. For $v = 11$, collisional dissociation is believed to be responsible for the enhanced loss rate. Also shown are earlier results,[97] where data were derived from afterglow studies and fluorescence of the products. The single point at $v = 2$ is an unpublished result, appearing in a table in a paper dealing with the $O_2(c^1\Sigma_u^-)$ state.[103] There is in fact no direct overlap, because levels below $v = 6$ could not be sampled in the REMPI measurements, while in the earlier kinetic studies results were limited to the lower vibrational levels seen in afterglows. We deduce from an afterglow spectrum published by Degen et al.[63] that the pertinent levels over the 250−400 nm range measured in the work of Kenner and Ogryzlo[97] are $v = 1-3$. The trend of the higher levels suggests that the afterglow results underestimate the magnitude of the removal rate coefficients, a conclusion previously reached by aeronomic modelers[166,174] to the extent that use of the $v = 1-3$ rate coefficients seemed inappropriate for interpretation of the nightglow emissions. Calculations by Kirillov[210] are also shown in Figure 16, indicating that the rate coefficients for the lower levels will behave roughly as an extrapolation of the higher levels, and that there is a discrepancy of an order of magnitude with the values reported by Kenner and Ogryzlo.[102−104] Measurements are needed to clarify this issue.

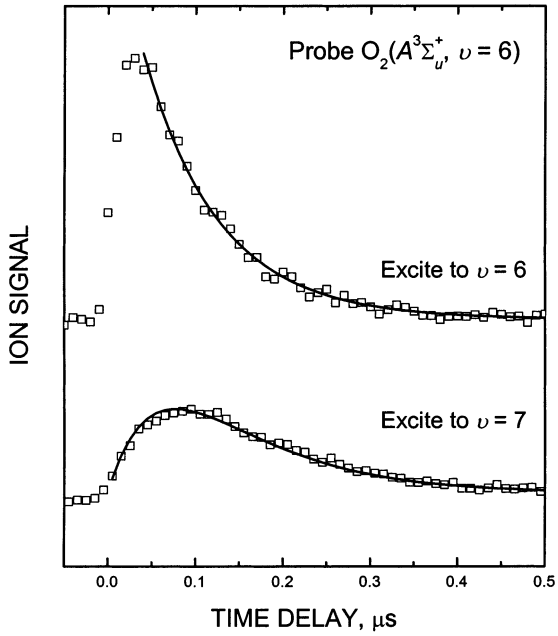

Figure 15. Ion signal for $O_2(A^3\Sigma_u^+, v = 6)$ as a function of time delay between the excitation and ionization laser pulse. In the upper plot the $A^3\Sigma_u^+(v = 6)$ level is excited directly, whereas in the lower plot excitation is to $A^3\Sigma_u^+(v = 7)$, and the fraction cascading into $v = 6$ is detected. The squares are the experimental data points, and the lines are calculated curves from the rate coefficients of Kalogerakis et al.,[167] scaled only in amplitude. The data were obtained at an O_2 pressure of 10 Torr at 235 K.

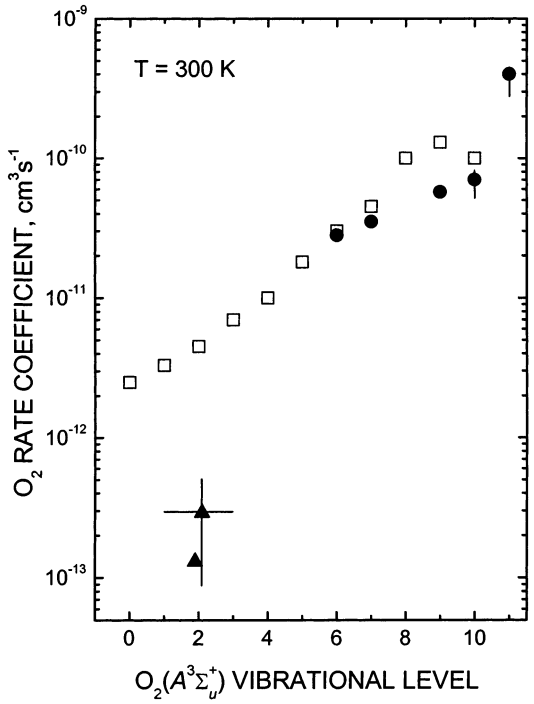

Figure 16. Rate coefficients for collisional removal of $O_2(A^3\Sigma_u^+, v)$ by O_2 at 300 K. Solid circles are data from REMPI measurements,[146,234] solid triangles are from studies by Kenner and Ogryzlo,[97,103] and open squares are calculations by Kirillov.[210]

The results of Wildt et al.,[225] in which $A^3\Sigma_u^+(v = 8)$ was excited and $b^1\Sigma_g^+(v = 0)$ promptly appeared, can now be more accurately quantified. Figure 17 is the counterpart of Figure 15, which showed a REMPI

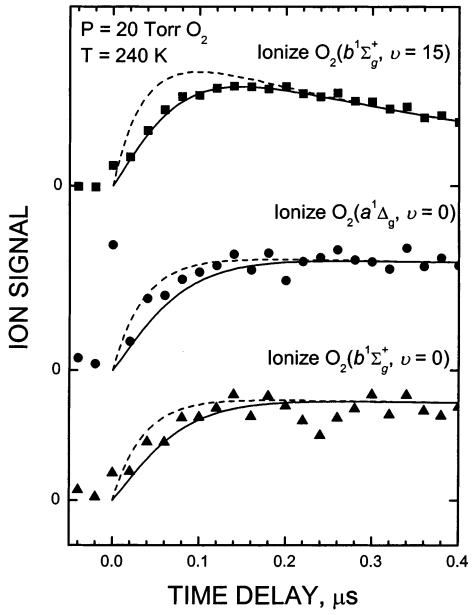

Figure 17. Temporal evolution of three excited levels of oxygen following excitation of O_2 to the $v = 7$ level of the $A^3\Sigma_u^+$ state. All of the measurements were recorded at 20 Torr of O_2 at 240 K.[67] The top curve (squares) shows the temporal evolution of the $O_2(b^1\Sigma_g^+,v = 15)$ state, the middle curve (circles) shows the temporal evolution of the $O_2(a^1\Delta_g,v = 0)$ state, and the bottom curve (triangles) shows the temporal evolution of the $O_2(b^1\Sigma_g^+,v = 0)$ state. The lines are the results of kinetic models with different assumptions about population of these states. The dashed line assumes these states are populated in one step via a collision of $O_2(A^3\Sigma_u^+,v = 7)$ with a ground-state O_2, and the solid line is a model where one-third of the molecules that populate the state come from $O_2(A^3\Sigma_u^+,v = 7)$ and two-thirds come from $O_2(A^3\Sigma_u^+,v = 6)$.

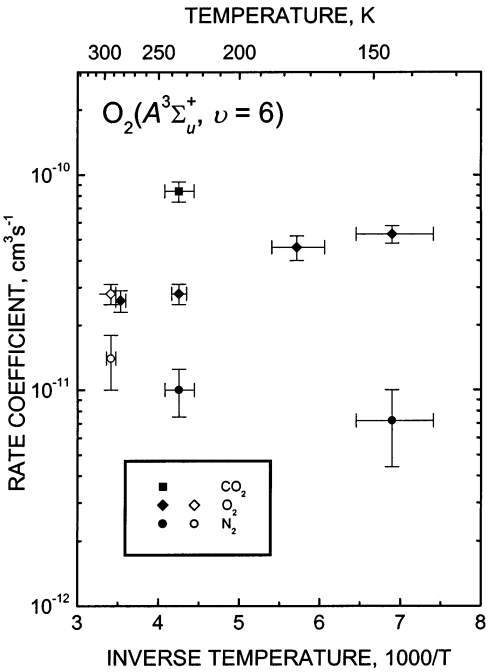

Figure 18. Arrhenius plot of the collisional removal rate coefficients for $O_2(A^3\Sigma_u^+,v = 6)$ for collider gases O_2, N_2, and CO_2. The open symbols are the results of Knutsen et al.,[146] and the closed symbols are the results of Kalogerakis et al.[167]

plot of the temporal behavior of $A^3\Sigma_u^+(v = 6)$ following $A^3\Sigma_u^+(v = 6, 7)$ excitation. In Figure 17 are shown temporal plots for three species following $A^3\Sigma_u^+(v = 7)$ excitation: $b^1\Sigma_g^+(v = 0)$, $b^1\Sigma_g^+(v = 15)$, and $a^1\Delta_g(v = 0)$. In each case the build-up is prompt, requiring about 50 ns at 20 Torr of O_2 (equivalent to 3 ns at the 300 Torr pressure used in the experiments of Wildt et al.[225]), which corresponds to a rate coefficient of about 3×10^{-11} cm^3 s^{-1}, close to the value shown in Figure 15 for $A^3\Sigma_u^+(v = 7) + O_2$ interaction. It is therefore evident that all three species rise at a similar rate to the fall of $A^3\Sigma_u^+(v = 7)$, leading to the conclusion that unless there is a still faster intermediate decay channel, they are primary products of $A^3\Sigma_u^+$ decay.

As the $a^1\Delta_g(v = 0)$ and $b^1\Sigma_g^+(v = 0)$ signals from $A^3\Sigma_u^+(v = 7)$ relaxation rise in a similar manner, there are parallel channels,

$$O_2(A^3\Sigma_u^+,v = 7) + O_2(X^3\Sigma_g^-,v = 0) \rightarrow O_2 + O_2(b^1\Sigma_g^+,v = 0) \quad +26\,564\ \text{cm}^{-1} \quad (8)$$

$$O_2(A^3\Sigma_u^+,v = 7) + O_2(X^3\Sigma_g^-,v = 0) \rightarrow O_2 + O_2(a^1\Delta_g,v = 0) \quad +31\,800\ \text{cm}^{-1} \quad (9)$$

We believe that these reactions proceed as written, in that the O_2 collider is converted to $a^1\Delta_g(v = 0)$ and $b^1\Sigma_g^+(v = 0)$. The excess energy in these highly exothermic interactions can be expected to appear as vibronic excitation of the partner O_2 molecule, and as we will show, this is indeed what happens; extremely high vibrational levels of the $a^1\Delta_g$ and $b^1\Sigma_g^+$ states are generated.

The temperature dependence of collisional removal rate coefficients has been measured in various cases. Examples are shown in Figure 18, where $A^3\Sigma_u^+(v = 6)$ is removed by three colliders over a wide range of low temperatures. There is an extremely small positive activation energy exhibited for N_2 collisions and a negative activation energy for O_2 collisions, complex formation possibly being important in the latter case.

15.2. The $^5\Pi_g$ State

The $^5\Pi_g$ state cannot be accessed by direct O_2 photoexcitation from the $v = 0$ levels of the low-lying electronic states. Figure 1 shows that there is a large difference between its internuclear distance and that of the ground state, making the FCFs out of the $X^3\Sigma_g^-(v = 0)$ level negligible. In the studies from our laboratory, the $^5\Pi_g$ state is populated via collisional processes, either via photoexcitation to the $O_2(A^3\Sigma_u^+$, $A'^3\Delta_u$, or $c^1\Sigma_u^-$) states or by reaction of $O(^1D)$ and O_3.

The first measurements on the quintet state investigated the collisional removal rates of the $v = 0$ level with O_2, N_2, and CO_2.[68] In subsequent work the spectroscopy was presented,[151] followed by determinations of the temperature dependence of the collisional removal process for the $v = 0$ level.[232,239] Measurements were also made on the quintet production efficiency as a function of temperature and vibrational level in the $A^3\Sigma_u^+$ state.[240]

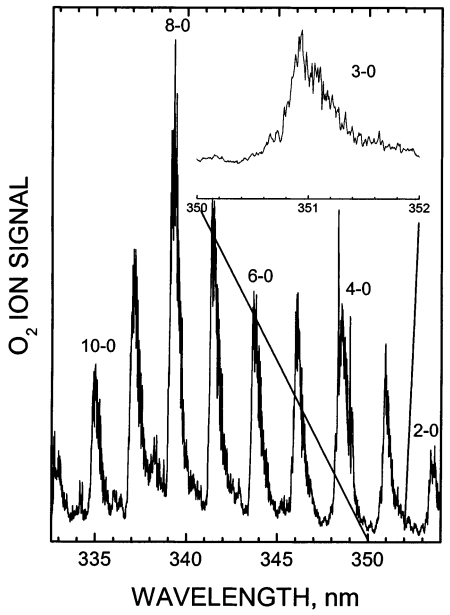

Figure 19. Ion signal as a function of ionization laser wavelength following excitation of O_2 to the $v = 9$ level of the $A^3\Sigma_u^+$ electronic state. The inset shows an expanded version of the same spectrum between 350 and 352 nm, corresponding to the 3−0 vibrational band of the $^5\Pi_g$−$^5\Pi_g$ transition.[68] The sharp feature near 349 nm corresponds to ionization of ground-state O_2 via a 3 + 1 REMPI process.[242]

Figure 19 presents a REMPI spectrum of the quintet band progression from the $v = 0$ level of $^5\Pi_g$, the initial excitation being to $A^3\Sigma_u^+(v = 9)$. Relaxation has taken place, because $A^3\Sigma_u^+(v = 9)$ corresponds to approximately $v = 2$ in the quintet state.[241] The spectrum that appears depends on the delay between photoexcitation and ionization; shorter delays result in appearance of the $^5\Pi_g$ $v = 1$, 2 levels, while with excitation to higher $A^3\Sigma_u^+$ levels, the quintet $v = 1$−4 levels become prominent. We see that the spectrum traces out a Franck−Condon envelope, maximizing at the 8−0 band (there are also other issues such as laser power). The expanded spectrum is the 3−0 band, and the shape of the 4−0 band is somewhat distorted because it is coincident with a 3 + 1 band of the O_2 ground state.[242] The upper state in this two-photon REMPI spectrum is a quintet ion-pair state, and the vibrational numbering given is tentative in the ion-pair intermediate state. These measurements are the first experimental characterization of the O_2 ion-pair states that previously had only been calculated for singlets and triplets.[243]

Figure 20 shows an excitation spectrum probing the $v = 4$ level of the quintet state, in the vicinity of the first dissociation limit, and shows that all levels lying in the excitation energy region convert to the quintet state. For this experiment, the ionization laser is set on the quintet−quintet 9−4 band, and the excitation laser is scanned. The three lower spectra are simulations of Herzberg bands in the excitation region: the A−X 11−0, A'−X 12−0, and c−X 16−0 bands. There is a one-to-one correlation between the features in the experimental spectrum and the three band simulations. From these observations, it is evident that, as each of the three transitions is excited, it feeds into the quintet state; there is no selectivity governed by multiplicity or symmetry. This demonstrates that the mixing of identity between the four states is efficient, at least near the dissociation limit, and illustrates the futility of attempting to determine the distribution of electronic states as oxygen atoms recombine in the atmosphere.[7,127,129]

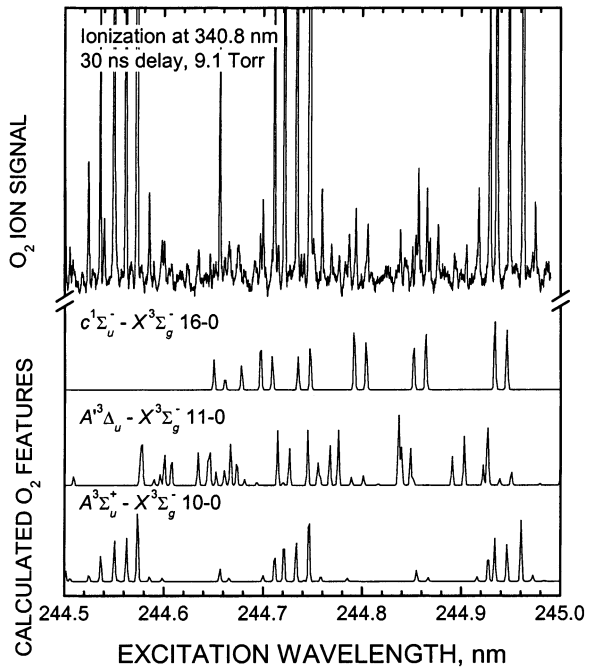

Figure 20. Ion signal as a function of excitation laser wavelength with the ionization laser wavelength set to 340.8 nm, along with calculated absorption spectra for the Herzberg transitions. The upper spectrum was obtained at 9.1 Torr of O_2, with the delay between the excitation and ionization laser pulses set to 30 ns.[68] At 340.8 nm, the strongest ionization feature is the 9−4 band of the $^5\Pi_g$−$^5\Pi_g$ transition. The calculated spectra shown in the three lower traces are obtained using the DIATOM computer program.[201]

The experiment carried out by Wildt et al.[225] is analogous, but instead of watching the Herzberg states evolve into the quintet, they observed the collisional production of the $b^1\Sigma_g^+(v = 0)$ level following excitation at the $A^3\Sigma_u^+(v = 8)$ level. The results were similar: the excitation spectrum mirrors the absorption spectrum. Thus, the efficiency with which conversion to $b^1\Sigma_g^+(v = 0)$ occurs is also independent of the identity of the initially excited state, implying that, at the excitation energy of the states (substantially lower than that displayed in Figure 20), collisional mixing erases the memory of the state being photoexcited.

Considering that there has been no previous evidence for the presence of the $^5\Pi_g$ state in O_2 photochemistry, it is interesting to find that, as Figure 19 shows, it is relatively easy to detect via REMPI. Figure 21 shows that the quintet population is not present initially but develops as a result of collisions. For a series of delays between the excitation laser and the ionization laser, one sees that it takes approximately 50 ns for the quintet population to

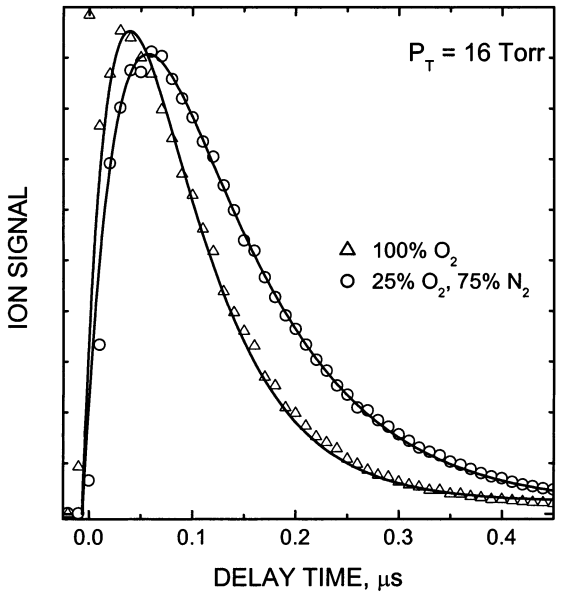

Figure 21. Comparison of the temporal evolution of the population in the $O_2(^5\Pi_g,v = 0)$ state as a function of gas composition. The data shown as the triangles were obtained in 16 Torr of O_2, while the circles were obtained in 4 Torr of O_2 and 12 Torr of N_2.[68]

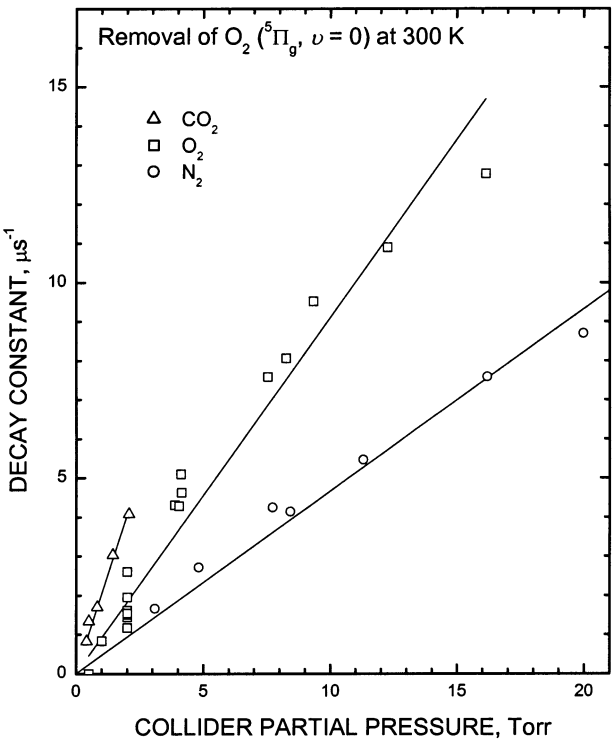

Figure 22. Pressure dependence of the $O_2(^5\Pi_g,v = 0)$ signal decay constant for O_2(squares), N_2 (circles), and CO_2 (triangles) colliders at room temperature. Contributions to the decay constants from diffusion and from O_2 in the mixed gas systems are subtracted.[240] The solid lines are the best linear fit to the data for each collider, and the slope of the line yields the rate coefficient.

maximize. Figure 22 shows decay plots of the $^5\Pi_g$ population, where the decay constant is plotted against the collider partial pressure. We see that collisional removal by CO_2 is about twice as fast as that by O_2, with that by N_2 being about half as fast.[68,147,232,239,240]

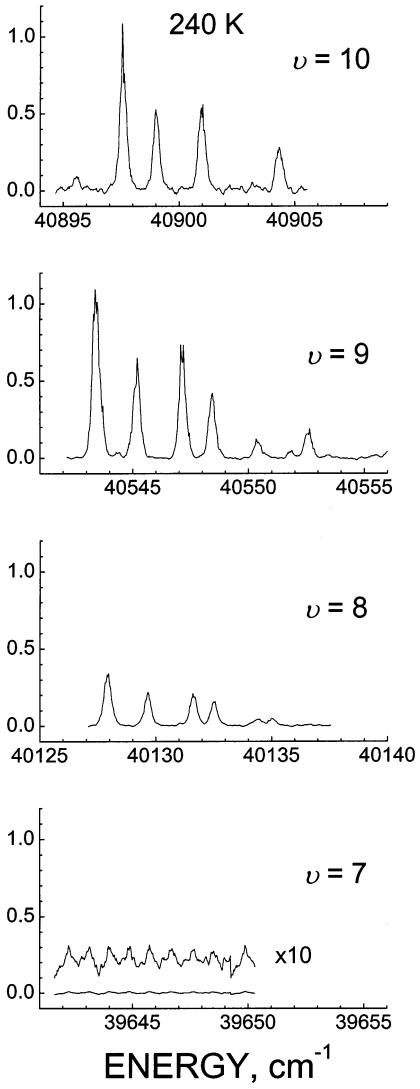

Figure 23. Ion signal exciting different vibrational levels in the $A^3\Sigma_u^+$ electronic state while detecting O_2 in the $v = 0$ level of the $^5\Pi_g$ state. Amaral et al. detected the $^5\Pi_g$ state via the 9−0 transition near 337.025 nm.[240] The oxygen pressure was 10 Torr, and the temperature was 240 K. The delay position between the excitation and ionization laser pulses was set to the maximum of the temporal evolution for each vibrational level excited.

The ion-pair quintet state is of Π_g symmetry, the energy of which is uncertain. As a result, although the $^5\Pi_g-^5\Pi_g$ energy difference is accurately measurable, the absolute energy of the lower $^5\Pi_g$ state can only be roughly defined. This is done by investigating the $^5\Pi_g$ levels that are generated relative to the $A^3\Sigma_u^+$ state levels initially excited.

Figure 23 shows excitation spectra at 240 K of the $v = 0$ level of the $^5\Pi_g$ state, where individual $A^3\Sigma_u^+(v)$ levels are interrogated to determine at what point no more quintet signal is produced. That the probed level is in fact $v = 0$ is based on the lack of observation of any lower level attributable to the quintet. It is evident that the quintet signal becomes weak for $A^3\Sigma_u^+(v = 8)$ excitation and is absent for $A^3\Sigma_u^+(v = 7)$ excitation at low temperature. With a decrease in temperature, the $v = 8$ signal weakens and the $v = 10$ signal becomes stronger; the latter

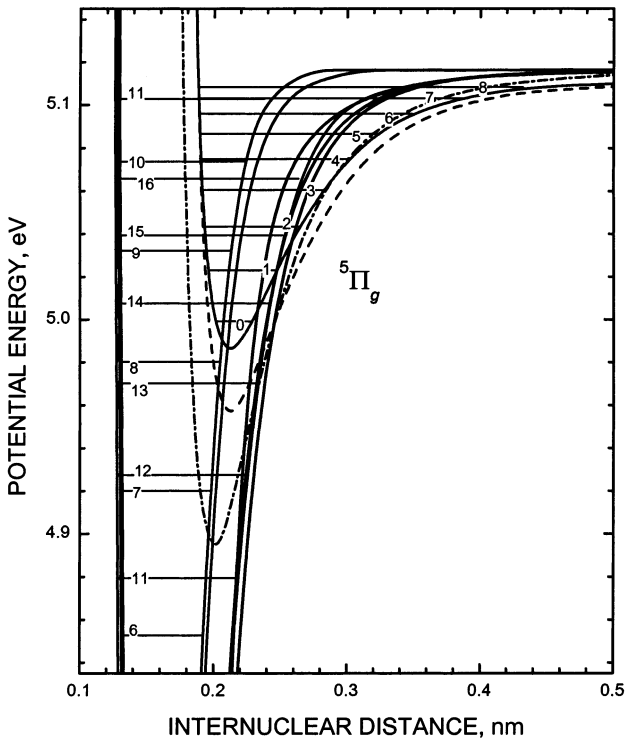

Figure 24. Calculated potential energy curves for the $^5\Pi_g$ state of O_2. The solid line is the calculated value of Partridge et al.,[241] the dashed line is the recommended value from the previous reference, and the dot−dash line is the calculated value from Saxon and Liu.[50] The vibrational levels labeled 11−16 on the left side of the figure correspond to vibrational levels in the $c^1\Sigma_u^-$ electronic state, and those numbered 6−11 correspond to vibrational levels in the $A^3\Sigma_u^+$ electronic state.

observation is probably related to the decreasing importance of the process[236]

$$O_2(A^3\Sigma_u^+, v = 10) + O_2 \rightarrow O_3 + O(^3P) \qquad (10)$$

the $A^3\Sigma_u^+(v = 10)$ level being only 335 cm^{-1} away from the O_2 dissociation limit.

Figure 24 shows the $A^3\Sigma_u^+$ and $^5\Pi_g$ potentials close to the dissociation limit, with three calculated sources for the latter. The lowest is from Saxon and Liu,[50] while the upper two are given by Partridge et al.[241] On the basis of the results shown in Figure 23, we believe that the $^5\Pi_g(v = 0)$ level lies slightly above $A^3\Sigma_u^+(v = 8)$, and the binding energy is 1000 ± 100 cm^{-1}. The vibrational levels of the quintet state are shown, based on the higher of Partridge's potentials,[241] as are the vibrational levels of the $A^3\Sigma_u^+$ and $c^1\Sigma_u^-$ states, the former for $v = 6-11$, and the latter for $v = 11-16$.

15.3. The $A'^3\Delta_u$ State

Only limited experiments on the $A'^3\Delta_u$ state have been carried out.[244] By generating the $A'^3\Delta_u(v = 10)$ state and probing the neighboring $A^3\Sigma_u^+(v = 9)$ level by REMPI, rapid energy transfer with O_2 collider is demonstrated. It is not yet known if this is specific to the $A'^3\Delta_u(v = 10)$ level or is a more general phenomenon.

It would be of considerable interest to study the collisional transfer between the $\Omega = 1$, 2, and 3 spin−orbit sublevels, to learn about the rates of interconversion across the 150 cm^{-1} gap between each one. Photoexcitation (the Herzberg III system) is much stronger from the ground state into the two upper levels, $\Omega = 1$ and 2, than into the lowest level, $\Omega = 3$, from which the Chamberlain bands originate.[24,28,43,245] The intermediate $C^3\Pi_g(v = 5)$ level, by means of which the $A^3\Sigma_u^+$ state levels are probed, can also be used for the $A'^3\Delta_u$ state, and the $^3\Pi_g$ valence state near the $O(^1S) + O(^3P)$ dissociation limit has also been used for $A^3\Sigma_u^+(v = 9)$ and $A'^3\Delta_u(v = 10)$ probing.

15.4. The $c^1\Sigma_u^-$ State

The $O_2(c^1\Sigma_u^-)$ state is sampled by means of the $d^1\Pi_g(v = 2)-c^1\Sigma_u^-$ bands in 1 + 1 REMPI. Measurements have been made on the vibrational levels $v = 8-12$ and 16. In the case of $v = 16$, the ionization transition is unknown. REMPI spectra of the $d-c$ 2−10 and 2−11 bands are shown in Figure 25, and delay data provide removal rate coefficients, given in Table 6.

Copeland et al.[144] published the first $c^1\Sigma_u^-$ laser pump−probe experiments with REMPI detection at room temperature for the colliders O_2, N_2, CO_2, and He. Preliminary pathway information was included in that work. Next, temperature-dependent measurements were made for $v = 9$, showing the surprising result that the rate decreased significantly as the temperature decreased, in contrast to the findings on the $A^3\Sigma_u^+$ and quintet states.[246] Recently, higher vibrational levels have been measured and cascading contributions studied.[213,247]

As noted in the discussion on the $A^3\Sigma_u^+$ state, it is difficult to carry out photoexcitation to levels below $v = 6$ because of decreasing FCFs. However, one may take advantage of the nesting of the Herzberg state potentials, resulting in improved overlap with the $X^3\Sigma_g^-(v = 0)$ level on going from $A^3\Sigma_u^+$ to $A'^3\Delta_u$ to $c^1\Sigma_u^-$ (see Figure 1). The same is true for ionization into the Rydberg levels. Thus, it is possible to make measurements on the c state to somewhat lower energies than for the $A^3\Sigma_u^+$ state. The lowest $A^3\Sigma_u^+$ state level measured is $v = 6$, whereas measurements have been made on $c^1\Sigma_u^-(v = 8)$, which lies 1200 cm^{-1} lower. In line with the idea that the Herzberg states are collisionally coupled, it is found that for O_2 collisional removal, $c^1\Sigma_u^-$ and $A^3\Sigma_u^+$ state levels at similar excitation energies exhibit similar rate coefficients.

Two important characteristics of the $c^1\Sigma_u^-$ $v = 9$ and 10 levels are that $v = 10$ is lost much more rapidly than $v = 9$ for collisions with O_2, and that vibrational cascading from $v = 10$ to $v = 9$ is the dominant pathway. Furthermore, $v = 9$ production is an important product of $O_2(A^3\Sigma_u^+, v = 7)$ collisional removal by O_2. As we discuss below, it is likely that the pathways by which deactivation occurs are dictated to a large extent by the availability of nearly resonant intermolecular processes. However, that is

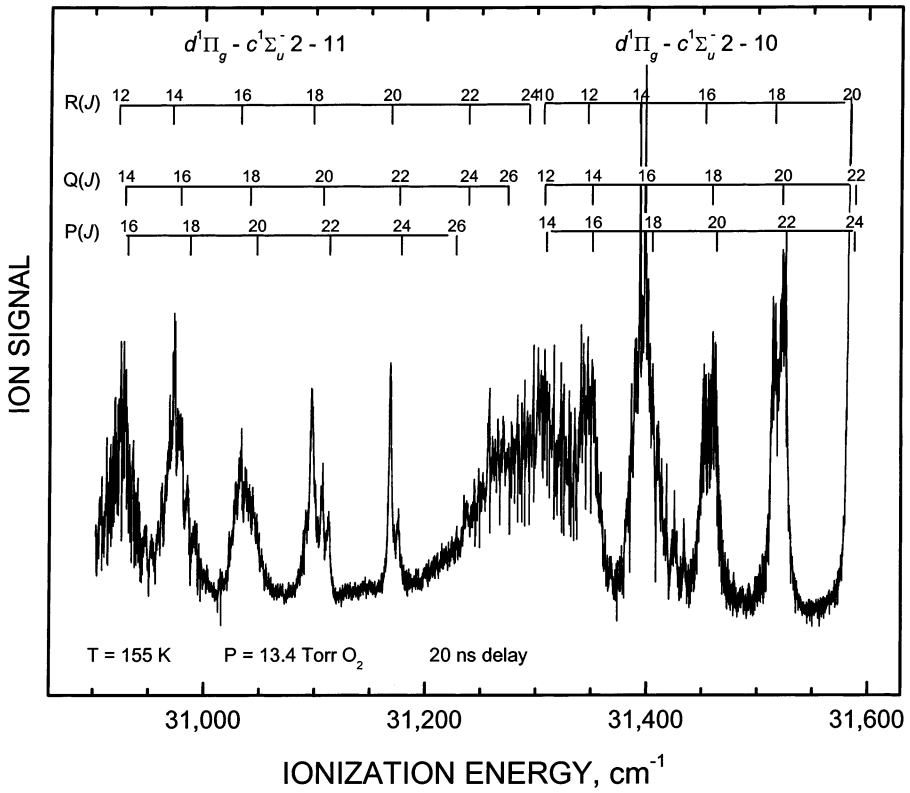

Figure 25. Ion signal as a function of photon energy following excitation of O_2 to the $v = 11$ level of the $c^1\Sigma_u^-$ electronic state. The data were obtained at 13.4 Torr of oxygen at 155 K and 20 ns delay between the excitation and ionization laser pulses.[247] The assignment is based on the level positions of Morrill et al.[230]

Table 6. Temperature-Dependent Removal Rate Coefficients for $O_2(c^1\Sigma_u^-,v)$ by O_2[a]

vibrational level, v	at 155 K	at 245 K	at 300 K
8[b]		$(1.5 \pm 0.4) \times 10^{-11}$	
9[c]	$(1.5 \pm 0.2) \times 10^{-12}$	$(4.2 \pm 0.2) \times 10^{-12}$	$(5.4 \pm 0.5) \times 10^{-12}$
10[d]	$(2.4 \pm 0.2) \times 10^{-11}$	$(1.5 \pm 0.3) \times 10^{-11}$	$(3.0 \pm 0.3) \times 10^{-11}$
11[d]	$(5.0 \pm 0.3) \times 10^{-11}$	$(2.1 \pm 0.1) \times 10^{-11}$	
12[d]	$(5-10) \times 10^{-11}$		
16[e]			$\sim 10^{-10}$

[a] Units for the removal rate coefficients are $cm^3\ s^{-1}$. The error estimates are two standard deviations. [b] Measurements of Kalogerakis et al.[67] [c] Room-temperature measurements from Copeland et al.[144] Low-temperature measurements from Bergman et al.[246] [d] Measurements of Wouters et al.[213] [e] Unpublished results from C. B. Bressler and R. A. Copeland.

not the only criterion, and there is at least one example where a resonant spin-forbidden process clearly does not occur. We consider three examples,

$$O_2(A^3\Sigma_u^+,v=7) + O_2(X^3\Sigma_g^-,v=0) \rightarrow O_2(a^1\Delta_g,v=19) + O_2(a^1\Delta_g,v=0) \quad +353\ cm^{-1} \quad (11)$$

$$O_2(c^1\Sigma_u^-,v=11) + O_2(X^3\Sigma_g^-,v=0) \rightarrow O_2(a^1\Delta_g,v=19) + O_2(a^1\Delta_g,v=0) \quad +26\ cm^{-1} \quad (12)$$

$$O_2(A^3\Sigma_u^+,v=6) + O_2(X^3\Sigma_g^-,v=0) \rightarrow O_2(a^1\Delta_g,v=19) + O_2(a^1\Delta_g,v=0) \quad -190\ cm^{-1} \quad (13)$$

The experimental results, shown in Figure 26, demonstrate that when the ionization laser is tuned to $a^1\Delta_g(v = 19)$ detection and the excitation laser is scanned over the appropriate region, there is a strong signal in the rather nonresonant but exothermic $A^3\Sigma_u^+(v = 7)$ case, a weak signal in the endothermic $A^3\Sigma_u^+(v = 6)$ case, and no discernible signal in the case of nearly resonant $c^1\Sigma_u^-(v = 11)$. Thus, although $c^1\Sigma_u^-(v = 11)$ loss is rapid, the deactivation channel does not include $a(19)$ production. It should be noted that the $c-X$ 11−0 FCF is considerably larger than that for $A-X$ 6−0 and 7−0, so the difference in $a^1\Delta_g$-$(v = 19)$ yields is not a result of decreased production of the initial states in the case of $c^1\Sigma_u^-(v = 11)$, where the four lines in the central panel mark the expected positions of $c^1\Sigma_u^-(v = 11)$ features.

In a similar manner, it is found that the high $b^1\Sigma_g^+$ state levels are not made from $c^1\Sigma_u^-(v)$ levels, even when there is energetic resonance, cf. $c^1\Sigma_u^-(v = 10) \rightarrow b^1\Sigma_g^+(v = 15)$, with generation of $a^1\Delta_g(v = 0)$. It appears that the preferred $c^1\Sigma_u^-(v)$ deactivation

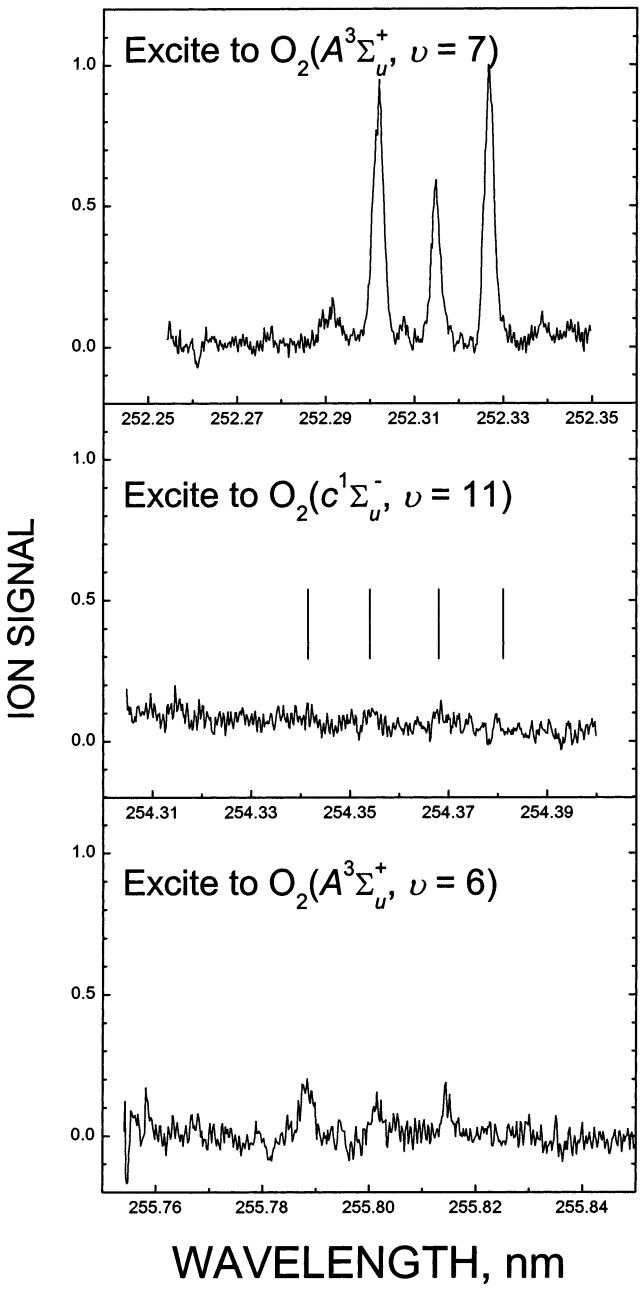

Figure 26. Ion signal from $O_2(a^1\Delta_g,v = 19)$ as a function of excitation wavelength. Amaral et al. obtained the spectra at 10 Torr of oxygen at a temperature of 240 K.[247] The displayed excitation spectra are obtained by subtracting the spectrum obtained off resonance at 31 548.7 cm^{-1} from the spectrum on resonance with the Q(3) rotational feature of the 5−19 band of the $3d\pi_g{}^1\Delta_g-a^1\Delta_g$ transition at 31 547.4 cm^{-1}. The top panel shows a group of rotational lines attributed to $O_2(A^3\Sigma_u^+,v = 7)$ excitation, and the bottom panel shows a group of rotational lines attributed to $O_2(A^3\Sigma_u^+,v = 6)$ excitation. In the middle panel, no appreciable ion signal is observed in the region of $O_2(c^1\Sigma_u^-$, $v = 11)$ excitation. The vertical lines show the position of the $O_2(c^1\Sigma_u^-)$ features present in both the on- and off-resonance ion signals but not in the difference.

pathway is vibrational cascading (which has been confirmed for O_2), a conclusion that is probably directly relevant to the Venus nightglow, where collisions with CO_2 bring the $O_2(c^1\Sigma_u^-)$ state population down to $v = 0$.

15.5. The $b^1\Sigma_g^+$ State

The $O_2(b^1\Sigma_g^+)$ state has been extensively studied in the laboratory in its $v = 0$ level.[4] Quenching being a slow process for $v = 0$, occurring in the atmosphere only with N_2, emission can be relatively intense despite a radiative lifetime of 13 s (Figure 2). By contrast, there are few studies on the vibrationally excited levels because collisional removal is very rapid.

Because of the convenient preparative technique for the $v = 1$ level, the energy transfer from $O(^1D)$ to O_2 (reaction 3), collisional removal of that level has been studied by Gauthier and Snelling,[216] Schurath,[248] and Lee and Slanger,[217] with general agreement that the 300 K rate coefficient with O_2 is about 2×10^{-11} cm^3 s^{-1}, some 6 orders of magnitude greater than the $v = 0$ rate coefficient.[4]

In a unique experiment carried out in the famous Bonn sphere, a 2.2×10^5-L reaction vessel, Schurath[248] obtained a rate coefficient for $v = 2$ collisional removal by O_2 at the same time as the $v = 1$ value, finding that it was smaller by a factor of 10−15. This seemed a surprising result, but subsequent state-specific excitation followed by REMPI detection[249−251] has substantiated the validity of this rapid falloff in rate coefficients with increasing vibrational level.

Measurements on $b^1\Sigma_g^+(v = 1-3)$ were carried out by direct O_2 photoexcitation, followed by REMPI probing.[249−251] One of the important conclusions from these studies, based on the temperature behavior and also on the analogous observations with $a^1\Delta_g(v)$, is that O_2 relaxation of at least the lower vibrational levels involves electronic-to-electronic (E−E) energy transfer with retention of the vibrational quanta, not vibrational cascading within the $b^1\Sigma_g^+$ state. Thus,

$$O_2(b^1\Sigma_g^+,v) + O_2(X^3\Sigma_g^-,v = 0) \rightarrow O_2(X^3\Sigma_g^-,v) + O_2(b^1\Sigma_g^+,v = 0) \quad (14)$$

Figure 27 shows the results of recent measurements on $b^1\Sigma_g^+(v = 1-3)$ removal by O_2 as a function of temperature, and one sees that at the low temperatures found in the mesosphere, near 200 K, the difference in rate coefficients becomes very large.

For $b^1\Sigma_g^+(v)$ generation above $v = 3$, production via direct photoexcitation of O_2 is limited by the FCFs, which maximize for $v' = v''$ transitions at low v. For accessing $b^1\Sigma_g^+(v = 4)$, the $b-X$ 4−0 FCF is 1×10^{-6}, a factor of 70 smaller than the 3−0 FCF. Thus, direct excitation in this manner becomes increasingly difficult. Further progress requires a less direct method of excitation.

Such a method is provided by collisional relaxation by O_2 of the higher levels, the Herzberg states. Any and all permutations of relaxation processes can take place—E−E, E−V, V−V, and V−R—so that the initial population becomes distributed in a number of ways. In particular, one pathway is the generation of highly vibrationally excited levels of the $b^1\Sigma_g^+$ and $a^1\Delta_g$ states, in the $v = 10-15$ and $v = 17-19$ ranges, respectively. Information on such high levels with any spectroscopic precision is directly available only

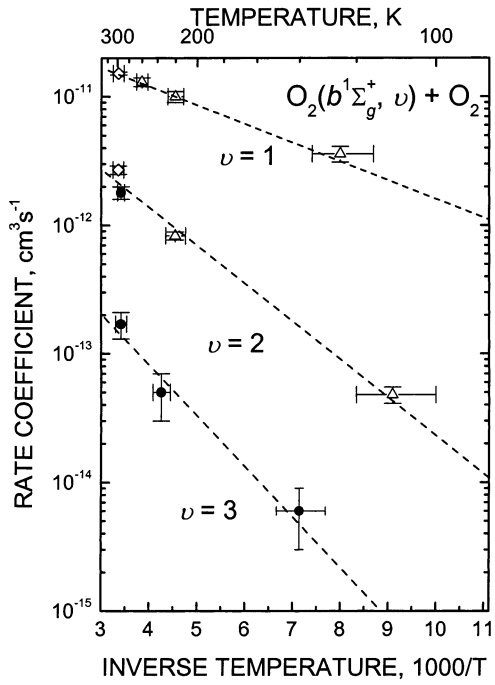

Figure 27. Arrhenius plot of the collisional removal rate coefficients for $O_2(b^1\Sigma_g^+, v = 1, 2,$ and 3) by oxygen. The open diamonds are the results of Bloemink et al.,[249] the open triangles are the results of Hwang et al.,[250] and the solid circles are the results of Kalogerakis et al.[261] The error bars represent two standard deviations. The solid lines are the results from Arrhenius fits to the experimental rate coefficient data.[261] Reprinted with permission from ref 251. Copyright 2002 American Institute of Physics.

from the Keck sky spectra, and even in that case extrapolation is needed for the $a^1\Delta_g$ state. For the $b^1\Sigma_g^+$ state, the Keck data go up to $v = 15$ in the $b-X$ bands,[150] while for $a^1\Delta_g$ the limit is $v = 10$ in the $A'-a$ bands.

Figure 11 has shown the wide range of species that are collisionally generated and detected by REMPI following excitation of O_2 to $A^3\Sigma_u^+(v = 7)$. Prompt production of the $a^1\Delta_g(v = 0)$ and $b^1\Sigma_g^+(v = 0)$ levels occurs in this process,[225] by the mechanisms of reactions 8 and 9. The 3−4 eV excess energy is then disposed of in various ways, and the production of the very high vibrational levels of the $a^1\Delta_g$ and $b^1\Sigma_g^+$ states represents one type of process. We see from reactions 11 and 13 that $a^1\Delta_g(v = 19)$ generation is close to resonant for an accompanying $a^1\Delta_g(v = 0)$, and the same is true for $b^1\Sigma_g^+(v = 15)$ generation. Lower levels of both states also appear, and they seem to arise from the high vibrational levels in the Herzberg states rather than vibrational cascading in the $b^1\Sigma_g^+$ or $a^1\Delta_g$ states. The fraction of $A^3\Sigma_u^+(v = 7)$ molecules that pass through the high-v $a^1\Delta_g$ and $b^1\Sigma_g^+$ pathways is as yet unknown.

The kinetics of the $b^1\Sigma_g^+$ levels has been followed for $v = 11-15$, and the 155 K rate coefficients for collisional removal by O_2 are shown in Table 7. The rise times are slightly different for each level and compatible with single-step or multistep processes from the $A^3\Sigma_u^+$ state as the source for each lower level, as opposed to vibrational cascading from higher $b^1\Sigma_g^+$ levels. Remarkable is the great difference between collisional removal rates of $b^1\Sigma_g^+(v = 12)$ and $b^1\Sigma_g^+(v = 13)$. In the nightglow, the $b^1\Sigma_g^+(v = 12)$ population is about 3 times larger than that of $b^1\Sigma_g^+(v = 13)$, whereas Table 7 and Figure 9 show that the 155 K removal rate of $b^1\Sigma_g^+(v = 13)$ is 60 times larger than that of $b^1\Sigma_g^+(v = 12)$ at 155 K. This could be interpreted as an indication that $O(^3P)$, not O_2, is the dominant quencher for $v = 12$; the rate coefficient for $v = 13$ is too large to be affected by collisional removal by O-atoms. N_2 is relatively inert for the high-v $b^1\Sigma_g^+$ levels.

It is interesting to compare the production of $b^1\Sigma_g^+(v = 15)$ from the $A^3\Sigma_u^+(v = 6)$ and $A^3\Sigma_u^+(v = 7)$ levels. For $A^3\Sigma_u^+(v = 6)$ the process is 114 cm^{-1} exothermic, while for $A^3\Sigma_u^+(v = 7)$ it is 657 cm^{-1} exothermic. As a result, what is observed is that following $A^3\Sigma_u^+(v = 6)$ excitation, its loss with O_2 collider matches the $b^1\Sigma_g^+(v = 15)$ build-up. On the other hand, following $A^3\Sigma_u^+(v = 7)$ excitation, the $A^3\Sigma_u^+(v = 7)$ loss is faster than that for $A^3\Sigma_u^+(v = 6)$, but the $b^1\Sigma_g^+(v = 15)$ build-up is noticeably slower. To model the $b^1\Sigma_g^+(v = 15)$ temporal behavior requires a two-thirds contribution from collisionally produced $A^3\Sigma_u^+(v = 6)$ and a one-third contribution directly from $A^3\Sigma_u^+(v = 7)$. No $b^1\Sigma_g^+(v = 16)$ is detected from $A^3\Sigma_u^+(v = 7)$ relaxation, the process being 288 cm^{-1} endothermic.

15.6. The $a^1\Delta_g$ State

Literature information on collisional energy transfer in the vibrationally excited levels of $O_2(a^1\Delta_g)$ is very sparse,[252,253] although of course the $v = 0$ level has been extensively studied for many years in chemistry, physics, and biology.[254] The reason that there is so little data on higher levels is the very long radiative lifetime of the $a^1\Delta_g$ state and, as is now known, the very large energy-transfer rate coefficients of such levels with O_2.

Table 7. Temperature-Dependent Removal Rate Coefficients for $O_2(b^1\Sigma_g^+, v)$ by O_2[a]

vibrational level, v	at 155 K	at 205 K	at 240 K	at 300 K
11	$(2.2 \pm 0.4) \times 10^{-13}$			
12	$(1.8 \pm 0.4) \times 10^{-13}$	$(3.2 \pm 0.8) \times 10^{-13}$	$(7 \pm 2) \times 10^{-13}$	
13	$(1.1 \pm 0.2) \times 10^{-11}$			
14	$(2.9 \pm 0.8) \times 10^{-12}$	$(3.3 \pm 1.0) \times 10^{-12}$	$(4.0 \pm 0.9) \times 10^{-12}$	
15	$(2.7 \pm 0.3) \times 10^{-12}$	$(2.0 \pm 0.2) \times 10^{-12}$	$(2.1 \pm 0.1) \times 10^{-12}$	$(2.7 \pm 0.2) \times 10^{-12}$

[a] Units for the removal rate coefficients are $cm^3\ s^{-1}$. The error estimates are two standard deviations. Measurements from Amaral et al. and Wouters et al.[213,247]

Table 8. Vibrational Distribution Percentages of $O_2(a^1\Delta_g)$ from Ozone Photodissociation[a]

λ (nm)	$v=0$	$v=1$	$v=2$	$v=3$	$v=4$	$v=5$	$v=6$	$v=7$
235	30	24	15	7	7	7	5	6
245	34	23	20	8	8	4		
255	39	30	14	10	8			
265	44	32	14	10				
275	59	26	15					
285	71	29						

[a] Measurements from Dylewski et al.[256]

Table 9. Wavelength Thresholds for Optically Allowed $O_2(a^1\Delta_g,v)$ Generation from O_3

vibrational level, v	wavelength threshold, nm
0	310
1	296
2	284
3	273
4	263
5	254
6	245
7	238

It is impractical to generate $a^1\Delta_g(v>0)$ by direct O_2 photoexcitation; the FCFs become small much more rapidly than is the case for the $b-X$ transition. For the $2-0$ $a-X$ band the FCF is 6.8×10^{-5}, compared to 2.6×10^{-3} for the $2-0$ $b-X$ band,[58] but in addition the intrinsic transition strength for $a-X$ is much smaller than for $b-X$. For these reasons, the preferable preparation technique is ozone photodissociation, from which Nieh and Valentini[69] have demonstrated with CARS spectroscopy that a broad range of vibrational levels can be produced. Thelen et al.[255] showed that the distribution of vibrationally excited $a^1\Delta_g$ molecules is not a simple function of input energy but also reflects interference effects, related to the small-scale absorption variability of the Hartley band. Subsequently, Dylewski et al.[256] made measurements over a range of wavelengths (Table 8), showing the expanding vibrational population with decreasing wavelength. They give comparisons with other measurements, showing significant differences from the earlier work[69] for the shorter wavelengths.

Generating vibrationally excited O_2 molecules in the presence of ozone has its own set of problems. Not only are there many vibrational levels of both the $X^3\Sigma_g^-$ and $a^1\Delta_g$ states produced, but the $O(^1D)$ atom can react with ozone to make all the O_2 states below the first dissociation limit. For this reason, such experiments require the suppression of the $O(^1D)$ reaction, as well as a limit on the photodissociation wavelength so that no higher $a^1\Delta_g$ levels than the one being studied are formed. In Table 9 are shown the threshold wavelengths for production of O_2 in a given $a^1\Delta_g$ vibrational level from the spin-allowed Hartley band photodissociation of ozone. Comparison with Table 8 shows that the observed distributions reach the thermodynamic limit in each case.

Experiments have been performed on $a^1\Delta_g(v=1,2)$ using ozone photodissociation followed by REMPI probing.[212] Although $O_2(a^1\Delta_g,v=0)$ loss by all colliders is extremely slow, the $a^1\Delta_g(v)$ levels are removed by O_2 even faster than the equivalent $b^1\Sigma_g^+(v)$ levels, presumably as a result of closer energy matching, cf.

$$O_2(a^1\Delta_g,v=2)+O_2(X^3\Sigma_g^-,v=0)\rightarrow O_2(X^3\Sigma_g^-,v=2)+O_2(a^1\Delta_g,v=0)\quad -149\ \mathrm{cm}^{-1} \quad (15)$$

$$O_2(b^1\Sigma_g^+,v=2)+O_2(X^3\Sigma_g^-,v=0)\rightarrow O_2(X^3\Sigma_g^-,v=2)+O_2(b^1\Sigma_g^+,v=0)\quad -309\ \mathrm{cm}^{-1} \quad (16)$$

The 300 K rate coefficients for $a^1\Delta_g(v=1)$ and $a^1\Delta_g(v=2)$ removal by O_2 are $(5.6\pm1.1)\times10^{-11}$ and $(3.6\pm0.4)\times10^{-11}$ cm^3 s^{-1}, respectively.[212] Although $a^1\Delta_g(v=0)$ removal is slower by some 7 orders of magnitude, isotope exchange—the equivalent E−E process for $v=0$—is very fast. A lower limit of 1.7×10^{-11} cm^3 s^{-1} has been reported,[257] compatible with an estimated value of 1×10^{-10} cm^3 s^{-1} based on extrapolation of the $v=1$ and $v=2$ rate coefficients. Because the E−E process with low-v $a^1\Delta_g(v)$ levels is fast and efficient, it represents an attractive method of generating vibrationally excited ground-state levels with reasonable specificity. In the next section we discuss the kinetics of low-v $O_2(X^3\Sigma_g^-)$ using this method of preparation.

As mentioned previously, very high $a^1\Delta_g(v)$ levels are produced from $A^3\Sigma_u^+$ state relaxation by O_2. As was done for the high-v $b^1\Sigma_g^+$, the decay rate coefficients can be measured, and they are presented in Table 10.[67,213,247] Figure 28 compares the decay of the $a^1\Delta_g(v=18,19)$ levels, demonstrating the major difference that can occur between adjacent levels. It can be postulated that the effect is attributable to some resonant process, in this case

$$O_2(a^1\Delta_g,v=19)+O_2(X^3\Sigma_g^-,v=0)\rightarrow O_2(b^1\Sigma_g^+,v=8)+O_2(a^1\Delta_g,v=0)\quad -6\ \mathrm{cm}^{-1} \quad (17)$$

However, such speculation is premature. REMPI measurements have not been performed on $b^1\Sigma_g^+$ state levels below $v=11$, spin is not conserved in reaction 17, and REMPI detection of the $a^1\Delta_g(v=0)$ and $b^1\Sigma_g^+(v=0)$ levels following $A^3\Sigma_u^+$ excitation indicates that they appear extremely rapidly, on the time scale of the disappearance of the photoexcited level, with no subsequent production corresponding

Table 10. Temperature-Dependent Removal Rate Coefficients for $O_2(a^1\Delta_g,v)$ by O_2[a]

vibrational level, v	at 155 K	at 240 K
17	$(1.2\pm0.8)\times10^{-13}$	
18	$(4.9\pm0.6)\times10^{-13}$	
19	$(1.4\pm0.2)\times10^{-11}$	$(1.5\pm0.2)\times10^{-11}$

[a] Units for the removal rate coefficients are cm^3 s^{-1}. The error estimates are two standard deviations. Measurements from Amaral et al. and Wouters et al.[213,247]

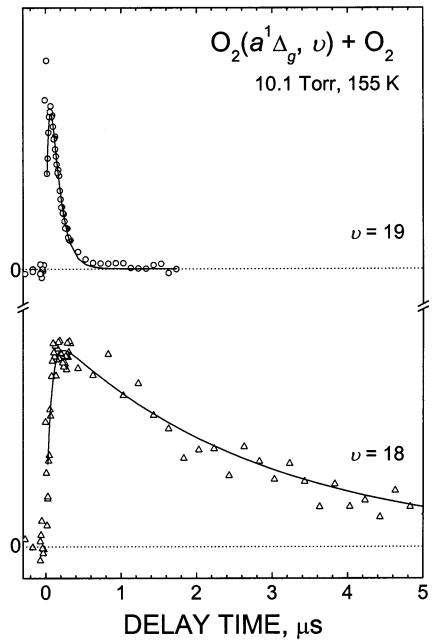

Figure 28. Oxygen ion signal as a function of delay between the excitation and ionization laser pulses monitoring $O_2(a^1\Delta_g, v = 19)$ in the top trace (circles) and $O_2(a^1\Delta_g, v = 18)$ in the bottom trace (triangles). Amaral et al. performed the measurements at 10.1 Torr of oxygen at 155 K.[247] The solid lines are the best two-exponential fits to the experimental data, and the dashed line shows the baseline. The $O_2(a^1\Delta_g, v = 19)$ data were obtained by exciting the O_2 via the $A^3\Sigma_u^+ - X^3\Sigma_g^-$ 7−0 transition and monitoring the excited oxygen via the Q(3) rotation feature in the $3d\pi_g{}^1\Delta_g - a^1\Delta_g$ 5−19 transition.[67] The $O_2(a^1\Delta_g, v = 19)$ data were obtained by exciting the O_2 via the $A^3\Sigma_u^+ - X^3\Sigma_g^-$ 6−0 transition and monitoring the excited oxygen via the Q(4) rotational feature in the $3d\pi_g{}^1\Delta_g - a^1\Delta_g$ 4−18 transition.[67] The ion signal rises are consistent with a one-step filling process from the initially prepared excited molecule for $O_2(a^1\Delta_g, v = 19)$, but inconsistent with a one-step process for $O_2(a^1\Delta_g, v = 18)$.

to further stepwise $a^1\Delta_g(v = 0)$ or $b^1\Sigma_g^+(v = 0)$ generation. Furthermore, there have been no relevant measurements on the ground-state vibrational manifold to see if that is an energy repository.

15.7. The $X^3\Sigma_g^-$ State

Experiments on vibrationally excited ground-state O_2 have an extensive history,[82,84,85,87,91,113,115,258,259] primarily because absorption and emission processes from the ground state connect to the $B^3\Sigma_u^-$ state in the optically allowed Schumann−Runge (SR) system. It has therefore been possible to make optical measurements on a broad array of vibrational levels in both upper and lower states. That the Schumann−Runge system has a large oscillator strength offsets the fact that the upper state is severely predissociated, resulting in line broadening for many bands[106−110] and low emission quantum efficiencies.

Generation of $X^3\Sigma_g^-(v)$ molecules can be accomplished in a variety of ways. Ozone photodissociation in the Hartley band is effective because the vibrational distribution of ground-state molecules is very broad. These molecules have been observed via absorption,[87] by LIF,[82,84,85,115] and by MPI imaging.[88]

Wodtke and co-workers have contributed greatly to the study of vibrationally excited ground-state O_2 using the approach of stimulated emission pumping in a three-laser system, where the first photon excites $X^3\Sigma_g^-(v = 0)$ to a level in the $B^3\Sigma_u^-$ state, the second stimulates the population down to a high-lying $X^3\Sigma_g^-(v)$ level, and the third samples that level by LIF, still in the SR system.[84,89,91,107,229,260]

Yet another method for $X^3\Sigma_g^-(v)$ generation involves O-atoms reacting with NO_2 to produce $X^3\Sigma_g^-$ ($8 \le v \le 12$), while sampling by LIF in the SR system.[114,115] Below $v = 8$, probing becomes difficult because shorter wavelength lasers are needed, and predissociation effects become more important.

Investigation of the kinetics of quenching the broad range of $X^3\Sigma_g^-(v)$ levels has been pursued, and it has been determined that collisional quenching by O_2 and N_2 is relatively slow, with rate coefficients in the $10^{-15}-10^{-13}$ cm^3 s^{-1} range.[82,84,85] There is a minimum in the O_2 rate coefficients at $v = 20$, caused by a crossover in mechanism between V−V and V−T processes. This minimum approximately coincides with a maximum in the two-quantum rate coefficient for the process[82,89]

$$O_2(X^3\Sigma_g^-, v) + N_2(v = 0) \rightarrow O_2(X^3\Sigma_g^-, v - 2) + N_2(v = 1) \quad (18)$$

In the atmosphere, there is therefore a wide range of ground-state vibrational levels, roughly $v = 14-22$, where relaxation could be due to N_2 collisions. To determine if this is the case, one must consider the possibility, alluded to several times here, that O-atoms are the dominant quencher.

There have been investigations of the low ground-state O_2 vibrational levels, prepared from an $a^1\Delta_g(v)$ distribution as described in the previous section. In this case, $X^3\Sigma_g^-(v = 1-3)$ are probed by Schumann−Runge LIF. Collisional removal rates by O_2 have been determined for $X^3\Sigma_g^-(v = 2,3)$ and by $O(^3P)$ for $X^3\Sigma_g^-(v = 1)$.[261] The 300 K experimental value for the rate coefficient for the V−T reaction

$$O_2(X^3\Sigma_g^-, v = 1) + O(^3P) \rightarrow O_2(X^3\Sigma_g^-, v = 0) + O(^3P) \quad (22)$$

is $(3 \pm 1) \times 10^{-12}$ cm^3 s^{-1}.[261] Approximately the same value has been obtained for the O + O_2 isotope exchange reaction,[262] although one would expect the exchange rate to be only half as fast as the V−T rate, due to the complex formation mechanism. There are no measurements for higher vibrational levels, but if values of this magnitude are valid for higher levels and lower temperatures, then O-atom quenching will be the dominant loss process for a large range of $X^3\Sigma_g^-(v)$ molecules in the 90−100 km region. The above rate coefficient is 20−30 times larger than the $v = 2,3$ O_2 rate coefficients, which will become smaller with increasing v,[13] and the typical $[O(^3P)]/[O_2]$ ratio at 95 km is 0.1; N_2 vibrational relaxation will not effectively compete with the $O(^3P)$ V−T process.[82,89]

The possible significance of $O_2(X^3\Sigma_g^-,v)$ in the atmosphere was discussed in connection with the observation that when an O_3/O_2 mixture was photodissociated at 248 nm, the amount of ozone increased.[263] The explanation was found to be that ozone photodissociation generates a large range of $X^3\Sigma_g^-(v)$ levels, and that the 2−7 band of the Schumann−Runge system lies at 248 nm. Thus, $v = 7$ molecules were dissociated within the laser pulse, and photodestruction of a molecule of ozone resulted in production of three O-atoms, and subsequently three ozone molecules. The efficiency of the process need not be large to see a net increase in ozone.

It was realized that if such a source was significant in the atmosphere, it might help alleviate the "ozone deficit problem", where modeled ozone profiles seem to underestimate the amount of ozone actually present in the 50−70 km region.[264−266] $O_2(X^3\Sigma_g^-,v)$ in highly vibrationally excited levels could thus be photodissociated in the Schumann−Runge bands at much longer wavelengths, where there is greater solar flux, than the 174−205 nm wavelength range appropriate to $v = 0$ dissociation. The critical point was whether collisional removal of these levels was slow enough that photodissociation could be a competing process. It thus became important to determine the rate coefficients for collisional removal of $O_2(X^3\Sigma_g^-,v)$ by O_2 and N_2.

It was soon established that although the rate coefficients are small, collisional removal still dominates photodissociation, and the additional ozone produced was insufficient to explain the apparent deficit.[265] However, subsequent research showed both that ozone photodissociation in the Hartley band results in a bimodal distribution of $X^3\Sigma_g^-(v)$, with a portion of the distribution at $v > 25$, and that such high-v molecules are lost quite rapidly in O_2 collisions.[84,89] It was suggested that this rapid high-v deactivation was an indicator of a reactive channel

$$O_2(X^3\Sigma_g^-,v > 25) + O_2 \rightarrow O_3 + O(^3P) \quad (19)$$

and that inclusion of this reaction in the models could help alleviate the ozone deficit.[267,268] It has not been possible to experimentally verify this reaction, but there have been a number of calculations, and these have all concluded that a reactive pathway is not expected.[12,14,269−271] Nevertheless, there are interesting features associated with the high-v levels.

Jongma and Wodtke have shown that in the $X^3\Sigma_g^-(v = 28)$ level there is a perturbation involving the $b^1\Sigma_g^+$ state, the first such example between the two states.[91] By extrapolating the Keck sky spectral data parameters from their present limit of $v = 15$, they were able to show that the perturber is the $b^1\Sigma_g^+(v = 19)$ level. Removal of population out of $v = 28$ was initially reported as being extremely rapid, involving a dark channel, possibly reaction 18 because no population appeared in the $v = 27$ level by an expected V−V transfer process.[84] In subsequent work, it was discovered that multiquantum relaxation was much more important, and that a fraction of about 40% of the $v = 28$ population was rapidly converted to $v = 19$ and 20.[107] The lower limit on the rate coefficient for $v = 28$ removal is 2×10^{-13} cm^3 s^{-1}, a much more modest figure than the limit of 1.2×10^{-11} cm^3 s^{-1} initially reported.

The $v = 30$ level was also investigated, and in this case the observed $X^3\Sigma_g^-$ products are $v = 19-22$. However, the yield is much smaller, 7−8%, and this may bear a relationship to the fact that the $v = 28$ level is perturbed and the $v = 30$ level is not. The perturbation may act as a gateway into the $b^1\Sigma_g^+$ state manifold, with subsequent collisions giving a different array of products than is the case for the ground-state levels.

Jongma and Wodtke[107] noted that the amount of energy removed in these multiquantum processes corresponds approximately to the energy of the $a^1\Delta_g(v = 0)$ level, 7889 cm^{-1}. It has recently become quite clear that processes of the type

$$O_2^* + O_2(X^3\Sigma_g^-,v = 0) \rightarrow O_2(b^1\Sigma_g^+,v) + O_2(a^1\Delta_g,v = 0) \quad (20)$$

$$O_2^* + O_2(X^3\Sigma_g^-,v = 0) \rightarrow O_2(a^1\Delta_g,v) + O_2(b^1\Sigma_g^+,v = 0) \quad (21)$$

are quite common, where O_2^* is one of the Herzberg states, and we have discussed in the previous sections the formation of the $a^1\Delta_g(v = 19)$ and $b^1\Sigma_g^+(v = 15)$ levels. Because $X^3\Sigma_g^-(v = 22)$ is produced from $X^3\Sigma_g^-(v = 30)$, a process that is 400 cm^{-1} endothermic to make $a^1\Delta_g(v = 0)$, Jongma and Wodtke express doubt that the reaction proceeds by that path, but because the yield to make $X^3\Sigma_g^-(v = 22)$ is only 2.6%, and there are a variety of possible pathways, including transfer into the Herzberg states, we believe that reactions 20 and 21 represents a generalized model for relaxation of highly energetic O_2 molecules.

There is by now a substantial body of data, both experimental and theoretical, on the $O_2(v) + O_2$ V−V rate coefficient.[11−13,82,84,85,89,91,107,114,115,260,271] In Figure 29 we plot all existing data for $X^3\Sigma_g^-(v = 1-28)$ at 300 K. It is apparent that there is now rather good agreement over the entire range. Above $v = 22$, the O_2 rate coefficients increase as V−T quenching becomes more important than V−V, but it can be seen that the data for the highest vibrational levels rise faster than calculations predict. There are calculations for the rate coefficients at 200 K (C. Coletti, private communication, 2003), pertinent to the mesosphere, and the rate coefficients are smaller than the 300 K values of Coletti and Billing[13] by factors of 0.78 at $v = 2$, 0.48 at $v = 8$, 0.22 at $v = 15$, and 0.15 at $v = 22$.

16. Relating Laboratory Kinetics to Nightglow Intensities

Volume emission rates (I) in the atmosphere can be related to the production rate (P) of the observed species if the collisional loss rates (L) and the radiative lifetime (τ) are known, via the steady-state equation

$$P(\text{cm}^{-3}\ \text{s}^{-1}) = L(\text{s}^{-1}) \times I(h\nu\ \text{cm}^{-3}\ \text{s}^{-1}) \times \tau(\text{s}) \quad (22)$$

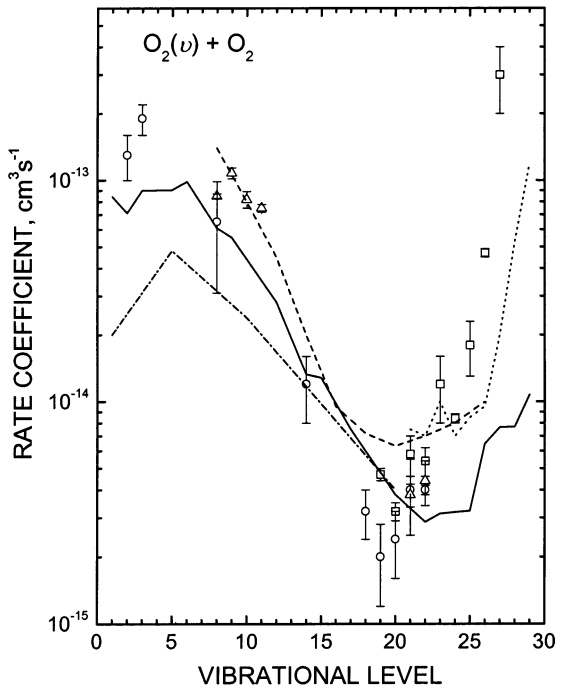

Figure 29. Removal rate coefficients for vibrationally excited levels of ground-state O_2 at 300 K. Open circles, Slanger et al.;[82,251] open triangles, Smith et al.;[85,114,115] open squares, Wodtke et al.[84,89,229,260] solid line, Coletti and Billing;[13] dashed line, Hernández et al.;[12] dot−dashed line, Billing and Kolesnick;[11] dotted line, Campos-Martínez et al.[14]

Comparison can then be made to the atom recombination rate. We approximate this rate by taking average values for the total density at 95 km of 3×10^{13} cm^{-3}, for the O-atom density of 5×10^{11} cm^{-3}, and a three-body recombination coefficient at 200 K of 1×10^{-32} cm^6 s^{-1},[66] resulting in a recombination rate of 7.5×10^4 cm^{-3} s^{-1}.

We consider two examples: the $A^3\Sigma_u^+(v = 7)$ level and the $b^1\Sigma_g^+(v = 13)$ level. According to Stegman's tabulations,[155] the intensity of the $A^3\Sigma_u^+(v = 7)-X^3\Sigma_g^-(v)$ emission is 17% of the total system intensity. McDade[223] gives an average Herzberg I intensity of 500 rayleighs, so that the $A^3\Sigma_u^+(v = 7)$ emission intensity is 85 rayleighs, which we approximate as a volume emission rate of 85 $h\nu$ cm^{-3} s^{-1}. The loss rate is $k_{N_2}[N_2] + k_{O_2}[O_2]$, where $k_{N_2} = 2.3 \times 10^{-11}$ and $k_{O_2} = 5.1 \times 10^{-11}$ cm^{-3} s^{-1}, which are estimates for a temperature of 195 K, based on averages of data obtained at 155 and 235 K (the rate coefficients for both colliders become about a factor of 2 larger on going from 235 to 155 K).[147,167] Using a radiative lifetime of 160 ms,[24] the $A^3\Sigma_u^+(v = 7)$ production rate is found to be 1.1×10^4 cm^{-3} s^{-1}, so that 15% of the excited molecules produced in the recombination event appear in a *single* vibrational level of a single state. Similar calculations can be made for other vibrational levels, but it is not obvious how to sum them because we do not yet know all the details of vibrational cascading, although we know that cascading from $A^3\Sigma_u^+(v = 7)$ to $A^3\Sigma_u^+(v = 6)$ is a minor process in air. Figure 15 shows a 0.35 cascading fraction for O_2 collider, but N_2 is the principal atmospheric collider, and in that case the cascading fraction is only 0.1. It is now evident that much of the O_2^* production derived from recombination is to be found in the $A^3\Sigma_u^+$ state; in a recent review[147] it was concluded that 100% of the recombining atoms go through the Herzberg states.

An additional consideration is our belief that the $A^3\Sigma_u^+$ and $A'^3\Delta_u$ states are collisionally coupled: the $A'^3\Delta_u(v = 8,\Omega = 2)$ state lies only 27 cm^{-1} above $A^3\Sigma_u^+(v = 7)$. REMPI measurements indicate very rapid rotational transfer between the states at $A^3\Sigma_u^+(v = 9)$ and $A'^3\Delta_u(v = 10)$, and it seems that the two levels should be considered together. The intensity used in eq 22 should be the sum of the intensities out of each level.[244] According to McDade,[223] the total Chamberlain band intensity is 40% that of Herzberg I, and from Stegman's tabulation[155] the intensity out of $A'^3\Delta_u(v = 8,\Omega = 3)$ is 16% of the total Chamberlain band intensity. As a consequence, the intensity out of the combined $A^3\Sigma_u^+(v = 7)/A'^3\Delta_u(v = 8)$ superlevel is 40% greater than that out of $A^3\Sigma_u^+(v = 7)$ alone and represents 20% of the molecules undergoing recombination.

This conclusion is radically different from that reached in earlier field measurements, where the fraction of recombination into the *total* Herzberg I system is typically quoted as 0.03−0.06.[166,177,272−275] The choice of these values has been constrained by statistical considerations,[274] and from what has been said, we are not persuaded of the relevance of that approach. Siskind and Sharp[276] performed $A^3\Sigma_u^+$ state modeling and reached a tentative conclusion that the efficiency factor for its production could be as high as 0.23, well above other estimates, but still too low because they used too low an air quenching rate coefficient. It thus appears that, in the nightglow, the excited O_2 molecules are not mysteriously undetected but are primarily represented by the UV emission.

We now consider the $b^1\Sigma_g^+(v = 13)$ level, where analysis of the Keck sky spectra shows a $b^1\Sigma_g^+(v = 13)-X^3\Sigma_g^-$ intensity of 3.5 rayleighs. Collisional loss of this level is due only to O_2 removal, with a rate coefficient at 155 K of 1.1×10^{-11} cm^3 s^{-1}, which from data on other levels and their temperature dependence appears to be a good estimate for 200 K.[67,213,247] The loss rate is therefore 65 s^{-1}. With a radiative lifetime of 17 s (Figure 2), the production rate from eq 22 is 4×10^3 cm^{-3} s^{-1}, or 5% of the number of molecules undergoing recombination. Again, this number is surprisingly large for a single (vibrationally excited) level of a single state, particularly in comparison with emission from the intense $b-X$ 0−0 band, where a similar calculation leads to a production rate of $(1.0-1.5) \times 10^4$ cm^{-3} s^{-1} for $b^1\Sigma_g^+(v = 0)$. With knowledge of the collisional loss rates of these metastable molecules, it is possible to make considerable progress in elucidating the nightglow processes.

17. Conclusions

Understanding the photochemistry, kinetics, and dynamics of O_2 excited states, both in the atmosphere

and in the laboratory, is a considerable challenge. However, progress is being made on both fronts. In the atmosphere, there are new tools available, in particular the sky spectra that are generated at large telescopes. In the laboratory, REMPI studies are producing rate coefficients for specific vibrational levels and tracing out deactivation pathways.

The O_2 Herzberg states are quenched very rapidly by both O_2 and N_2. Although N_2 is slower, in air N_2 quenching dominates. For this reason the N_2 deactivation pathways must be determined, and there is as yet little information available. For O_2 collisional removal, it has been shown that major channels for the $O_2(A^3\Sigma_u^+)$ state are those in which the colliding molecule is excited to the $a^1\Delta_g(v = 0)$ level, or to a lesser extent the $b^1\Sigma_g^+(v = 0)$ level. Exchange of this amount of energy leaves some fraction of the original molecules in high vibrational levels of the $a^1\Delta_g$ and $b^1\Sigma_g^+$ states. For the $A^3\Sigma_u^+$ levels investigated, the $a^1\Delta_g(v = 19)$ and $b^1\Sigma_g^+(v = 15)$ levels are favored. Further deactivation of these levels occurs in air via O_2, not N_2.

On the basis of the large quenching rate coefficients for the $A^3\Sigma_u^+$ state by O_2 and N_2, we find that previous modeling of the Herzberg I altitude profiles seriously underestimates the fraction of O-atom recombination events that produce the Herzberg states. We believe that the fraction is very high and could approach unity.

The manifold of vibrational levels in the $a^1\Delta_g$ and $b^1\Sigma_g^+$ states can show very large differences in collisional loss rate coefficients between adjacent levels. For instance, $a^1\Delta_g(v = 19)$ is quenched 30 times more rapidly by O_2 than is $a^1\Delta_g(v = 18)$, while $b^1\Sigma_g^+(v = 13)$ is quenched 60 times faster than $b^1\Sigma_g^+(v = 12)$.

Sky spectra show that in the atmosphere there is discernible population in the $b^1\Sigma_g^+$ manifold up to $b^1\Sigma_g^+(v = 15)$, which may be related to the fact that in the laboratory higher levels have not been detected either. The nightglow intensities from the $b^1\Sigma_g^+(v)$ levels are not inversely related to O_2 quenching rate coefficients, as might be the case if the $b^1\Sigma_g^+$ state vibrational populations were controlled by simple vibrational cascading caused by O_2. It may be that O-atoms are significant quenchers of the $a^1\Delta_g$ and $b^1\Sigma_g^+$ states.

Laboratory data are now in good agreement with calculations for V−V relaxation of the O_2 ground-state manifold. It is not yet known whether O-atom recombination leads to a large yield of vibrational energy in the ground-state manifold, but nightglow studies indicate that production of the $a^1\Delta_g(v = 0)$ level corresponds approximately to one such molecule for each recombination event. In terms of the available energy, this leaves 80% going elsewhere.

The sky spectra are having a big impact on O_2 spectroscopy. In the $b^1\Sigma_g^+$ state, the $v = 4-15$ levels are new in terms of spectroscopic parameters. Observation of many $A^3\Sigma_u^+-X^3\Sigma_g^-$ bands provides new information on ground-state levels, including a number which have been uncertain. The $A'^3\Delta_u-a^1\Delta_g$ Chamberlain bands are observed up to $a^1\Delta_g(v = 10)$, again leading to levels not previously seen.

The main O_2 emission system in the visible spectral region of the Venus nightglow is the $c^1\Sigma_u^- - X^3\Sigma_g^-$ transition. These bands are seen only with difficulty in the terrestrial atmosphere. However, the sky spectra have led to the discovery of a new O_2 transition, the $c^1\Sigma_u^- - b^1\Sigma_g^+$ bands, the study of which may aid in our further understanding of nightglow processes.

Another feature new to the nightglow is high-altitude emission in the $O_2(b-X)$ bands, specifically in the 1−1 band. This is a consequence of enhanced concentrations of $O(^1D)$ originating with O_2^+ dissociative recombination. Collisional transfer of the $O(^1D)$ energy to O_2 results in ionospheric $b^1\Sigma_g^+(v = 0,1)$ emission, which can at times reach an intensity as viewed from space of 500 rayleighs.

18. Acknowledgments

We gratefully acknowledge our funding sources for the work described herein: NSF Aeronomy, NASA Planetary Atmospheres, NASA Planetary Astronomy, and NASA Ionospheric, Mesospheric, and Thermospheric Physics. SRI has an active NSF-sponsored Research Experience for Undergraduates (REU) program, (Grant PHY-0097861), and the people who have been involved in these studies are Aaron Bergman, Olivia Cheriton, Kelly Cone, Ashley Espy, Seth Koterba, Wannasiri Lapcharoensap, Marc Onishi, Andrea Santoro, Ryan Thom, Apolka Totth, Aurea Tucay, Tim Shiau, and Emily Spangler. Past and present postdoctoral students involved in the laboratory studies, and whose results are quoted prior to publication, are Gabriel Amaral, Christian Bressler, Bor-Yu Chang, Eunsook Hwang, Kostas Kalogerakis, Karen Knutsen, Eloy Wouters, and Talat Yalçin. We also thank our SRI colleagues who have been intimately associated with the work—David Huestis and Philip Cosby—as well as others who have shared their results and expertise: Brenton Lewis, Jeff Morrill, Marshall Ginter, Andrei Kirillov, and Cecilia Coletti. For the astronomical sky spectra we are particularly grateful to Don Osterbrock, who introduced us to the astronomers' secrets, and to our providers, particularly Wal Sargent and Tom Barlow.

19. References

(1) Meriwether, J. W., Jr. *J. Geophys. Res.* **1989**, *94*, 14629.
(2) Solomon, S. C. *Rev. Geophys.* **1991**, *29*, 1089.
(3) Slanger, T. G.; Cosby, P. C. *J. Phys. Chem.* **1988**, *92*, 267.
(4) Sander, S. P.; Friedl, R. R.; Golden, D. M.; Kurylo, M. J.; Huie, R. E.; Orkin, V. L.; Moortgat, G. K.; Ravishankara, A. R.; Kolb, C. E.; Molina, M. J.; Finlayson-Pitts, B. J. *Chemical Kinetics and Photochemical Data for Use in Stratospheric Modeling*, Evaluation No. 14; National Aeronautics and Space Administration, Jet Propulsion Laboratory, 2003.
(5) Meier, R. R. *Space Sci. Rev.* **1991**, *58*, 1.
(6) Fox, J. L. In *Atomic, Molecular, & Optical Physics Handbook*; Drake, G. W. F., Ed.; AIP Press: Woodbury, NY, 1996.
(7) Bates, D. R. In *Progress and Problems in Atmospheric Chemistry*; Barker, J. R., Ed.; World Scientific: River Edge, NJ, 1995.
(8) Slanger, T. G.; Copeland, R. A. In *Progress and Problems in Atmospheric Chemistry*; Barker, J. R., Ed.; World Scientific: Singapore, 1995.
(9) Slanger, T. G.; Wolven, B. C. In *Atmospheres in the Solar System: Comparative Aeronomy*; Mendillo, M., Nagy, A., Waite, J. H., Eds.; American Geophysical Union: Washington, D.C., 2002; Vol. 130.

(10) Kunc, J. A. *J. Phys. B* **1991**, *24*, 3741.
(11) Billing, G. D.; Kolesnick, R. E. *Chem. Phys. Lett.* **1992**, *200*, 382.
(12) Hernández, R.; Toumi, R.; Clary, D. C. *J. Chem. Phys.* **1995**, *102*, 9544.
(13) Coletti, C.; Billing, G. D. *Chem. Phys. Lett.* **2002**, *356*, 14.
(14) Campos-Martínez, J.; Carmona-Novillo, E.; Echave, J.; Hernández, M. I.; Hernández-Lamoneda, R.; Palma, J. *Chem. Phys. Lett.* **1998**, *289*, 150.
(15) Saxon, R. P.; Slanger, T. G. *J. Geophys. Res.* **1986**, *91*, 9877.
(16) Klotz, R.; Peyerimhoff, S. D. *Mol. Phys.* **1986**, *57*, 573.
(17) Slanger, T. G.; Cosby, P. C.; Huestis, D. L. *J. Geophys. Res.* **2003**, *108*, 1089.
(18) Tachiev, G. I.; Fischer, C. F. *Astron. Astrophys.* **2002**, *385*, 716.
(19) Kernahan, J. A.; Pang, P. H.-L. *Can. J. Phys.* **1974**, *53*, 455.
(20) Greer, R. G. H.; Murtagh, D. R.; McDade, I. C.; Dickinson, P. H. G.; Thomas, L.; Jenkins, D. B.; Stegman, J.; Llewellyn, E. J.; Witt, G.; Mackinnon, D. J.; Williams, E. R. *Planet. Space Sci.* **1986**, *34*, 771.
(21) Tinsley, B. A.; Christensen, A. B.; Bittencourt, J.; Gouveia, H.; Angreji, P. D.; Takahashi, H. *J. Geophys. Res.* **1973**, *78*, 1174.
(22) Merienne, M. F.; Jenouvrier, A.; Coquart, B.; Carleer, M.; Fally, S.; Colin, R.; Vandaele, A. C.; Hermans, C. *J. Mol. Spectrosc.* **2000**, *202*, 171.
(23) England, J. P.; Lewis, B. R.; Gibson, S. T. *Can. J. Phys.* **1996**, *74*, 185.
(24) Huestis, D. L.; Copeland, R. A.; Knutsen, K.; Slanger, T. G.; Jongma, R. T.; Boogaarts, M. G. H.; Meijer, G. *Can. J. Phys.* **1994**, *72*, 1109.
(25) Bates, D. R. *Planet. Space Sci.* **1989**, *37*, 811.
(26) Yoshino, K.; Murray, J. E.; Esmond, J. R.; Sun, Y.; Parkinson, W. H.; Thorne, A. P.; Learner, R. C. M.; Cox, G. *Can. J. Phys.* **1994**, *72*, 1101.
(27) Yoshino, K.; Esmond, J. R.; Parkinson, W. H.; Thorne, A. P.; Learner, R. C. M.; Cox, G. *J. Chem. Phys.* **1999**, *111*, 2960.
(28) Yoshino, K.; Esmond, J. R.; Parkinson, W. H.; Thorne, A. P.; Learner, R. C. M.; Cox, G.; Cheung, A. S.-C. *J. Chem. Phys.* **2000**, *112*, 9791.
(29) Mlynczak, M. G.; Olander, D. S. *Geophys. Res. Lett.* **1995**, *22*, 1377.
(30) Newman, S. M.; Lane, I. C.; Orr-Ewing, A. J.; Newnham, D. A.; Ballard, J. *J. Chem. Phys.* **1999**, *110*, 10749.
(31) Miller, H. C.; McCord, J. E.; Choy, J.; Hagen, G. D. *J. Quant. Spectrosc. Radiat. Transfer* **2001**, *69*, 305.
(32) Gamache, R. R.; Goldman, A. *J. Quant. Spectrosc. Radiat. Transfer* **2001**, *69*, 389.
(33) Cheah, S.-L.; Lee, Y.-P.; Ogilvie, J. F. *J. Quant. Spectrosc. Radiat. Transfer* **2000**, *64*, 467.
(34) Ritter, K. J.; Wilkerson, T. D. *J. Mol. Spectrosc.* **1987**, *121*, 1.
(35) Miller, J. H.; Giver, L. P.; Boese, R. W. *J. Quant. Spectrosc. Radiat. Transfer* **1976**, *16*, 595.
(36) Naus, H.; van der Wiel, S. J.; Ubachs, W. *J. Mol. Spectrosc.* **1998**, *192*, 162.
(37) Schermaul, R.; Learner, R. C. M. *J. Quant. Spectrosc. Radiat. Transfer* **1999**, *61*, 781.
(38) Minaev, B.; Vahtras, O.; Agren, H. *Chem. Phys.* **1996**, *208*, 299.
(39) Fink, E. H.; Kruse, H.; Ramsay, D. A.; Vervloet, M. *Can. J. Phys.* **1986**, *64*, 242.
(40) Hasson, V.; Nicholls, R. W.; Degen, V. *J. Phys. B* **1970**, *3*, 1192.
(41) Hasson, V.; Nicholls, R. W. *J. Phys. B* **1971**, *4*, 1778.
(42) Yoshino, K.; Esmond, J. R.; Murray, J. E.; Parkinson, W. H.; Thorne, A. P.; Learner, R. C. M.; Cox, G. *J. Chem. Phys.* **1995**, *103*, 1243.
(43) Jenouvrier, A.; Merienne, M.-F.; Coquart, B.; Carleer, M.; Fally, S.; Vandaele, A. C.; Hermans, C.; Colin, R. *J. Mol. Spectrosc.* **1999**, *198*, 136.
(44) Offermann, D.; Conway, R. R. *EOS, Trans. Am. Geophys. Union* **1995**, *76*, 337.
(45) O'Brien, D. M.; English, S. A.; Costa, G. D. *J. Atmos. Ocean. Technol.* **1997**, *114*, 105.
(46) Naus, H.; Ubachs, W. *J. Mol. Spectrosc.* **1999**, *193*, 442.
(47) Lafferty, W. J.; Solodov, A. M.; Lugez, C. L.; Fraser, G. T. *Appl. Opt.* **1998**, *37*, 2264.
(48) Cheung, A. S.-C.; Yoshino, K.; Parkinson, W. H.; Guberman, S. L.; Freeman, D. E. *Planet. Space Sci.* **1986**, *34*, 1007.
(49) Lee, L. C.; Slanger, T. G.; Black, G.; Sharpless, R. L. *J. Chem. Phys.* **1977**, *67*, 5602.
(50) Saxon, R. P.; Liu, B. *J. Chem. Phys.* **1977**, *67*, 5432.
(51) Lacoursière, J.; Meyer, S. A.; Faris, G. W.; Slanger, T. G.; Lewis, B. R.; Gibson, S. T. *J. Chem. Phys.* **1999**, *110*, 1949.
(52) Lewis, B. R.; Gibson, S. T.; Emami, M.; Carver, J. H. *J. Quant. Spectrosc. Radiat. Transfer* **1988**, *40*, 469.
(53) Lewis, B. R.; Gibson, S. T.; Emami, M.; Carver, J. H. *J. Quant. Spectrosc. Radiat. Transfer* **1988**, *40*, 1.
(54) Lewis, B. R.; Gibson, S. T.; Banerjee, S. S.; Lefebvre-Brion, H. *J. Chem. Phys.* **2000**, *113*, 2214.
(55) Lewis, B. R.; Gibson, S. T.; Tucay, A. A.; Roberston, R.; Hwang, E. S.; Bergman, A.; Copeland, R. A. *J. Chem. Phys.* **2001**, *114*, 8364.
(56) Lee, P. C.; Nee, J. B. *J. Chem. Phys.* **2000**, *112*, 1763.
(57) Nee, J. B.; Lee, L. C. *J. Chem. Phys.* **1984**, *81*, 3811.
(58) Krupenie, P. H. *J. Phys. Chem. Ref. Data* **1972**, *1*, 423.
(59) Broida, H. P.; Peyron, M. *J. Chem. Phys.* **1960**, *32*, 1068.
(60) Barth, C. A.; Patapoff, M. *Astrophys. J.* **1962**, *136*, 1144.
(61) Young, R. A.; Sharpless, R. L. *J. Chem. Phys.* **1963**, *39*, 1071.
(62) Young, R. A.; Black, G. *J. Chem. Phys.* **1966**, *44*, 3741.
(63) Degen, V.; Innanen, S. H.; Hebert, G. R.; Nicholls, R. W. Identification Atlas of Molecular Spectra. 6. The O_2 $A-X$ Herzberg I System; York University, 1968.
(64) McNeal, R. J.; Durana, S. C. *J. Chem. Phys.* **1969**, *51*, 2955.
(65) Smith, I. W. M. *Int. J. Chem. Kinet.* **1984**, *16*, 423.
(66) Campbell, I. M.; Gray, C. N. *Chem. Phys. Lett.* **1973**, *18*, 607.
(67) Kalogerakis, K. S.; Totth, A.; Cosby, P. C.; Slanger, T. G.; Copeland, R. A. *EOS, Trans. Am. Geophys. Union* **2000**, *81*, F944.
(68) Thom, R. L.; Bressler, C. G.; Hwang, E. S.; Copeland, R. A. *EOS, Trans. Am. Geophys. Union* **1998**, *79*, F669.
(69) Nieh, J.-C.; Valentini, J. J. *J. Phys. Chem.* **1987**, *91*, 1370.
(70) Taherian, M.-R.; Slanger, T. G. *J. Chem. Phys.* **1985**, *83*, 6246.
(71) Turnipseed, A. A.; Vaghjiani, G. L.; Gierczak, T.; Thompson, J. E.; Ravishankara, A. R. *J. Chem. Phys.* **1991**, *95*, 3244.
(72) Stranges, D.; Yang, X.; Chesko, J. D.; Suits, A. G. *J. Chem. Phys.* **1995**, *102*, 6067.
(73) Levene, H.; Nieh, J.-C.; Valentini, J. J. *J. Chem. Phys.* **1987**, *87*, 2583.
(74) Ball, S. M.; Hancock, G.; Pinot de Moira, J. C.; Sadowski, C. M.; Winterbottom, F. *Chem. Phys.* **1995**, *245*, 1.
(75) Ball, S. M.; Hancock, G.; Martin, S. E.; Moira, J. C. P. *Chem. Phys. Lett.* **1997**, *264*, 531.
(76) Ball, S. M.; Hancock, G.; Murphy, I. J.; Rayner, S. P. *Geophys. Res. Lett.* **1993**, *20*, 2063.
(77) Takahashi, K.; Matsumi, Y.; Kawasaki, M. *J. Phys. Chem.* **1996**, *100*.
(78) Takahashi, K.; Kishigami, M.; Matsumi, Y.; Kawasaki, M.; Orr-Ewing, A. J. *J. Chem. Phys.* **1996**, *105*, 5290.
(79) Talukdar, R. K.; Longfellow, C. A.; Gilles, M. K.; Ravishankara, A. R. *Geophys. Res. Lett.* **1998**, *25*, 143.
(80) O'Keeffe, P.; Ridley, T.; Lawley, K. P.; Maier, R. R. J.; Donovan, R. J. *J. Chem. Phys.* **1999**, *110*, 10803.
(81) Ravishankara, A. R.; Hancock, G.; Kawasaki, M.; Matsumi, Y. *Science* **1998**, *280*, 60.
(82) Park, H.; Slanger, T. G. *J. Chem. Phys.* **1994**, *100*, 287.
(83) Kinugawa, T.; Sato, T.; Arikawa, T.; Matsumi, Y.; Kawasaki, M. *J. Chem. Phys.* **1990**, *93*, 3289.
(84) Rogaski, C. A.; Mack, J. A.; Wodtke, A. M. *Faraday Discuss. Chem. Soc.* **1995**, *100*, 229.
(85) Hickson, K. M.; Sharkey, P.; Smith, I. W. M.; Symonds, A. C.; Tuckett, R. P.; Ward, G. N. *J. Chem. Soc., Faraday Trans.* **1998**, *94*, 533.
(86) Webster, H.; Bair, E. J. *J. Chem. Phys.* **1972**, *56*, 6104.
(87) Fitzsimmons, R. V.; Bair, E. J. *J. Chem. Phys.* **1964**, *40*, 451.
(88) Miller, R. L.; Suits, A. G.; Houston, P. L.; Toumi, R.; Mack, J. A.; Wodtke, A. M. *Science* **1994**, *265*, 1831.
(89) Mack, J. A.; Mikulecky, K.; Wodtke, A. M. *J. Chem. Phys.* **1996**, *105*, 4105.
(90) Parker, D. H.; Eppink, A. T. J. B. *J. Chem. Phys.* **1997**, *107*, 2357−2362.
(91) Jongma, R. T.; Shi, S.; Wodtke, A. M. *J. Chem. Phys.* **1999**, *111*, 2588.
(92) Geiser, J. D.; Dylewski, S. M.; Mueller, J. A.; Wilson, R. J.; Toumi, R.; Houston, P. L. *J. Chem. Phys.* **2000**, *112*, 1279.
(93) Syage, J. *J. Chem. Phys.* **1996**, *105*, 1007.
(94) Syage, J. *J. Phys. Chem.* **1995**, *99*, 16530.
(95) Degen, V. *Can. J. Phys.* **1968**, *46*, 783.
(96) Degen, V. *J. Geophys. Res.* **1972**, *27*, 6213.
(97) Kenner, R. D.; Ogryzlo, E. A. *Int. J. Chem. Kinet.* **1980**, *12*, 501.
(98) Chamberlain, J. W. *Astrophys. J.* **1955**, *123*, 277.
(99) Slanger, T. G.; Huestis, D. L. *J. Chem. Phys.* **1983**, *78*, 2274.
(100) Herzberg, G. *Can. J. Phys.* **1953**, *31*, 657.
(101) Slanger, T. G.; Degen, V. *Planet. Space Sci.* **1986**, *34*, 971.
(102) Kenner, R. D.; Ogryzlo, E. A. *Chem. Phys. Lett.* **1983**, *103*, 209.
(103) Kenner, R. D.; Ogryzlo, E. A. *Can. J. Chem.* **1983**, *61*, 921.
(104) Kenner, R. D.; Ogryzlo, E. A. *Can. J. Phys.* **1984**, *62*, 1599.
(105) Ogryzlo, E. A.; Shen, Y. Q.; Wassell, P. T. *J. Photochem.* **1984**, *25*, 389.
(106) Dooley, P. M.; Lewis, B. R.; Gibson, S. T.; Baldwin, K. G. H.; Cosby, P. C.; Price, J. L.; Copeland, R. A.; Slanger, T. G.; Thorne, A. P.; Murray, J. E.; Yoshino, K. *J. Chem. Phys.* **1998**, *109*, 3856.
(107) Jongma, R. T.; Wodtke, A. M. *J. Chem. Phys.* **1999**, *111*, 10957.
(108) Lewis, B. R.; Berzins, L.; Carver, J. H. *J. Quant. Spectrosc. Radiat. Transfer* **1986**, *36*, 209.
(109) Lewis, B. R.; Gibson, S. T.; Dooley, P. M. *J. Chem. Phys.* **1994**, *100*, 7012.
(110) Lewis, B. R.; Berzins, L.; Carver, J. H.; Gibson, S. T. *J. Quant. Spectrosc. Radiat. Transfer* **1986**, *36*, 187.
(111) Lewis, B. R.; Berzins, L.; Carver, J. H. *J. Quant. Spectrosc. Radiat. Transfer* **1987**, *37*, 243.
(112) Lewis, B. R.; Gibson, S. T.; Dooley, P. M. *J. Chem. Phys.* **1993**, *100*, 7012.

(113) Creek, D. M.; Nicholls, R. W. *Proc. R. Soc. London A* **1975**, *341*, 517.
(114) Klatt, M.; Smith, I. W. M.; Tuckett, R. P.; Ward, G. N. *Chem. Phys. Lett.* **1994**, *224*, 253.
(115) Klatt, M.; Smith, I. W. M.; Symonds, A. C.; Tuckett, R. P.; Ward, G. N. *J. Chem. Soc., Faraday Trans.* **1996**, *92*, 193.
(116) Johnson, R. D.; Long, G. R.; Hudgens, J. W. *J. Chem. Phys.* **1987**, *87*, 1977.
(117) Ogorzalek-Loo, R.; Marinelli, W. J.; Houston, P. L.; Arepalli, S.; Wiesenfeld, J. R.; Field, R. W. *J. Chem. Phys.* **1989**, *91*, 5185.
(118) Morrill, J. S.; Ginter, M. L.; Lewis, B. R.; Gibson, S. T. *J. Chem. Phys.* **1999**, *111*, 173.
(119) Morrill, J. S. Ph.D. thesis, University of Maryland, 1999.
(120) Yntema, L. *Publ. Astron. Groningen* **1909**, *22*, 1.
(121) Chapman, S. *Proc. R. Soc.* **1931**, *A 132*, 353.
(122) Barth, C. A.; Hildebrandt, A. F. *J. Geophys. Res.* **1961**, *66*, 985.
(123) Herzberg, G. *Naturewissenschaften* **1932**, *20*, 577.
(124) Krasnopolsky, V. A.; Krysko, A. A.; Rogachev, V. N.; Parshev, V. A. *Cosmic Res.* **1976**, *14*, 789.
(125) Slanger, T. G.; Huestis, D. L. *J. Geophys. Res.* **1983**, *88*, 4137.
(126) Brasseur, G.; Solomon, S. *Aeronomy of the Middle Atmosphere*; D. Reidel: Boston, 1984.
(127) Bates, D. R. *Planet. Space Sci.* **1992**, *40*, 211.
(128) Wraight, P. C. *Planet. Space Sci.* **1982**, *30*, 251.
(129) Eppink, A. T. J. B.; Parker, D. H.; Janssen, M. H. M.; Buijsse, B.; Zande, W. J. v. d. *J. Chem. Phys.* **1998**, *108*, 1305.
(130) Lewis, B. R.; Gibson, S. T.; Slanger, T. G.; Huestis, D. L. *J. Chem. Phys.* **1999**, *110*, 11129.
(131) Traub, W. A.; Carleton, N. P.; Connes, P.; Noxon, J. F. *Astrophys. J.* **1979**, *229*, 846.
(132) Noxon, J. F.; Traub, W. A.; Carleton, N. P.; Connes, P. *Astrophys. J.* **1976**, *207*, 1025.
(133) Slysh, V. I. *Cosmic Res.* **1976**, *14*, 796.
(134) Lawrence, G. M.; Barth, C. A.; Argabright, V. *Science* **1977**, *195*, 573.
(135) Slanger, T. G. *J. Chem. Phys.* **1978**, *69*, 4779.
(136) Slanger, T. G.; Black, G. *Geophys. Res. Lett.* **1978**, *5*, 947.
(137) Bougher, S. W.; Borucki, W. J. *J. Geophys. Res.* **1994**, *99*, 3759.
(138) Crisp, D.; Meadows, V. S.; Bezard, B.; Bergh, C. d.; Maillard, J.-P.; Mills, F. P. *J. Geophys. Res.* **1996**, *101*, 4577.
(139) Slanger, T. G.; Cosby, P. C.; Huestis, D. L.; Bida, T. A. *Science* **2001**, *291*, 463.
(140) Krasnopolsky, V. A. *Planet. Space Sci.* **1986**, *34*, 511.
(141) Broadfoot, A. L.; Bellaire, P. J. *J. Geophys. Res.* **1999**, *104*, 17127.
(142) Chamberlain, J. W. *Astrophys. J.* **1958**, *128*, 713.
(143) Broadfoot, A. L.; Kendall, K. R. *J. Geophys. Res.* **1968**, *73*, 426.
(144) Copeland, R. A.; Knutsen, K.; Onishi, M. E.; Yalçin, T. *J. Chem. Phys.* **1996**, *105*, 10349.
(145) Hwang, E. S.; Copeland, R. A. *Geophys. Res. Lett.* **1997**, *24*, 643.
(146) Knutsen, K.; Dyer, M. J.; Copeland, R. A. *J. Chem. Phys.* **1994**, *101*, 7415.
(147) Huestis, D. L. In *Atmospheres in the Solar System: Comparative Aeronomy*; Mendillo, A., Nagy, A., Waite, J. H., Eds.; American Geophysical Union: Washington, D.C., 2002; Vol. 130.
(148) McDade, I. C.; Murtagh, D. P.; Greer, R. G. H.; Dickinson, P. H. G.; Witt, G.; Stegman, J.; Llewellyn, E. J.; Thomas, L.; Jenkins, D. B. *Planet. Space Sci.* **1986**, *34*, 789.
(149) Slanger, T. G.; Cosby, P. C.; Huestis, D. L. *J. Atmos. Terr. Phys.* **2003**, in press.
(150) Slanger, T. G.; Cosby, P. C.; Huestis, D. L.; Osterbrock, D. E. *J. Geophys. Res.* **2000**, *105*, 20557.
(151) Huestis, D. L.; Chang, B.-Y.; Cosby, P. C.; Bressler, C. G.; Copeland, R. A. *EOS, Trans. Am. Geophys. Union* **1999**, *80*, F780.
(152) Bates, D. R. *Chem. Phys. Lett.* **1989**, *162*, 313.
(153) Stegman, J.; Murtagh, D. P. *Planet. Space Sci.* **1988**, *36*, 927.
(154) Stegman, J.; Murtagh, D. P. *Planet. Space Sci.* **1991**, *39*, 595.
(155) Stegman, J. Ph.D. thesis, Stockholm University, 1991.
(156) Taylor, M. J.; Turnbull, D. N.; Lowe, R. P. *Geophys. Res. Lett.* **1995**, *22*, 2849.
(157) Taylor, M. J.; Bishop, M. B.; Taylor, V. *Geophys. Res. Lett.* **1995**, *22*, 2833.
(158) Hecht, J. H.; Howatt, S. K. R.; Walterscheid, R. L.; Isler, J. R. *Geophys. Res. Lett.* **1995**, *22*, 2817.
(159) Reisin, E. R.; Scheer, J. *J. Geophys. Res.* **1996**, *101*, 21.
(160) Scheer, J.; Reisin, E. R. *J. Atmos. Terr. Phys.* **1990**, *52*, 47.
(161) Sica, R. J. *J. Geophys. Res.* **1993**, *98*, 1057.
(162) Rodrigo, R.; Lopez-Moreno, J. J.; Lopez-Puertas, M.; Molina, A. *J. Atmos. Terr. Phys.* **1985**, *47*, 1099.
(163) Melo, S. M. L.; McDade, I. C.; Takahashi, H. *J. Geophys. Res.* **2001**, *106*, 15377.
(164) Slanger, T. G.; Huestis, D. L.; Cosby, P. C.; Bida, T. A. *Adv. Space Res.* **2001**, *27*, 1135.
(165) McDade, I. C.; Llewellyn, E. J.; Greer, R. G. H.; Murtagh, D. P. *Planet. Space Sci.* **1986**, *34*, 801.
(166) Murtagh, D. R.; McDade, I. C.; Greer, R. G. H.; Stegman, J.; Witt, G.; Llewellyn, E. J. *Planet. Space Sci.* **1986**, *34*, 811.
(167) Kalogerakis, K. S.; Hwang, E. S.; Copeland, R. A. The Temperature Dependence of the Collisional Removal of $O_2(A^3\Sigma_u^+, v = 6, 7, 9)$, in preparation.
(168) Deans, A. G.; Shepherd, G. G.; Evans, W. F. J. *J. Geophys. Res.* **1976**, *81*, 6227.
(169) Witt, G.; Stegman, J.; Solheim, B. H.; Llewellyn, E. J. *Planet. Space Sci.* **1979**, *27*, 341.
(170) Witt, G.; Stegman, J.; Murtagh, D. P.; McDade, I. C.; Greer, R. G. H.; Dickinson, R. H. G.; Jenkins, D. B. *J. Photochem.* **1984**, *25*, 365.
(171) McDade, I. C.; Llewellyn, E. J.; Solheim, B. H. *Can. J. Phys.* **1985**, *63*, 983.
(172) Heller, J. W.; Christensen, A. B.; Yee, J. H.; Sharp, W. E. *J. Geophys. Res.* **1991**, *96*, 19499.
(173) Yee, J.-H.; Niciejewski, R.; Luo, M. Z. *Geophys. Res. Lett.* **1991**, *18*, 1357.
(174) Thomas, R. J. *J. Geophys. Res.* **1981**, *86*, 206.
(175) Sharp, W. E. *Planet. Space Sci.* **1985**, *33*, 571.
(176) Sharp, W. E.; Siskind, D. E. *Geophys. Res. Lett.* **1989**, *16*, 1453.
(177) Kita, K.; Iwagami, N.; Ogawa, T. *Planet. Space Sci.* **1992**, *40*, 1269.
(178) Melo, S. M. L.; Takahashi, H.; Clemesha, B. R.; Stegman, J. *J. Atmos. Terr. Phys.* **1996**, *59*, 295.
(179) Melo, S. M.; Takahashi, H.; Clemesha, B. R.; Batista, P. P.; Simonich, D. M. *J. Atmos. Terr. Phys.* **1996**, *58*, 1935.
(180) Dymond, K. F.; McCoy, R. P.; Thonnard, S. E.; Budzien, S. A.; Thomas, R. J.; Bullett, T. N.; Bucsela, E. J. *J. Geophys. Res.* **2000**, *105*, 23025.
(181) Owens, J. K.; Torr, D. G.; Torr, M. R.; Chang, T.; Fennelly, J. A.; Richards, P. G.; Morgan, M. F.; Baldridge, T. W.; Fellows, C. W.; Dougani, H.; Swift, W.; Tejada, A.; Orme, T.; Germany, G. A.; Yung, S. *Geophys. Res. Lett.* **1993**, *20*, 515.
(182) Shepherd, G. G.; Thuillier, G.; Solheim, B. H.; et al. *Geophys. Res. Lett.* **1993**, *20*, 1303.
(183) Morgan, F.; Romick, G. J.; Yee, J. H.; Morrison, D.; Anderson, D. E.; Paxton, L.; Meng, C. I. IAGA, Uppsala, Sweden, 1997.
(184) Eastes, R. W.; Huffman, R. E.; LeBlanc, F. J. *Planet. Space Sci.* **1992**, *40*, 481.
(185) Santoro, A. L.; Huestis, D. L.; Slanger, T. G. *EOS, Trans. Am. Geophys. Union* **1994**, *75*, F496.
(186) Mlynczak, M. G.; Solomon, S.; Zaras, D. S. *J. Geophys. Res.* **1993**, *98*, 18639.
(187) Evans, W. F. J.; McDade, I. C.; Yuen, J.; Llewellyn, E. J. *Can. J. Phys.* **1988**, *66*, 941.
(188) Mlynczak, M. G.; Morgan, F.; Yee, J.-H.; Espy, P.; Murtagh, D.; Marshall, B.; Schmidlin, F. *Geophys. Res. Lett.* **2001**, *28*, 999.
(189) Badger, R. M.; Wright, A. D.; Whitlock, R. F. *J. Chem. Phys.* **1965**, *43*, 4345.
(190) Mlynczak, M. G.; Nesbitt, D. J. *Geophys. Res. Lett.* **1995**, *22*, 1381.
(191) Sandor, B. J.; Clancy, R. T.; Rusch, D. W.; Randall, C. E.; Eckman, R. S.; Siskind, D. S.; Muhleman, D. O. *J. Geophys. Res.* **1997**, *102*, 9013.
(192) Wayne, R. P. *J. Photochem.* **1984**, *25*, 345.
(193) Noxon, J. F. *Space Sci. Rev.* **1968**, *8*, 92.
(194) Wallace, L.; Hunten, D. M. *J. Geophys. Res.* **1968**, *73*, 4813.
(195) Babcock, H. D.; Herzberg, L. *Astrophys. J.* **1948**, *108*, 167.
(196) Green, J. G.; Shi, J.; Barker, J. R. *J. Phys. Chem. A* **2000**, *104*, 6218.
(197) Knickelbein, M. B.; Marsh, K. L.; Ulrich, O. E.; Busch, G. E. *J. Chem. Phys.* **1987**, *87*, 2392.
(198) Borrell, P. M.; Borrell, P.; Ramsay, D. A. *Can. J. Phys.* **1986**, *64*, 721.
(199) Coquart, B.; Ramsay, D. A. *Can. J. Phys.* **1986**, *64*, 726.
(200) Ramsay, D. A. *Can. J. Phys.* **1986**, *64*, 717.
(201) Huestis, D. L. DIATOM Spectral Simulation Computer Program, v. 7.0, SRI International, 1994.
(202) Slanger, T. G.; Huestis, D. L.; Cosby, P. C.; Osterbrock, D. E. *J. Chem. Phys.* **2000**, *113*, 8514.
(203) Rouillé, G.; Millot, G.; Saint-Loup, R.; Berger, H. *J. Mol. Spectrosc.* **1992**, *154*, 372.
(204) Richards, J. L.; Johnson, P. M. *J. Chem. Phys.* **1976**, *65*, 3948.
(205) Slanger, T. G.; Huestis, D. L. *J. Geophys. Res.* **1981**, *86*, 3551.
(206) Wilkinson, P. G.; Mulliken, R. S. *J. Chem. Phys.* **1959**, *31*, 674.
(207) Gattinger, R. L.; Vallance Jones, A. *J. Geophys. Res.* **1976**, *81*, 4789.
(208) Slanger, T. G.; Huestis, D. L.; Osterbrock, D. E.; Fulbright, J. P. *Science* **1997**, *277*, 1485.
(209) Bates, D. R. *Proc. R. Soc. London A* **1993**.
(210) Kirillov, A. Committee on Space Research (COSPAR), Houston, TX, 2002.
(211) Hwang, E. S.; Copeland, R. A.; Slanger, T. G. Collisional removal of $O_2(a^1\Delta_g, v = 1,2)$ by O_2, N_2, and CO_2, in preparation.
(212) Hwang, E. S.; Copeland, R. A.; Robertson, R. M.; Slanger, T. G. *EOS, Trans. Am. Geophys. Union* **1998**, *79*, F85.
(213) Wouters, E. R.; Amaral, G. A.; Cone, K. V.; Spangler, E. L.; Kalogerakis, K. S.; Copeland, R. A. *EOS, Trans. Am. Geophys. Union* **2002**, *83*, SA72A.

(214) Howell, C. D.; Michelangeli, D. V.; Allen, M.; Yung, Y. L. *Planet. Space Sci.* **1990**, *38*, 529.
(215) McDade, I. C.; Llewellyn, E. J.; Greer, R. G. H.; Murtagh, D. P. *Planet. Space Sci.* **1987**, *35*, 1541.
(216) Gauthier, M. J. E.; Snelling, D. R. *Can. J. Chem.* **1974**, *52*, 4007.
(217) Lee, L. C.; Slanger, T. G. *J. Chem. Phys.* **1978**, *69*, 4053.
(218) Slanger, T. G.; Cosby, P. C.; Huestis, D. L. *J. Geophys. Res.* **2003**, *108*, 10.1029/2003JA009885.
(219) Slanger, T. G.; Osterbrock, D. E. *J. Geophys. Res.* **2000**, *105*, 1425.
(220) Wallace, L.; Chamberlain, J. W. *Planet. Space Sci.* **1959**, *2*, 60.
(221) Henriksen, K.; Sivjee, G. G. *Planet. Space Sci.* **1990**, *38*, 835.
(222) Slanger, T. G. *Can. J. Phys.* **1986**, *64*, 1657.
(223) McDade, I. C. *Adv. Space Res.* **1997**, *19*, 6653.
(224) Slanger, T. G.; Bischel, W. K.; Dyer, M. J. *Chem. Phys. Lett.* **1984**, *108*, 472.
(225) Wildt, J.; Bednarek, G.; Fink, E. H.; Wayne, R. P. *Chem. Phys.* **1991**, *156*, 497.
(226) Bednarek, G.; Wayne, R. P.; Wildt, J.; Fink, E. H. *Chem. Phys.* **1994**, *185*, 251; **1997**, *222*, 113 (erratum).
(227) Shiau, T. P.; Hwang, E. S.; Buijsse, B.; Copeland, R. A. *Chem. Phys. Lett.* **1998**, *282*, 369.
(228) Ali, A. A.; Ogryzlo, E. A.; Shen, Y. Q.; Wassell, P. T. *Can. J. Phys.* **1986**, *64*, 1614.
(229) Yang, X.; Price, J. M.; Mack, J. A.; Morgan, C. G.; Rogaski, C. A.; McGuire, D.; Kim, E. H.; Wodtke, A. M. *J. Phys. Chem.* **1993**, *97*, 3944.
(230) Morrill, J. S.; Ginter, M. L.; Hwang, E. S.; Slanger, T. G.; Copeland, R. A.; Lewis, B. R.; Gibson, S. T. *J. Mol. Spectrosc.* **2003**, *219*, 200.
(231) Morrill, J. S.; Ginter, M. L.; Lewis, B. R.; Gibson, S. T. *J. Mol. Spectrosc.* **2003**, *219*, 217.
(232) Copeland, R. A.; Kalogerakis, K. S.; Chang, B.-Y.; Huestis, D. L. *EOS, Trans. Am. Geophys. Union* **2001**, *82*, S283.
(233) Cosby, P. C.; Copeland, R. A.; Slanger, T. G. *EOS, Trans. Am. Geophys. Union* **2001**, *82*, F954.
(234) Copeland, R. A. *J. Chem. Phys.* **1994**, *100*, 744.
(235) Copeland, R. A.; Kalogerakis, K. S. *EOS, Trans. Am. Geophys. Union* **2000**, *81*, F943.
(236) Copeland, R. A.; Knutsen, K.; Slanger, T. G. In *Proceedings of the International Conference on Lasers '93*; Corcoran, V. J., Goldman, T. A., Eds.; STS Press: McLean, VA, 1994.
(237) Hwang, E. S.; Buijsse, B.; Copeland, R. A.; Riris, H.; Carlisle, C. B.; Slanger, T. G. *J. Chem. Soc., Faraday Trans.* **1997**, *93*, 2657.
(238) Kalogerakis, K. S.; Slanger, T. G.; Copeland, R. A. *EOS, Trans. Am. Geophys. Union* **1999**, *81*, S332.
(239) Chang, B.-Y.; Huestis, D. L.; Copeland, R. A. *EOS, Trans. Am. Geophys. Union* **1999**, *80*, S239.
(240) Amaral, G. A.; Lapcharoensap, W.; Copeland, R. A.; Huestis, D. L. *EOS, Trans. Am. Geophys. Union* **2001**, *82*, F955.
(241) Partridge, H.; Bauschlicher, C. W., Jr.; Langhoff, S. R.; Taylor, P. R. *J. Chem. Phys.* **1991**, *95*, 8292.
(242) Lewis, B. R.; Gibson, S. T.; Copeland, R. A.; Bressler, C. G. *Phys. Rev. Lett.* **1999**, *82*, 4212.
(243) Saxon, R. P.; Liu, B. *J. Chem. Phys.* **1980**, *73*, 876.
(244) Knutsen, K.; Yalçin, T.; Onishi, M. E.; Copeland, R. A. *EOS, Trans. Am. Geophys. Union* **1994**, *75*, 496.
(245) Kerr, C. M. L.; Watson, J. K. G. *Can. J. Phys.* **1986**, *64*, 36.
(246) Bergman, A.; Bressler, C. G.; Hwang, E. S.; Copeland, R. A. *EOS, Trans. Am. Geophys. Union* **1997**, *78*, F527.
(247) Amaral, G. A.; Kalogerakis, K. S.; Copeland, R. A. *EOS, Trans. Am. Geophys. Union* **2002**, *83*, S236.
(248) Schurath, U. *J. Photochem.* **1975**, *4*, 215.
(249) Bloemink, H. I.; Copeland, R. A.; Slanger, T. G. *J. Chem. Phys.* **1998**, *109*, 4237.
(250) Hwang, E. S.; Bergman, A.; Copeland, R. A.; Slanger, T. G. *J. Chem. Phys.* **1999**, *110*, 18.
(251) Kalogerakis, K. S.; Copeland, R. A.; Slanger, T. G. *J. Chem. Phys.* **2002**, *116*, 4877.
(252) Klais, O.; Laufer, A. H.; Kurylo, M. J. *J. Chem. Phys.* **1980**, *73*, 2696.
(253) Collins, R. J.; Husain, D. *J. Photochem.* **1973**, *1*, 481.
(254) Wayne, R. P. *Res. Chem. Intermed.* **1994**, *20*, 395.
(255) Thelen, M.-A.; Gejo, T.; Harrison, J. A.; Huber, J. R. *J. Chem. Phys.* **1995**, *103*, 7946.
(256) Dylewski, S. M.; Geiser, J. D.; Houston, P. L. *J. Chem. Phys.* **2001**, *115*, 7460.
(257) Jones, I. T. N.; Bayes, K. D. *J. Chem. Phys.* **1972**, *57*, 1003.
(258) Copeland, R. A.; Cosby, P. C.; Crosley, D. R.; Jeffries, J. B.; Slanger, T. G. *J. Chem. Phys.* **1987**, *86*, 2500.
(259) Andresen, P.; Schluter, H.; Wolff, D.; Voges, H.; Koch, A.; Hentschel, W.; Oppermann, W.; Rothe, E. *Appl. Opt.* **1992**, *31*, 7684.
(260) Price, J. M.; Mack, J. A.; Rogaski, C. A.; Wodtke, A. M. *Chem. Phys.* **1993**, *175*, 83.
(261) Kalogerakis, K. S.; Copeland, R. A.; Slanger, T. G. *EOS, Trans. Am. Geophys. Union* **2001**, *82*, F964.
(262) Wiegell, M. R.; Wessel Larsen, N.; Pedersen, T.; Esgaard, H. *Int. J. Chem. Kinet.* **1997**, *29*, 745.
(263) Slanger, T. G.; Jusinski, L. E.; Black, G.; Gadd, G. E. *Science* **1988**, *241*, 945.
(264) Eluszkiewicz, J.; Allen, M. *J. Geophys. Res.* **1993**, *98*, 1069.
(265) Patten, K. O., Jr.; Connell, P. S.; Kinnison, D. E.; Wuebbles, D. J.; Slanger, T. G.; Froidevaux, L. *J. Geophys. Res.* **1994**, *99*, 1211.
(266) Crutzen, R. J.; Grooss, J.-U.; Brühl, C.; Müller, R.; Russell, J. M., III. *Science* **1995**, *268*, 705.
(267) Rogaski, C. A.; Price, J. M.; Mack, J. A.; Wodtke, A. M. *Geophys. Res. Lett.* **1993**, *20*, 2885.
(268) Toumi, R.; Houston, P. L.; Wodtke, A. M. *J. Chem. Phys.* **1996**, *104*, 775.
(269) Balakrishnan, N.; Dalgarno, A.; Billing, G. D. *Chem. Phys. Lett.* **1998**, *288*, 657.
(270) Balakrishnan, N.; Billing, G. D. *J. Chem. Phys.* **1996**, *104*, 9482.
(271) Mack, J. A.; Huang, Y.; Wodtke, A. M.; Schatz, G. C. *J. Chem. Phys.* **1996**, *105*, 7495.
(272) Melo, S. M. L.; Takahashi, H.; Clemesha, B. R.; Stegman, J. *J. Atmos. Terr. Phys.* **1997**, *59*, 295.
(273) Murtagh, D. P.; Witt, G.; Stegman, J. *Can. J. Phys.* **1986**, *64*, 1587.
(274) Bates, D. R. *Planet. Space Sci.* **1988**, *36*, 875.
(275) Lopez-Gonzalez, M. J.; Lopez-Moreno, J. J.; Rodrigo, R. *Planet. Space Sci.* **1992**, *40*, 913.
(276) Siskind, D. E.; Sharp, W. E. *Planet. Space Sci.* **1991**, *39*, 627.

CR0205311